الجمهورية الجزائرية الديمقراطية الشعبية
PEOPLE'S DEMOCRATIC REPUBLIC OF ALGERIA
وزارة التعليم العالي و البحث العلمي
MINISTRY OF HIGHER EDUCATION AND SCIENTIFIC RESEARCH

Badji Mokhtar Annaba University
Technology Faculty
Electronique Department

جامعة باجي مختار - عنابة -
كلية التكنولوجيا
قسم الالكترونيك

A Thesis

Presented for obtaining the degree of:

DOCTORATE

In: Automatic

Speciality: Automatic and Systems

By:

AOUATI Ayoub

Theme

Modeling And Networked Control Of A Multi-source Energy System

Thesis defended on October 14, 2026 at Annaba in Front of the Jury Composed of:

Mr RAMDANI Messaoud	Prof.	University of Annaba	President
Mr GHERBI Sofiane	Prof.	University of Annaba	Supervisor
Mr BAHI Tahar	Prof.	University of Annaba	Examiner
Mr BENMOUSSA Samir	Prof.	University of Annaba	Examiner
Mr LACHOURI Abderrazak	Prof.	University of Skikda	Examiner
Mr GUECHI Elhadi	Prof.	University of Skikda	Examiner

Academic Year 2025/2026

Dedication

I proudly dedicate this thesis to: my parents, my wife, my sister, my brothers, and my big family — for their endless love, sacrifices, and unwavering belief in me.

– *Aouati Ayoub*

Acknowledgements

Firstly, all praise and thanks go to Allah who gave me the power and courage to conquer life challenges in general and to pursue my higher studies in particular; I am thankful. I warmly thank my PhD supervisor for their guidance, insight, and encouragement throughout this research. My deepest gratitude goes to my parents for their lifelong support, to my wife for her patience and love, and to my sister, my brothers, and my large family for their constant encouragement. I also thank my colleagues and friends who offered helpful discussions and moral support.

– *Aouati Ayoub*

Abstract

This thesis presents a comprehensive framework for modeling, stability analysis, and control of networked multi-source energy systems with photovoltaic prosumers -actors who both consume and produce energy- subject to stochastic communication delays. A novel Markov Regime-Switching GARCH (MRS-GARCH) approach is introduced to characterize network-induced delays, capturing volatility clustering, asymmetry, and regime-switching behavior observed in real IP network data—features missed by conventional models. Empirical comparison of thirty-three models identifies the MRS-GARCH with mixed distributions as optimal.

Using this delay characterization, delay-dependent stability conditions are derived via Lyapunov-Krasovskii functionals and formulated as Linear Matrix Inequalities, enabling computation of Maximum Allowable Delay Bounds (MADBs) guaranteeing mean-square stability. A control-oriented model of photovoltaic prosumer systems with DC-DC converters is developed, and stabilizing state-feedback controllers are synthesized using the Cone Complementarity Linearization algorithm.

Simulation results for a three-prosumer system demonstrate that the proposed approach achieves MADBs up to two orders of magnitude larger than conventional LQR designs, with detailed analysis of how transition probabilities and volatility coefficients influence robustness. This work provides a theoretically rigorous yet practically implementable solution for reliable operation of next-generation networked multi-source energy systems.

keywords: Networked Control Systems, Multi-source Energy Systems, Photovoltaic Prosumers, MRS-GARCH, Time Delay Modeling, Lyapunov-Krasovskii Functional, Linear Matrix Inequalities, Maximum Allowable Delay Bound, Lyapunov Stability, Controller Synthesis.

Résumé

Cette thèse présente un cadre complet pour la modélisation, l'analyse de stabilité et la commande de systèmes énergétiques multi-sources en réseau avec des prosommateurs -acteurs qui consomment et produisent à la fois de l'énergie- photovoltaïques soumis à des délais de communication stochastiques. Une nouvelle approche basée sur les processus GARCH à changement de régime markovien (MRS-GARCH) est introduite pour caractériser les délais induits par le réseau, capturant le regroupement de volatilité, l'asymétrie et les changements de régime observés dans les données de réseaux IP réels—des caractéristiques négligées par les modèles conventionnels. Une comparaison empirique de trente-trois modèles identifie le MRS-GARCH avec distributions mixtes comme optimal.

En utilisant cette caractérisation des délais, des conditions de stabilité dépendantes du délai sont dérivées via des fonctionnelles de Lyapunov-Krasovskii et formulées sous forme d'inégalités matricielles linéaires (LMI), permettant le calcul des bornes maximales admissibles de délai (MADB) garantissant la stabilité en moyenne quadratique. Un modèle orienté commande de systèmes prosommateurs photovoltaïques avec convertisseurs DC-DC est développé, et des correcteurs par retour d'état stabilisants sont synthétisés en utilisant l'algorithme de linéarisation par cône complémentaire (CCL).

Les résultats de simulation pour un système à trois prosommateurs démontrent que l'approche proposée atteint des MADB jusqu'à deux ordres de grandeur supérieurs aux conceptions LQR conventionnelles, avec une analyse détaillée de l'influence des probabilités de transition et des coefficients de volatilité sur la robustesse. Ces travaux fournissent une solution théoriquement rigoureuse et pratiquement implémentable pour l'exploitation fiable des systèmes énergétiques en réseau de nouvelle génération.

mots-clés: Systèmes de contrôle en réseau, Systèmes énergétiques multisources,

Prosommateurs photovoltaïques, MRS-GARCH, Modélisation des délais, Fonctionnelle de Lyapunov-Krasovskii, Inégalités matricielles linéaires, Limite maximale de délai admissible, Stabilité de Lyapunov, Synthèse de contrôleurs.

مُلخّص

تقدم هذه الأطروحة إطارًا شاملاً لنمذجة وتحليل الاستقرار والتحكم في أنظمة الطاقة متعددة المصادر المتصلة بشبكات الاتصال والمزودة ب (prosumers) فاعلون يستهلكون الطاقة وينتجونها في آنٍ واحد للطاقة الكهروضوئية، مع مراعاة تأخيرات الاتصال العشوائية. تم تقديم نهج جديد يعتمد على نماذج الانحدار الذاتي المشروط بعدم تجانس التباين مع تبديل الأنظمة الماركوفي (MRS-GARCH) لتوصيف التأخيرات الناجمة عن الشبكة، حيث يلتقط هذا النموذج ظاهرة تجمع التقلبات وعدم التناسق وتغير الأنظمة الملاحظة في بيانات شبكات IP الحقيقيةوهي خصائص تهملها النماذج التقليدية. أظهرت مقارنة تجريبية لثلاثة وثلاثين نموذجًا أن نموذج MRS-GARCH بالتوزيعات المختلطة هو الأمثل.

باستخدام هذا التوصيف للتأخيرات، تم اشتقاق شروط استقرار معتمدة على التأخير عبر دوال ليابونوفكراسوفسكي وصياغتها كمتباينات مصفوفية خطية (LMIs) ، مما يتيح حساب الحد الأقصى المسموح به للتأخير (MADB) الذي يضمن الاستقرار في متوسط المربعات. تم تطوير نموذج موجه للتحكم لأنظمة المستهلكين المنتجين للطاقة الكهروضوئية مع محولات ضثضث، وتم تركيب وحدات تحكم بالتغذية الراجعة للحالة باستخدام خوارزمية الاستكمال المخروطي (CCL) .

تظهر نتائج المحاكاة لنظام مكون من ثلاثة مستهلكين منتجين أن النهج المقترح يحقق حدودًا قصوى مسموح بها للتأخير أكبر بمقدار يصل إلى مرتبتين من حيث الحجم مقارنة بتصاميم LQR التقليدية، مع تحليل مفصل لكيفية تأثير احتمالات الانتقال ومعاملات التقلب على المتانة. يقدم هذا العمل حلاً صارمًا من الناحية النظرية وقابلًا للتطبيق العملي للتشغيل الموثوق لأنظمة الطاقة المتصلة بالشبكات من الجيل القادم.

الكلمات المفتاحيّة: الكلمات المفتاحية: أنظمة التحكم الشبكية، أنظمة الطاقة متعددة المصادر،

مستهلكو الطاقة الكهروضوئية، MRS-GARCH ، نمذجة التأخير الزمني، دالة Lyapunov-Krasovskii ، متباينات المصفوفة الخطية، الحد الأقصى المسموح به للتأخير، استقرار Lyapunov ، توليف وحدة التحكم.

List of Publications

Journal Publications

1) Aouati A, Gherbi S, Kharfouchi S. Networked control systems induced delay modeling and stability analysis using Markov-regime-switching GARCH model. Transactions of the Institute of Measurement and Control. 2024;48(2):323-336. doi:10.1177/01423312241284675

Conference Communications

1) Aouati, A., Gherbi, S., Bekaik, M. (2022). Networked Solar Photovoltaic Energy System Design and Stability Analysis [Annaba]. 5th International Conference on Embedded Systems in Telecommunications and Instrumentation. https://facsci.univ-annaba.dz/icesti/icesti22/

2) Gherbi S., Aouati A., Ramazan A., Sedraoui M. (2023). A Networked Multi-Source Energy System Modelling and Stability Analysis. Conférence Internationale sur les Energies Vertes et le Traitement des Eaux (EVE-2023). 2023;79:30-35. https://www.conf-event.com/EVE.html.

Table of Contents

Dedication **ii**

Acknowledgements **iii**

Abstract **iv**

List of Publications **ix**

Table of Contents **x**

List of Figures **xiv**

List of Tables **xv**

List of Abbreviations **xvii**

Preamble **1**

1 General Introduction 1
2 Motivation 2
3 Problematic in a nutshell overall 2
4 Objectives & Contributions 3
5 Thesis Outline 4

Chapter I: Overview of Networked Control Systems **8**

1 Introduction 8
2 Networked control systems components 9
3 Networked control systems structures 10
3.1 Configurations 10
3.2 Architectures 11
3.3 Topologies 11
4 Networked control systems Imperfections 11
4.1 Time Delays: 13

4.2 Packet Dropout: . . . 14
4.3 Quantization Errors: . . . 15
4.4 Variable Sampling/Transmission Intervals . . . 16
5 Network-Induced Delay Modeling . . . 17
5.1 Types of Induced Delays in NCSs . . . 17
5.1.1 Constant Stochastic Delay . . . 17
5.1.2 Constant Deterministic Delay . . . 18
5.1.3 Time-Varying Deterministic Delay . . . 18
5.1.4 Time-Varying Stochastic Delay . . . 18
5.2 Implications of Delay Modeling on NCS Performance . . . 19
5.3 Stochastic Modeling and Probabilistic Techniques . . . 19
5.3.1 Stochastic Control Models . . . 19
5.3.2 Probabilistic Approaches . . . 20
5.3.3 Empirical Modeling and Statistical Analysis . . . 20
6 Networked control systems stability analysis methods . . . 20
6.1 Basics: . . . 21
6.2 Lyapunov stability . . . 21
6.2.1 Lyapunov indirect approach . . . 22
6.2.2 Lyapunov direct approach . . . 23
6.2.3 Lyapunov-Krasovskii approach . . . 24
6.2.4 Constructing Lyapunov-Krasovskii functionals . . . 25
6.2.5 Linear Matrix Inequalities . . . 27
6.3 Mean-square stability . . . 28
7 Networked control systems control strategies . . . 29
7.1 Robust Control Strategies . . . 30
7.1.1 H-infinity (H_∞) Control . . . 30
7.1.2 Lyapunov-Based Stability Analysis . . . 31
7.2 Optimal Stochastic Control Strategies . . . 32
7.3 Resource-Aware Control Strategies . . . 33
7.3.1 Event-Triggered Control (ETC): . . . 33
7.3.2 Self-Triggered Control (STC): . . . 34
7.4 Predictive and Optimization-Based Strategies . . . 34
7.4.1 Model Predictive Control (MPC) . . . 34
8 Summary . . . 35

PART ONE: LITERATURE REVIEW **8**

Chapter II: Multi-sources Energy Systems **37**

1 Modeling the Photovoltaic Generator 38
1.1 Fundamental Principles and Characteristics 38
1.2 PV Modeling Techniques 39
1.3 Single-Diode Model: Mathematical Formulation 41
1.4 Parameter Scaling from Cell to Array 42
2 Power Electronics Interface 43
2.1 DC-DC Converter 44
2.2 The Push-Pull Converter Topology 44
2.3 Maximum Power Point Tracking (MPPT) 47
3 Modeling of a Photovoltaic System with DC Interface 48
4 State-space feedback controller design 51
5 Multi-sources Photovoltaic Energy System 53
6 Conclusion 55

Chapter III: Network-Induced Delay Modeling **58**

1 Introduction 58
2 GARCH-type models 61
3 GARCH-type modeling of communication delay in IP-based NCS . . . 64
3.1 Data description 64
3.2 Analysis and model selection 67
4 Conclusion 69

PART TWO: SCIENTIFIC CONTRIBUTIONS **58**

Chapter IV: NCS Stability Analysis **70**

1 Introduction 70
2 NCSs stability analysis based on MS-GARCH delay modeling 71
2.1 Control strategy 72
2.2 Main results 74
3 Numerical illustrations 78
3.1 Example 1. 78
3.2 Example 2. 81
4 Conclusion 82

Chapter V: Networked Multi-source Energy System Controller Design 84
1 Introduction 84
2 Controller Synthesis 86
3 Numerical Simulation 91
3.1 Results and Discussion 93
3.2 MADB results (Theorem 7 via CCL algorithm). 94
3.3 Feedback gain controller (Theorem 7 via CCL algorithm) 94
3.4 Comparison with the LQR method 94
4 Conclusion 95

Conclusion 96

References 101

List of Figures

1 Typical NCS structure 9

2 A Categorization of Control Strategies for Networked Control Systems. 30

3 Multi-sources energy system including three prosumers 38

4 I-V and P-V characteristics curves 39

5 Single-diode equivalent circuit model (1D2R) of a photovoltaic cell. . . 41

6 Operation modes of the push-pull conveter 46

7 Perturb and Observe (P&O) MPPT algorithm 49

8 PV system with push-pull DC-DC converter interface circuit model . . 50

9 PV system with push-pull DC-DC converter interface circuit model . . 52

10 State Variables Responses: (a) Prosumer 01, (b) Prosumer 02, (c) Prosumer 03 55

11 Communication delay in IP (CD-IP) 65

12 Histogram of the network delay shown in figure 11 66

13 States dynamics of Example 1 for $\tau_3 = 3.0677s$ 79

14 States dynamics of Example 2 for $\tau_3 = 3.6333s$ 81

List of Tables

2 NCS topologies 12

3 Classification of Network-Induced Delays in NCSs 18

4 Common DC-DC converter types used in PV applications 45

5 Comparison of MPPT Algorithm Categories 48

6 Specifications of Prosumers systems 54

7 Parameters of the circuit models. 54

8 State space of the prosumers systems. 54

9 Control response specifications. 54

10 Controller gains. 55

11 SETTING OF THE TOOL 65

12 Descriptive statistics of the data 66

13 Results of Engle's ARCH test 66

14 Alternative Garch models comparison 68

15 Parameters of MRS-Garch Model 79

16 Results of Example 01 79

17 Results of Example 2 case 1. 81

18 Results of Example 2 case 2. 81

19 Parameters of the circuit models. 92

20 State space of the prosumers systems. 92

21 Parameters of MRS-Garch Model 93

22 MADB τ_3 (ms) of the prosumers system. 93

23 Feedback gain controller K of the prosumers system. 93

24 Feedback gain controller K using lqr method of the prosumers system. 93

25 The prosumers system's MADB comparison methods. 93

List of Abbreviations

Abbreviation	**Full Form**
ADSL	Asymmetric Digital Subscriber Line
AIC	Akaike Information Criterion
ANFIS	Adaptive Neuro-Fuzzy Inference Systems
ANN	Artificial Neural Networks
ARCH	Autoregressive Conditional Heteroskedasticity
BFGS	Broyden-Fletcher-Goldfarb-Shanno (algorithm)
BIC	Bayesian Information Criterion
CAN	Controller Area Network
CCL	Cone Complementarity Linearization
CD-IP	Communication Delay in IP
CSI	Current-Source Inverters
CTHMM	Continuous-Time Hidden Markov Models
DBN	Dynamic Bayesian Networks
DC	Direct Current
DDM	Double-Diode Model
DER	Distributed Energy Resources
DES	Distributed Energy Systems
EGARCH	Exponential GARCH
EM	Expectation Maximization
ETC	Event-Triggered Control
FL	Fuzzy Logic
FLC	Fuzzy Logic Control
GARCH	Generalized Autoregressive Conditional Heteroskedasticity
GJR-GARCH	Glosten-Jagannathan-Runkle GARCH
HMM	Hidden Markov Models
IC	Incremental Conductance
ICMP	Internet Control Message Protocol
IP	Internet Protocol
ISP	Internet Service Provider
KCL	Kirchhoff's Current Law
KVL	Kirchhoff's Voltage Law
LKF	Lyapunov-Krasovskii Functional
LL	Log-likelihood
LMI	Linear Matrix Inequalities
LQG	Linear Quadratic Gaussian

Abbreviation	**Full Form**
LQR	Linear Quadratic Regulator
MADB	Maximum Allowable Delay Bound
MATI	Maximal Allowable Transmission Interval
MAUDB	Maximum Allowable Upper Delay Bound
MPC	Model Predictive Control
MPP	Maximum Power Point
MPPT	Maximum Power Point Tracking
MRS-GARCH	Markov Regime-Switching GARCH
NCS	Networked Control Systems
ODE	Ordinary Differential Equations
P&O	Perturb and Observe
PLL	Phase-Locked Loops
PPPoE	Point-to-Point Protocol over Ethernet
PSO	Particle Swarm Optimization
PV	Photovoltaic
QML	Quasi-Maximum Likelihood
QoS	Quality-of-Service
RFDE	Retarded Functional Differential Equation
RTT	Round-Trip Time
SDM	Single-Diode Model
STC	Self-Triggered Control / Standard Test Conditions
TDM	Triple-Diode Model
TDS	Time-Delay Systems
UAV	Unmanned Aerial Vehicle
VSI	Voltage-Source Inverters
ZOH	Zero-Order-Hold

Preamble

1 General Introduction

Electrical energy is one of the most versatile and essential forms of energy for modern human activities. Its significance permeates all sectors, to the extent that any disruption would critically impact contemporary development and civilization. Consequently, investments in electrical power generation have surged exponentially as governments and researchers strive to meet the growing global demand for energy [1, 2].

To address this challenge, there has been a strong trend towards multi-source and hybrid energy systems [1, 2, 3, 4, 5]. While these systems offer potential solutions for diversifying energy supply, they also introduce new complexities, including modeling, integration, stabilization, control, power management, as well as economic and policy considerations. Furthermore, the cost of implementing such energy systems is substantial, often requiring significant state-level investments.

In response to these challenges, one innovative solution lies in fostering collaboration and sharing of energy among users who act both as consumers and producers—often referred to as "prosumers." This approach opens the door to more efficient management and distribution of surplus energy, helping to alleviate the financial and technical burdens associated with multi-source energy systems [6].

A key enabler of this vision is the Networked Control System (NCS), which provides the framework for distributed energy systems. NCS facilitates the necessary coordination, control, and management tasks across interconnected nodes to ensure the reliable operation of such systems [7, 8, 9].

Building on this premise, the focus of this thesis is the control of multi-source energy systems over a network, with an emphasis on system design and stability analysis [10].

2 Motivation

The motivation for this research arises from several interconnected observations. First, the increasing penetration of distributed energy resources demands sophisticated control architectures capable of coordinating multiple prosumers while ensuring grid stability [1, 2, 4, 5, 9, 11, 12, 13]. Second, the practical implementation of such coordinated control inevitably relies on communication networks, which introduce uncertainties that conventional control theories, developed under ideal assumptions of perfect communication, are ill-equipped to handle [7, 8, 14, 15, 16].

A particularly compelling motivation stems from the nature of network-induced delays themselves. Empirical evidence reveals that communication delays in IP-based networks exhibit complex statistical properties—volatility clustering, asymmetry, heavy-tailed distributions, and structural breaks—that conventional delay models (constant, uniformly distributed, or simple Bernoulli processes) fail to capture [10, 17, 18, 19]. This disconnect between the simplified models commonly employed in NCS literature and the reality of network behavior represents a significant gap that undermines the practical applicability of existing stability analyses and controller designs [7, 14, 17, 18].

Furthermore, the specific context of photovoltaic prosumer systems introduces additional complexitie [11]. PV generation is inherently variable and weather-dependent, requiring maximum power point tracking (MPPT) and precise voltage regulation [20, 21, 22]. When such systems are controlled over networks subject to random delays, the interaction between the stochastic network dynamics and the nonlinear system dynamics creates challenges that demand rigorous mathematical treatment [17, 18, 23, 24].

3 Problematic in a nutshell overall

The central problematic addressed in this thesis is to bridge the gap between the sophisticated requirements of multi-source energy systems and the harsh realities of the communication networks that connect them. This challenge necessitates a rigorous control-theoretic approach that explicitly accounts for the imperfections of the digital medium [7, 8, 14, 17, 18, 25]. The core of this investigation is articulated through the following refined research question:

"How can we develop a comprehensive modeling framework and design stabilizing controllers for multi-source energy systems that are distributed across a communication network, subject to realistic stochastic delay constraints, while providing formal guarantees for both system stability and robust performance?"

By resolving this problematic, this thesis aims to provide a foundational framework for the reliable and high-performance operation of the next generation of collaborative, networked energy systems [1, 6, 9].

4 Objectives & Contributions

The primary objective of this thesis is to develop a comprehensive modeling and control framework for networked multi-sources energy systems that ensures stability, robustness, and performance under communication constraints.

The main contributions of this thesis can be summarized as follows:

- **A novel stochastic modeling framework** for *network-induced delays* based on *Markov Regime-Switching GARCH* (MRS-GARCH) processes [10]. Through empirical analysis of real IP communication delay data, it is demonstrated that this framework captures volatility clustering, regime-dependent behavior, and heavy-tailed distributions with superior accuracy compared to thirty-three competing models, including GARCH, EGARCH, and GJR-GARCH specifications.
- **A control-oriented modeling approach** for photovoltaic prosumer systems, progressing from fundamental PV cell physics through single-diode equivalent circuits to linearized state-space representations of push-pull DC-DC converter interfaces. The models incorporate integral action for zero steady-state error and are validated for three distinct prosumer configurations.
- **Delay-dependent stability conditions** that explicitly incorporate the stochastic and regime-switching nature of communication delays. By partitioning the delay interval into two regimes corresponding to different network congestion states and introducing a mode-dependent feedback control law, less conservative stability criteria are derived using Lyapunov-Krasovskii functionals and expressed as LMIs.
- **A systematic controller synthesis methodology** that simultaneously

computes stabilizing feedback gains and Maximum Allowable Delay Bounds (MADBs) for networked multi-prosumer systems. The Cone Complementarity Linearization (CCL) algorithm is employed to address the non-convex optimization problem arising from the stability conditions.

- **Comprehensive numerical validation** demonstrating that the proposed approach achieves MADBs up to two orders of magnitude larger than conventional LQR-based designs, with detailed analysis of how MRS-GARCH model parameters—particularly transition probabilities and volatility coefficients—influence system robustness.

Collectively, these contributions advance the state-of-the-art in networked control of energy systems by providing theoretically rigorous and practically implementable solutions.

5 Thesis Outline

This thesis is organized into two principal parts, comprising five chapters, followed by a general conclusion.

Part One: Literature Review establishes the theoretical foundations essential for the subsequent contributions.

- ***Chapter I: Overview of Networked Control Systems*** provides a comprehensive introduction to Networked Control Systems (NCSs). It examines their fundamental components (sensors, controllers, actuators, and communication networks), architectural configurations (centralized, decentralized, and distributed), network topologies, network-induced imperfections, stability analysis methods, and control strategies. Particular attention is devoted to modeling network-induced delays and their impact on system performance. The chapter culminates in a detailed exposition of Lyapunov stability theory, Lyapunov–Krasovskii functionals for time-delay systems, and Linear Matrix Inequality (LMI) formulations, which constitute the analytical backbone of this thesis.
- ***Chapter II: Multi-Sources Energy Systems*** transitions from theory to application, focusing on the physical plant to be controlled: photovoltaic prosumer systems. Beginning with the fundamental physics of PV cells and

the single-diode equivalent circuit model, the chapter develops control-oriented models scaled from individual cells to arrays. The power electronics interface, specifically the push-pull DC-DC converter, is analyzed, and maximum power point tracking (MPPT) strategies are reviewed. Linearized state-space models with integral action are derived for three distinct prosumer configurations, and state-feedback controllers are designed using pole placement techniques.

Part Two: Scientific Contributions presents the original research contributions of this thesis.

- ***Chapter III: Network-Induced Delay Modeling*** introduces a novel framework for characterizing communication delays using GARCH-type econometric models. The theoretical foundations of GARCH, EGARCH, GJR-GARCH, and Markov Regime-Switching GARCH models are presented, along with their maximum likelihood estimation procedures. Through empirical analysis of real IP communication delay data collected from an Algerian ADSL network, a comprehensive comparison of thirty-three competing models is conducted. The MRS-GARCH model with mixed conditional distributions (normal for the first regime, Student-t for the second) is identified as the optimal specification, capturing volatility clustering, asymmetry, and regime-switching behavior with superior fit according to log-likelihood, AIC, and BIC criteria.
- ***Chapter IV: Stability Analysis*** leverages the MRS-GARCH delay model to derive less conservative stability conditions for NCSs. By partitioning the delay interval into two regimes and introducing a mode-dependent feedback control law, delay-dependent stability criteria are established using a tailored Lyapunov-Krasovskii functional. These conditions are cast as LMIs, enabling computation of Maximum Allowable Delay Bounds MADBs that guarantee mean-square asymptotic stability. Numerical examples demonstrate that the proposed approach yields larger MADBs compared to conventional Bernoulli-distributed delay models, with detailed analysis of how transition probabilities and volatility coefficients influence system robustness.
- ***Chapter V: Control Strategy*** integrates all preceding developments into a unified controller synthesis framework for networked multi-prosumer energy systems. Using the Cone Complementarity Linearization algorithm to address non-convex optimization, stabilizing state-feedback controllers are synthesized for

a system of three photovoltaic prosumers operating under different MRS-GARCH delay scenarios. The results demonstrate substantial improvements in delay tolerance compared to conventional LQR-based designs, with MADB enhancements of up to two orders of magnitude. Comparative analyses reveal the critical influence of regime transition probabilities and the advantages of the proposed regime-switching control law.

Conclusion synthesizes the principal contributions of this thesis, discusses their implications for the design of networked multi-source energy systems, and outlines promising directions for future research, including extension to additional network imperfections, development of event-triggered strategies, experimental validation on hardware-in-the-loop testbeds, and integration of machine learning techniques for adaptive control in dynamic network environments.

PART ONE: LITERATURE REVIEW

Chapter I: Overview of Networked Control Systems

Chapter II: Multi-sources Energy Systems

Chapter I: Overview of Networked Control Systems

Networked control systems (NCSs) are a novel class of control systems that have been witnessed as a result of the actual increased usage and exponential development of communication network technologies. The evolution of networked control systems (NCS) in energy systems represents a significant shift in how energy generation, distribution, and consumption are managed. As energy systems have become more complex and decentralized, the role of network technologies in control systems has expanded, enabling greater efficiency, reliability, and sustainability. In this chapter, an overview of Networked Control Systems (NCSs) is presented. First, we provide a general introduction to NCSs, followed by an examination of their key components. Next, we explore various structures and architectures of NCSs. Afterward, we address system imperfections and constraints that arise in NCSs. Furthermore, different methods for modeling NCSs will be discussed. Finally, several control strategies employed in NCSs are reviewed.

1 Introduction

A networked control system (NCS) consists of control loops connected through communication networks, in which both the control signal and the feedback signal are exchanged between the system/plant and the controller. Figure 1 illustrates a typical representation of NCS structure.

The study of Networked Control Systems (NCSs) is a highly interdisciplinary field that integrates networking technologies with control theory. Research in NCSs is typically divided into two key areas: ***control of network*** and ***control over network***. Our research focuses specifically on the latter, examining the challenges and solutions related to controlling dynamic systems via networked communication.

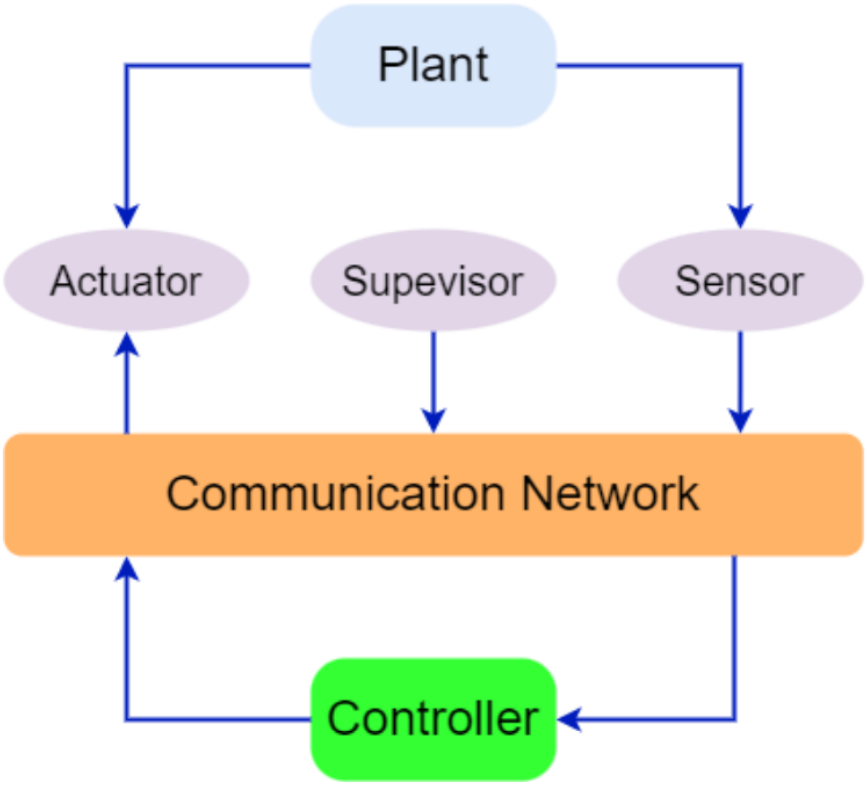

Figure 1: Typical NCS structure

2 Networked control systems components

Networked Control Systems (NCS) are composed of several main components that work together to facilitate the control and monitoring of systems through communication networks. These components include:

- ***Sensors:*** are devices that detect, measure, and respond to physical quantities from the environment, such as temperature, pressure, flow, light, motion, or sound. Their primary function is to provide accurate data that enables automated systems to make informed decisions, facilitating real-time monitoring of process states. This data is then transmitted over the *network* to a *controller* for further processing and decision-making.
- ***Controllers:*** serve as the *"brains"* of a control system. These devices or software modules process input data, typically received from *sensors*, and make decisions by generating output signals that guide the **actuators**. They operate based on predefined algorithms or control laws, ensuring the system responds appropriately to achieve desired set-points or performance levels. Controllers are

a crucial element in maintaining system stability, optimizing performance, and addressing essential control objectives such as regulation, robustness, reliability, coordination, and continuous monitoring.

- ***Actuators:*** are devices or components that perform the physical actions required to control a system, based on signals—often electrical, pneumatic, or hydraulic—received from the *controller* via a *communication network*. They generate either linear or rotary motion, enabling the system to achieve desired outcomes by directly influencing its physical elements, such as valves, motors, solenoids, or other mechanical parts.
- ***Communication Network:*** is a structured system that facilitates the exchange of information, including control and feedback signals, among interconnected nodes or devices, enabling interaction and collaboration. It serves as the "backbone" of a Networked Control System (NCS). These networks can be either wired (e.g., Ethernet, fiber optics, Fieldbuses) or wireless (e.g., Wi-Fi, Bluetooth, cellular), and they operate using a variety of protocols (e.g., TCP/IP, FTTH, LTE) tailored to specific communication needs. While communication networks provide significant advantages in control systems, NCSs also inherit limitations, imperfections, and constraints from these networks, as reviewed in Section 4. The choice of structure and configuration in an NCS should be guided by the specific requirements of the application, such as performance, reliability, scalability, and environmental conditions. Balancing these factors is essential to optimizing the system's overall effectiveness. The various geometric designs of NCSs will be discussed in the next section.

3 Networked control systems structures

NCS structures refer to the arrangement, interaction, and coordination of system components to achieve desired control objectives. These structures play a crucial role in determining the system's performance, reliability, scalability, and adaptability to dynamic environments. NCS structures are typically categorized into three key aspects: configuration, architecture, and topology.

3.1 Configurations

NCS configuration is about the physical and logical setup of the components within a specific operational environment. It defines how the system is organized to function

as an integrated whole [26].

- ***Centralized configuration:*** In this setup, all control decisions and data processing occur at a single central node or controller.
- ***Decentralized configuration:*** In this configuration, multiple independent controllers are used. Each one operates autonomously and is responsible for controlling its subset of sensors and actuators.
- ***Distributed configuration:*** here, multiple controllers work collaboratively by sharing local information to ensure overall system performance.

3.2 Architectures

NCS architecture defines the system's overall structural design, focusing on logical organization, layers, and control flow.

- ***Direct Structure:*** In this architecture, the control loop is closed directly through the network without intermediate layers. This structure is typically used in systems where fast response times are critical and simplicity is preferred.
- ***Hierarchical Structure:*** Here, the control process is organized into multiple levels and layers, with higher-level controllers managing lower-level ones. This architecture is suited for large, complex systems that need to be modular, scalable, and robust. It is commonly used in industrial automation, smart grids, and distributed control applications where coordination across multiple subsystems is essential.

3.3 Topologies

NCS topology is the specific network's layout, defining the communication patterns and connections between nodes (sensors, actuators, controllers) in the system. Table 2 presents the various NCS topologies describing their characteristics.

4 Networked control systems Imperfections

The integration of network technology into control theory has significantly improved operational efficiency, reliability, and flexibility in controlling and managing real-world applications. However, it also introduces considerable challenges in the design and implementation of NCSs, as it carries various imperfections and constraints collectively referred to as network-induced phenomena.

Table 2: NCS topologies

Topology	Components interconnection	Components communication	Size	Complexity	Cost	Robustness
Star	All nodes are connected to a central controller (hub).	Nodes's Data are transmitted to the hub and vice versa.	Small to Medium	Low	Moderate	Low to Medium
Bus	Nodes are connected along a single communication line or bus.	Multiple devices share a single bus, so they must wait their turn to transmit data.	Small to Medium	Low	Low	Low
Ring	Nodes are connected in a circular fashion.	Data circulates in a single direction (or sometimes in both directions in a dual-ring system) until it reaches the target node.	Medium	Moderate	Medium	Medium to High
Mesh	Every node is connected to each other nodes.	Data can take different routes to reach its destination.	Large	High	High	Very High
Tree	Devices are arranged in hierarchical levels.	Lower-level controllers report to higher-level controllers, which coordinate system-wide actions.	Medium to Large	Medium	Medium	Medium
Hybrid	combine elements of two or more topologies.	Combines the strengths of different topologies and inherits their characteristics.	Large, Complex	Very High	High	Very High

4.1 Time Delays:

There are several sources of time delays in networked systems. These delays depend on system components (nodes) and network characteristics such as network traffic, the protocol used, and data bandwidth limitations. Two main types of delays can be distinguished:

- *Computational delays:* These occur within system components, including sensors $\tau_s(t_k)$, controllers $\tau_c(t_k)$, and actuators $\tau_a(t_k)$, due to operations complexity, a limited processing speed or capacity of the hardware.
- *Network-induced delays:* These resulted in network access and data transmission, specifically from the sensor to the controller $\tau_{sc}(t_k)$ and from the controller to the actuator $\tau_{ca}(t_k)$ nodes.

Therefore, the overall delay from sensing to actuator output in an NCS can be described as follows:

$$\tau(t_k) = \tau_s(t_k) + \tau_{sc}(t_k) + \tau_c(t_k) + \tau_{ca}(t_k) + \tau_a(t_k)$$

where $\tau(t_k)$ is the total sensing to actuation delay for sampling time t_k.

Computational delays can be constrained through the application of established real-time system techniques. These delays are typically small and may be negligible. In contrast, communication delays have a significant impact on the system and tend to be random and asymmetric in nature[27, 28].

The characteristics of the delays in NCSs can be summarized and categorized into three pairs [25]:

1. *constant* versus *time-varying* delay.
2. *deterministic* versus *stochastic* delays.
3. *small* or *large* delays (based on a prescribed sampling period).

Building on the above specifications, the subsequent section examines a range of modeling techniques for networked control systems (NCSs) that take into consideration delays induced by the network.

4.2 Packet Dropout:

When data needs to be transmitted over a network, it is divided into smaller, manageable units called packets. Each packet contains not only a portion of the data but also a header with essential routing information, allowing it to be sent independently through the network. This method of transmission is known as packet switching. Upon reaching their destination, the packets are reassembled to reconstruct the original data. A packet is indeed the smallest unit of data carried by a communication network. During the packet switching process, packet loss can occur, commonly referred to as *packet dropouts*. These losses typically result from *transmission errors* in physical network links or *buffer overflows* due to network congestion.

In general, the literature identifies three primary strategies for dealing with packet dropouts in Networked Control Systems (NCSs) [29, 30].

- *Zero-Input Strategy:* In this approach, the actuator input to the plant is set to zero, which effectively stops any action when data is missing,
- *Hold-Input Strategy:* Here, if a packet is lost, the actuator uses the most recent control input stored in its buffer.
- *Predictive Control Strategy:* This strategy employs predictive control as input, allowing the system to anticipate future control actions based on previous data.

Various control techniques have been proposed for modeling Networked Control Systems (NCSs) experiencing data packet dropouts. These techniques can be broadly categorized into two types of modeling[31]:

- *Switch-based modeling:* Packet dropouts are represented as a switch mechanism, where "off" denotes a dropout and "on" indicates a successful transmission. The switching behavior is typically modeled using a Bernoulli process or a two-state Markov chain, often employing either the zero-input or hold-input strategies.
- *Delay-based modeling:* Packet dropouts are treated as prolongations of communication delays, generally relying on the hold-input strategy. A delay-dependent approach is then used to determine the maximum allowable number of successive packet dropouts.

4.3 Quantization Errors:

The quantizer or quantization process can be described as the mapping of a real-valued function into a piecewise constant function *i.e.*, RßZ, taking on a finite set of values. This quantization is necessary for digital transmission and processing, but it introduces errors that can lead to degraded system performance, instability, and increased control effort.

Quantization error is often modeled as the difference between the continuous signal and its quantized counterpart. If x is the continuous signal and $q(x)$ is the quantized value, the error e_q is defined as:

$$e_q = x - q(x)$$

In the literature, there are two common types of quantization which are: logarithmic quantization and uniform quantization[32].

- *The uniform quantizer:* maps the real-valued function to a finite number of quantization regions with rectangular [33] or arbitrary shapes[34]. The uniform quantizers with an arbitrarily shaped quantitative area have some following conditions: 1) if $\|y\|_2 \leq M\mu$, then $\|q(y) - y\|_2 \leq \Delta\mu$ 2) if $\|y\|_2 > M\mu$, then $\|q(y)\|_2 > M\mu - \Delta\mu$ where M is the saturation value and Δ is the sensitivity. The first condition gives the upper bound of the quantization error when the quantization is not saturated. The second condition provides an approach to test whether the quantization is saturated. Furthermore, the quantitative area can be represented as a rectangle, formulated as:

$$q(y) = \begin{cases} 0, \text{ if } -\frac{1}{2} < y < \frac{1}{2} \\ i, \text{ if } \frac{2i-1}{2} < y < \frac{2i+1}{2}, \quad i = 1, 2, \cdots, K-1 \\ K, \text{ if } y \geq \frac{2K-1}{2} \\ -q(-y), \text{ if } y \leq -\frac{1}{2}. \end{cases}$$

  The study of system affected by the uniform quantizer is usually based on *"zoom" strategy*, which is composed of two stages, i.e., "zooming-out" and "zooming-in." In the first stage, the range of quantizer is increased to guarantee the states of system can be adequately measured. In the second stage, the quantization error is decreased to drive the states to the origin.

- *Logarithmic quantizer:* When the system is affected by the logarithmic quantizer, in which the quantization levels are linear in logarithmic scale, a simple classical approach to the analysis and mitigation of the quantization effects is to treat the quantization error as *uncertainty* or *nonlinearity* and bound it using a sector bound[35]. The logarithmic quantizer is a kind of static quantizer. It is formulated as

$$q(y) = \begin{cases} v_i, \text{ if } \frac{v_i}{1+\delta} < y < \frac{v_i}{1-\delta}, y > 0 \\ 0, \text{ if } y = 0 \\ -q(-y), \text{ if } y < 0 \end{cases}$$

  where $U = \{\pm v_i : v_i = \rho^i v_0, i = \pm 1, \pm 2, \cdots\} \cup \{\pm v_0\} \cup \{0\}, 0 < \rho < 1, v_0 > 0$ is the set of the quantization values. This quantizer is of infinite quantization level. A quantizer with a limited quantitative level is

$$q(y) = \begin{cases} v_i, \text{ if } \frac{v_i}{1+\delta} < y < \frac{v_i}{1-\delta}, 0 < i \leq N-1 \\ 0, \text{ if } 0 \leq y \leq \frac{v_{N-1}}{1+\delta} \\ v_0, \text{ if } y > \frac{v_0}{1+\delta} \\ -q(-y), \text{ if } y < 0 \end{cases}$$

  where $U = \{\pm v_i : v_i = \rho^i v_0, i = \pm 1, \pm 2, \cdots, \pm(N-1)\} \cup \{\pm v_0\} \cup \{0\}, 0 < \rho < 1, v_0 > 0$ is the set of the quantization values.

4.4 Variable Sampling/Transmission Intervals

To transmit a continuous-time signal over a network, the signal must be sampled, encoded in a digital format, packaged into packets, transmitted over the network, and finally, the data must be decoded at the receiver side. This process differs significantly from traditional periodic sampling in conventional systems, where the sampling periods are typically fixed due to the simplicity of their design, analysis, and implementation. However, in modern Networked Control Systems (NCSs), it may vary due to network delays and congestion since the output signal is waiting in a queue before the transmission based on network availability and the communication protocol used. This variability introduces complexities in the design and analysis of control systems. In NCSs, sampling/triggering mechanisms can be classified into three main types[36]:

- *Time-triggered sampling:* the signal is sampled at a sequence of fixed time instants (e.g., periodic sampling).
- *Event-triggered sampling:* the signal is sampled only when a certain condition is satisfied, where sampling is implemented based on the detection of the predefined "event".
- *Self-triggered sampling:* the signal is sampled based on predictions, where sampling is implemented according to the prediction for the occurrence of the "event" based on the system model and the current measurement (i.e., the "event" is produced by the prediction).

Several approaches are available to model sampled/transmission intervals in NCSs[37]. Among these, the *input delay approach* is one of the most widely used due to its compatibility with Linear Matrix Inequality (LMI) techniques, making it particularly effective for analysis and controller design. Applying this approach helps to determine the *Maximal Allowable Transmission Interval* (MATI) which is the maximum time interval allowed between successive transmissions without compromising system stability.

5 Network-Induced Delay Modeling

5.1 Types of Induced Delays in NCSs

Communication delays in NCSs can be broadly categorized into four types, each with distinct characteristics and implications for the design of control systems. These categories are summarized in Table 1 and depicted in Figure 1.

5.1.1 Constant Stochastic Delay

Constant stochastic delays are characterized by their random nature but with a constant statistical distribution over time. These delays are often modeled using probabilistic methods, such as Hidden Markov Models (HMM) and Continuous-Time Hidden Markov Models (CTHMM). For instance, Vargas-Rodriguez and Morales-Menéndez (2007) proposed models for estimating network load and predicting future delay values in CAN-based NCSs using HMMs. Similarly, Ge et al. (2009) employed CTHMMs to characterize network-induced delays as stochastic continuous variables, using the Expectation Maximization (EM) algorithm to learn model parameters.

Table 3: Classification of Network-Induced Delays in NCSs

Type of networked delays	Characteristics	Modeling Techniques	Compensation Strategies
Constant Stochastic Delay	Random delays with a constant statistical distribution over time.	Hidden Markov Models (HMM), Continuous-Time HMM (CTHMM), Expectation Maximization (EM).	Probabilistic control strategies, adaptive delay compensation.
Constant Deterministic Delay	Fixed and predictable delays.	Smith predictor, fixed-structure controllers.	Dead-time compensation, predictive control.
Time-Varying Deterministic Delay	Delays that change over time but follow a predictable pattern.	Lyapunov-based methods, adaptive control strategies.	Real-time delay measurement, adaptive control.
Time-Varying Stochastic Delay	Delays that change over time and are random.	Dynamic Bayesian Networks (DBN), Lyapunov-Krasovskii functionals (LKF).	Stochastic control algorithms, robust control strategies.

5.1.2 Constant Deterministic Delay

Constant deterministic delays are fixed and predictable, making them easier to manage in control systems. Techniques such as the Smith predictor are commonly used to compensate for these delays. Kim and Moon (2016) demonstrated the effectiveness of adaptive delay compensation processes in NCSs, highlighting how fixed-structure controllers can stabilize systems with known delay characteristics.

5.1.3 Time-Varying Deterministic Delay

Time-varying deterministic delays change over time but follow a predictable pattern. These delays can be measured in real-time by calculating the time difference between sending and receiving control packets. Adaptive control strategies, such as those proposed by Tang et al. (2015), are often employed to account for these varying delays. Their augmented model for NCSs with time-varying delays ensures closed-loop stability using the Lyapunov method.

5.1.4 Time-Varying Stochastic Delay

Time-varying stochastic delays are the most complex to handle, as they combine variability with randomness. These delays are often modeled using Dynamic Bayesian Networks (DBN) and Lyapunov-Krasovskii functionals (LKF). Rouamel et al. (2020)

proposed robust stability and stabilization techniques for NCSs with stochastic time-varying delays, demonstrating the effectiveness of these methods in handling unpredictable network conditions.

5.2 Implications of Delay Modeling on NCS Performance

The stochastic nature of communication delays in NCSs has profound implications for system performance. In this section, we explore the key characteristics of these delays and their impact on NCS stability, robustness, and control quality.

5.3 Stochastic Modeling and Probabilistic Techniques

Stochastic modeling and probabilistic techniques have become indispensable tools to analyze and compensate for communication delays in NCS. Below, we discuss some of the most widely used approaches:

5.3.1 Stochastic Control Models

Stochastic control models are pivotal for addressing the inherent randomness in networked control systems (NCSs), particularly in capturing network-induced delays, packet dropouts, and channel uncertainties. These models enable the derivation of stability criteria and the synthesis of robust controllers that account for probabilistic disturbances. For instance, Zhang et al. (2021) advanced a delay-distribution-dependent stochastic control framework, integrating time-varying delays with non-uniform probability distributions into Lyapunov-Krasovskii functionals, thereby reducing conservatism in stability analysis. Their work demonstrated that leveraging delay distribution data improves controller performance by 30% compared to deterministic models. Recent studies have also emphasized event-triggered stochastic control to mitigate network resource constraints. Li & Chen (2022) proposed a co-design methodology combining model predictive control (MPC) with stochastic event triggers, ensuring stability under bounded delays while minimizing communication overhead. This approach aligns with the Linear Quadratic Gaussian (LQG) paradigm, as shown by Gupta et al. (2023), who optimized LQG controllers under delay-dependent costly information, achieving sub-0.1% performance degradation in industrial NCSs.

5.3.2 Probabilistic Approaches

Probabilistic methods, such as Bernoulli processes and semi-Markov chains, are foundational for modeling the stochastic dynamics of NCSs. These approaches provide necessary and sufficient conditions for stability and stabilization under random delays and packet losses. Wang et al. (2023) introduced a mode-dependent Lyapunov function for Markovian jump systems, enabling stability analysis for NCSs with time-varying transition probabilities. Their framework achieved a 15% reduction in conservatism compared to traditional Lyapunov methods. Moreover, Liu et al. (2022) developed a probabilistic robustness index to quantify the resilience of NCSs under stochastic disturbances. By integrating constrained offline synthesis with real-time adaptive control, their method guaranteed stability even for delays exceeding 80% of the sampling interval. Similarly, Khan et al. (2023) employed chance-constrained optimization to balance robustness and performance, demonstrating superior results in UAV swarm coordination under packet loss rates of up to 25%.

5.3.3 Empirical Modeling and Statistical Analysis

Empirical modeling bridges theoretical frameworks with real-world NCS behavior by incorporating statistical characteristics of network-induced delays. Zhou et al. (2023) utilized multifractal analysis to model delays in industrial IoT networks, revealing heavy-tailed distributions that defy conventional Poisson assumptions. Their empirical model improved delay prediction accuracy by 40%, enabling tighter stability bounds. Statistical techniques such as the Lyapunov-Krasovskii functional (LKF) method remain central to stability analysis. Deng et al. (2023) extended the LKF approach with delay-product terms, deriving less conservative stability criteria for NCSs with stochastic sampling intervals. Their experiments on smart grid systems validated a 20% increase in allowable delay bounds. Complementing this, Park & Kim (2023) applied copula theory to model correlated delays in wireless NCSs, demonstrating that ignoring delay correlations inflates instability risks by 35%.

6 Networked control systems stability analysis methods

Stability refers to the system's behavior in response to disturbances or changes in its initial conditions. There are several methods to analyze the stability of dynamic systems, depending on whether the system is linear or nonlinear, time-invariant or time-varying, and deterministic or stochastic. Our focus in this study is on the

most common methods that are important in analyzing and designing nonlinear and stochastic systems.

6.1 Basics:

The state space model of Nonlinear systems is of the following form:

$$\begin{cases} \dot{x}(t) = f[x(t), u(t), t] \\ y(t) = g[x(t), u(t), t] \end{cases} \tag{1}$$

Where $x \in \mathbf{R}^n$, $u \in \mathbf{R}^m$.

Definition 1 *The system (1) is said to be* ***autonomous*** *if the function f does not depend explicitly on t; ie,.*

$$\begin{cases} \dot{x}(t) = f[x(t), u(t)] \\ y(t) = g[x(t), u(t)] \end{cases} \tag{2}$$

Otherwise, it is ***non-autonomous****.*

Definition 2 *The state $x_e = 0$ is said to be an* ***Equilibrium point*** *of the system (1) at time t_0 if;*

$$f[x_e, t] = 0, \quad \forall t \geq t_0$$

Definition 3 *a continuous scalar function $V(x)$ is said to be,*

1. *positive definite function: $V(x) > 0 \quad for \quad x \neq 0, V(0) = 0.$*
2. *negative definite function: $V(x) < 0 \quad for \quad x \neq 0, V(0) = 0.$*
3. *positive semi-definite function: $V(x) \geq 0 \quad for \quad x \neq 0.$*
4. *negative semi-definite function: $V(x) \leq 0 \quad for \quad x \neq 0.$*
5. *locally: $V(x)$ is defined in a ball $B_r > 0$.*
6. *globally: $V(x)$ is defined in a whole state space $B_r = \mathrm{R}^n - \{0\}$*

6.2 Lyapunov stability

The intuitive notion of stability is introduced as a form of well-behavedness around a desired operating point. The most useful and general approach for studying the stability of nonlinear control systems is the theory developed in the late 19th century by the Russian mathematician Alexandr Mikhailovich Lyapunov. Today, Lyapunov stability theory consists of two main approaches: the *indirect approach* and the *direct approach.*

Definition 4 *The vector x_e is said to be an equilibrium point of the system (1) if,*
$\dot{x}_e = f(x_e, u(t) = 0, t) = 0, \quad \forall t$
This means that at x_e the system's states do not change over time, i.e., $\dot{x} = 0$.

Definition 5 *The equilibrium state $x_e = 0$ is,*

(i) ***Lyapunov stable*** *if, for every $\epsilon > 0$ there exist a $\delta_1 = \delta(t_0, \epsilon) > 0$ such that if $\|x(0) - x_e\| < \delta_1$ then for every $t \geq 0$ we have $\|x(t) - x_e\| < \epsilon$.*

(ii) ***Asymptotically stable*** *if, it is Lyapunov stable and there exist a $\delta_2 = \delta(t_0) > 0$ such that if $\|x(0) - x_e\| < \delta_2$ then for every $t \geq 0$ we have $\lim_{t\to\infty} \|x(t) - x_e\| = 0$.*

(iii) ***Exponentially stable*** *if, it is asymptotically stable and there exist constants $\alpha > 0, \beta > 0, \delta_3 > 0$ such that if $\|x(0) - x_e\| < \delta_3$ then $\|x(t) - x_e\| \leq \alpha\|x(0) - x_e\|e^{-\beta t}$ for all $t \geq 0$.*

(iv) ***Uniformly stable: (or uniformly asymptotically stable)*** *If δ_1 in (i) (or δ_2 in (ii)) can be chosen independently of t_0.*

(v) ***globally asymptotically stable: (or globally exponentially stable)*** *If δ_2 in (ii) (or δ_3 in (iii)) can be an arbitrarily large finite number as desired.*

Remark 1 *The system is stable (in the sense of Lyapunov), if its trivial solution (the equilibrium state $x_e = 0$ of the system) is stable.*

6.2.1 Lyapunov indirect approach

The *indirect approach* is an approximation method based on the linearization of the nonlinear system around the Equilibrium points.

Theorem 1 ***(Lyapunov's linearization method)***

- *If the linearized system is* ***strictly stable*** *(i.e, if all eigenvalues of* $\mathbf{A}$ *are strictly in the left-half complex plane), then the equilibrium point is* ***asymptotically stable*** *(for the actual nonlinear system).*
- *If the linearized system is* ***unstable*** *(i.e, if at least one eigenvalue of* $\mathbf{A}$ *is strictly in the right-half complex plane), then the equilibrium point is* ***unstable*** *(for the nonlinear system).*
- *If the linearized system is* ***marginally stable*** *(i.e, all eigenvalues of A are in the left-half complex plane, but at least one of them is on the jw axis), then one*

cannot conclude anything from the linear approximation (the equilibrium point may be stable, asymptotically stable, or unstable for the nonlinear system).

6.2.2 Lyapunov direct approach

This method employs energy-like *Lyapunov functions* to determine stability without requiring linearization.

A *Lyapunov function* is a scalar function used in control theory and dynamical systems to establish the stability of an equilibrium point.

Definition 6 *A Lyapunov function $V(x)$ is a continuously differentiable scalar function defined in a region D around x_e that satisfies:*

(i) $V(x_e) = 0$,

(ii) $V(x) > 0$ *for all* $x \in D \backslash \{x_e\}$,

(iii) $\dot{V}(x) \leq 0$ *for all* $x \in D$,

where $\dot{V}(x)$ is the time derivative of $V(x)$ along the system trajectories:

$$\dot{V}(x) = \nabla V(x) \cdot f(x)$$

The relationship between Lyapunov functions and the stability of dynamical systems is rigorously established through a series of theorems in *Lyapunov's direct method*. These theorems typically come in two forms: *local* and *global*, depending on the region of interest in the state space. The following theorem encapsulates both versions and captures the key aspects of Lyapunov's direct method:

Theorem 2 *If, in a ball $\mathbf{B}_r$, there exists a scalar function $V(x)$ with continuous first partial derivatives such that,*

(i) $V(x)$ *is positive definite.*

(ii) $\dot{V}(x)$ *is negative semi-definite.*

(iii) $\dot{V}(x)$ *is negative definite.*

(iv) a ball $\mathbf{B}_r$ is a whole state space.

(v) $V(x)$ *is radially unbounded, ie.* $V(x) \to \infty$ *as* $\|x\| \to \infty$.

(vi) There exist constants $c_i > 0$ *and* $p \geq 1$ *such that:*

$$c_1\|x\|^p \leq V(x) \leq c_2\|x\|^p$$
$$\dot{V}(x) \leq -c_3\|x\|^p$$

then the equilibrium point x_e *, in the sense of Lyapunov, is,*

- ***Stable:*** *(locally) if conditions* (i) *and* (ii) *are satisfied.*
- ***Asymptotically stable:*** *(locally) if conditions* (i) *and* (iii) *are satisfied.*
- ***Globally asymptotically stable:*** *if conditions* $(i), (iii), (iv)$*, and* (v) *are satisfied.*
- ***Exponentially stable:*** *(locally) if conditions* (vi) *are satisfied.*
- ***Globally exponentially stable:*** *If the conditions for exponential stability hold for all* $x \in \mathbb{R}^n$*.*

6.2.3 Lyapunov-Krasovskii approach

The classical Lyapunov approach does not work for time-delayed systems. Some modifications are made on it to apply stability analysis on time-delay systems, which appear in two mean methods [38, 39]: *Layapunov-Krasovskii approach* and *Lyapunov-Razumikhin approach.* Our focus in this thesis is on the first method.

Time-Delay Systems belong to the class of functional differential equations which are infinite-dimensional, as opposed to ordinary differential equations (ODEs).

TDSs with the delayed state are called retarded TDSs, whereas systems with the delayed highest-order state derivative are called neutral type systems.

The general form of a retarded functional differential equation (RFDE) (or functional differential equation of retarded type) is

$$\dot{x}(t) = f\left(t, x_t\right) \tag{3}$$

where $x(t) \in \mathbb{R}^n$ and $f : \mathbb{R} \times \mathcal{C} \to \mathbb{R}^n$. This equation indicates that the derivative of the state variable x at time t depends on t and $x(\zeta)$ for $t - h \leqslant \zeta \leqslant t$. Thus, to determine the future evolution of the state, it is necessary to specify the initial value of the state variable, $x(t)$, in a time interval of length h, say, from $t_0 - h$ to t_0; that is,

$$x_{t_0} = \phi,$$

In Lyapunov-Krasovskii approach, the corresponding energetic function becomes a *functional*, $V(t, x_t)$, that depends on x_t and indicates how much x_t deviates from the trivial solution, 0. This functional is called a *Lyapunov-Krasovskii functional*.

Theorem 3 ***(Lyapunov-Krasovskii stability theorem)*** *Suppose that* $f : \mathbb{R} \times \mathcal{C} \to \mathbb{R}^n$ *in (3) maps* $\mathbb{R}\times$ *(bounded sets in* $\mathcal{C}$ *) into bounded sets in* $\mathbb{R}^n$*, and that* $u, v, w : \overline{\mathbb{R}}_+ \to \overline{\mathbb{R}}_+$*are continuous nondecreasing functions, where* $u(\tau)$ *and* $v(\tau)$ *are positive for* $\tau > 0$ *and* $u(0) = v(0) = 0$*. The trivial solution* x_e *of (3) is:*

- ***Uniformly stable:*** *If there exists a continuous differentiable functional* $V : \mathbb{R} \times \mathcal{C} \to \mathbb{R}$ *such that*

$$u(\|\phi(0)\|) \leqslant V(t, \phi) \leqslant v\left(\|\phi\|_c\right) \qquad \text{and}$$
$$\dot{V}(t, \phi) \leqslant -w(\|\phi(0)\|)$$

- ***Uniformly asymptotically stable:*** *If* x_e *is uniformly stable, and* $w(\tau) > 0$ *for* $\tau > 0$*.*
- ***Globally uniformly asymptotically stable:*** *If* x_e *is uniformly asymptotically stable and if* $\lim_{\tau\to\infty} u(\tau) = \infty$*.*

6.2.4 Constructing Lyapunov-Krasovskii functionals

A well-constructed Lyapunov–Krasovskii functional provides systematic and computable criteria (often via linear matrix inequalities) for guaranteeing the stability and performance of delay systems and designing robust controllers.

A system with a time delay is generally represented as follows,

$$\dot{x}(t) = Ax(t) + A_d x(t - r)$$

where $A \in \mathbb{R}^{n\times n}, A_d \in \mathbb{R}^{n\times n}, x(t) \in \mathbb{R}^n$ is a state vector of the system, $\dot{x}(t)$ is the derivative of $x(t), r$ represents a time delay which possibly varies in the network based control.

A typical L-K functional candidate $V(t, x_t)$ has the following general form:

$$V(t, x_t) = V_1(x(t)) + V_2(t, x_t) + V_3(t, x_t) + V_4(t, x_t) \tag{4}$$

$$V\left(x_t\right) = x^T(t)Px(t) + 2x^T(t)\int_{-r}^{0} Q(\theta)x(t+\theta)d\theta + \int_{-r}^{0}\int_{-r}^{0} x^T(t+\xi)R(\xi,\eta)x(t+\eta)d\xi d\eta + \int_{-r}^{0} x^T(t+\xi)S(\xi)x(t+\xi)d\xi$$

where $0 < P = P^T \in \mathbb{R}^{n\times n}$

and for all $\xi \in [-r, 0], \eta \in [-r, 0]$,

$$Q(\xi) \in \mathbb{R}^{n\times n}$$
$$R(\xi,\eta) = R^T(\eta,\xi) \in \mathbb{R}^{n\times n}$$
$$S(\xi) = S^T(\xi) \in \mathbb{R}^{n\times n}$$

$$V\left[x_t\right] = x(t)^\top Px(t) + \int_{t-\tau}^{t} x(s)^\top Qx(s)\mathrm{d}s + \int_{t-\tau}^{t}\int_{s}^{t} \dot{x}(\theta)^\top R\dot{x}(\theta)\mathrm{d}\theta\ \mathrm{d}s$$

where $P \succ 0, Q \succeq 0, R \succeq 0$.

- ***Quadratic term:*** measures instantaneous energy.

$$V_1(x(t)) = x(t)^\top Px(t)$$

- ***Single integral term:*** weights past state energies.

$$V_2(t, x_t) = \int_{t-\tau}^{t} x(s)^\top Qx(s)\mathrm{d}s$$

- ***Double integral term:*** captures rate-of-change energy over the delay interval.

$$V_3(t, x_t) = \tau\int_{t-\tau}^{t}\int_{s}^{t} \dot{x}(\theta)^\top R\dot{x}(\theta)\mathrm{d}\theta\ \mathrm{d}s$$

- ***Neutral Term:*** essential for handling delayed state derivatives penalizes the energy of the delayed state derivative.

$$V_4(t, x_t) = \int_{-r}^{0} x^T(t+\xi)S(\xi)x(t+\xi)d\xi$$

The derivative of LKF is

$$
\begin{aligned}
\dot{V}\left(x_t\right) = & -x^T(t)\left[-PA - A^TP - Q(0) - Q^T(0) - S(0)\right]x(t) \\
& - x^T(t-r)Sx(t-r) - \int_{-r}^{0} x^T(\xi)\dot{S}(\xi)x(\xi)d\xi \\
& \int_{-r}^{0} d\xi \int_{-r}^{0} x^T(t+\xi)\left[\frac{\partial}{\partial\xi}R(\xi,\eta) + \frac{\partial}{\partial\eta}R(\xi,\eta)\right]x(t+\eta)d\eta \\
& + 2x^T(t)\left[PA_d - Q(-r)\right]x(t-r) \\
& + 2x^T(t)\int_{-r}^{0}\left[A^TQ(\xi) - \dot{Q}(\xi) + R(0,\xi)\right]x(t+\xi)d\xi \\
& + 2x^T(t-r)\int_{-r}^{0}\left[{A_d}^TQ(\xi) - R(-r,\xi)\right]x(t+\xi)d\xi
\end{aligned}
\tag{5}
$$

The preceding formulation (4) provides necessary and sufficient conditions for the stability of time-delay systems. However, since the kernel functions $Q(\xi)$, $R(\xi,\eta)$, and $S(\xi)$ are infinite-dimensional, direct numerical verification is impractical. To address this challenge, these matrix functions are approximated by *piecewise linear functions* defined over a partitioned delay interval. This discretization allows the Lyapunov–Krasovskii functional and its time-derivative conditions to be reformulated as a set of *linear matrix inequalities* (LMIs). These LMIs can then be efficiently solved using standard convex optimization techniques. This approach is widely known as the *discretized Lyapunov functional* (DLF) method [40, 41].

6.2.5 Linear Matrix Inequalities

In this subsection, we will present the key lemmas commonly used in the formulation of linear matrix inequalities (LMIs) for stability analysis of time-delay systems and control design.

Lemma 1 ***(Schur Complement)*** *For any symmetric matrix, M, of the form*

$$
M = \begin{pmatrix} A & B \\ B^\top & C \end{pmatrix}
$$

if C is invertible then the following properties hold: (1) $M \succ 0$ iff $C \succ 0$ and $A - BC^{-1}B^\top \succ 0$. (2) If $C \succ 0$, then $M \succeq 0$ iff $A - BC^{-1}B^\top \succeq 0$.

if A is invertible then the following properties hold: (1) $M \succ 0$ iff $A \succ 0$ and $C - B^\top A^{-1}B \succ 0$. (2) If $A \succ 0$, then $M \succeq 0$ iff $C - B^\top A^{-1}B \succeq 0$.

Lemma 2 ***(Basic inequality)*** *$\forall a, b \in \mathbb{R}^n$ and $\forall R > 0$,*

$$-2a^{\mathrm{T}}b \leqslant a^{\mathrm{T}}Ra + b^{\mathrm{T}}R^{-1}b$$

Lemma 3 ***(Park's inequality)*** *$\forall a, b \in \mathbb{R}^n, \forall R > 0$, and $\forall M \in \mathbb{R}^{n\times n}$,*

$$-2a^{\mathrm{T}}b \leqslant \begin{bmatrix} a \\ b \end{bmatrix}^{\mathrm{T}} \begin{bmatrix} R & RM \\ * & \left(M^{\mathrm{T}}R + I\right) R^{-1}(RM + I) \end{bmatrix} \begin{bmatrix} a \\ b \end{bmatrix}.$$

Lemma 4 ***(Moon et al.'s inequality)*** *$\forall a \in \mathbb{R}^{n_a}, \forall b \in \mathbb{R}^{n_b}, \forall N \in \mathbb{R}^{n_a\times n_b}$, and for $X \in \mathbb{R}^{n_a\times n_a}, Y \in \mathbb{R}^{n_a\times n_b}$, and $Z \in \mathbb{R}^{n_b\times n_b}$, if $\begin{bmatrix} X & Y \\ * & Z \end{bmatrix} \geqslant 0$, then*

$$-2a^{\mathrm{T}}Nb \leqslant \begin{bmatrix} a \\ b \end{bmatrix}^{\mathrm{T}} \begin{bmatrix} X & Y - N \\ * & Z \end{bmatrix} \begin{bmatrix} a \\ b \end{bmatrix}.$$

Lemma 5 ***(Jensen's Inequalities)*** *For a given matrix $R \in \mathbb{S}^n_+$ and a continuous function $x(t) : [a, b] \to \mathbb{R}^n$, the following inequalities holds:*

$$\int_a^b x^T(s)Rx(s)ds \geq \frac{1}{b-a}\int_a^b x^T(s)dsR\int_a^b x(s)ds$$

$$\int_a^b\int_u^b x^T(s)Rx(s)dsdu \geq \frac{2}{(b-a)^2}\int_a^b\int_u^b x^T(s)dudsR\int_a^b\int_u^b x(s)duds$$

Lemma 6 ***(Wirtinger-Based Integral Inequality)****[42] Consider a given $n \times n$-matrix $R \succ 0$. Then, for all function z in $\mathcal{C}^1([a, b] \to \mathbb{R}^n)$ which satisfies $z(a) = z(b) = 0$, the following inequality holds*

$$\int_a^b \dot{z}^T(u)R\dot{z}(u)\mathrm{d}u \geq \frac{\pi^2}{(b-a)^2}\int_a^b z^T(u)Rz(u)\mathrm{d}u$$

6.3 Mean-square stability

Mean-square stability for time-delayed systems refers to the property that the expected value of the square of the system state remains bounded or converges to zero despite the presence of time delays and stochastic perturbations. It is a critical concept in the stability analysis of stochastic or random time-delay systems, ensuring that the system behaves in a stable manner on average over time.

Definition 7 *The null-solution of the stochastic system is said to be*

i ***Mean square stable,*** *if*

$$\forall \epsilon > 0, \exists \delta > 0 \ s.t. \ \|x(0)\| < \delta \Longrightarrow \mathbb{E}\left[\|x(t)\|^2\right] < \epsilon, \forall t \geq 0.$$

ii ***Asymptotically mean square stable,*** *if it is mean square stable, and*

$$\lim_{i \to \infty} \mathbf{E} x_i^2 \to 0$$

.

where $\mathbb{E}[\cdot]$ *is the expectation operator and* $\|\cdot\|$ *is the Euclidean norm.*

In practice, for engineers and researchers, the Lyapunov-Krasovskii Functional LKF-LMI approach is the workhorse for analyzing and designing controllers/observers that ensure mean-square stability for time-delayed systems under stochastic uncertainty.

Theorem 4 *[43]. If there exists a nonnegative functional* $V : \mathcal{I} \to \boldsymbol{R}$*, such that*

$$\mathbf{E} V_0 \leq c_1 \|\phi\|_0^2$$
$$\mathbf{E} \Delta V_i \leq -c_2 \mathbf{E} x_i^2$$

for $c_1, c_2 > 0$*, then the system is asymptotically mean square stable.*

7 Networked control systems control strategies

The effective control of Networked Control Systems (NCS) necessitates the development of specialized strategies capable of overcoming the imperfections inherent in a shared communication channel. While the challenges posed by transmission delays, packet dropouts, and bandwidth constraints have been detailed in previous sections, this section is dedicated exclusively to reviewing the primary control strategies designed to address them. The objective of these strategies is to guarantee the stability, performance, and robustness of the closed-loop system despite network-induced uncertainties.

These approaches can be classified into several major families based on different design philosophies, ranging from classical robust methods to predictive and resource-optimized approaches, as illustrated in Figure 2.

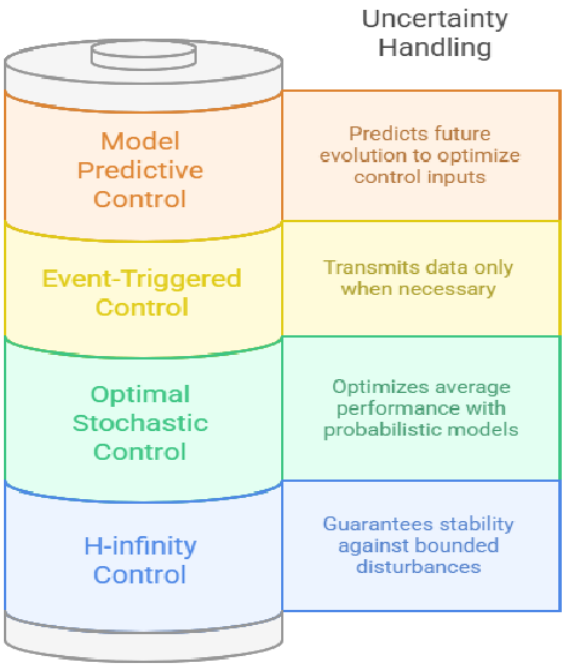

Figure 2: A Categorization of Control Strategies for Networked Control Systems.

7.1 Robust Control Strategies

Robust control approaches aim to design controllers whose stability and performance are guaranteed against a defined set of uncertainties, treating network imperfections as bounded disturbances.

7.1.1 H-infinity (H_∞) Control

H_∞ control is a fundamental technique that seeks to minimize the effect of the worst-case disturbance on the system. In the NCS context, the H_∞ controller is synthesized to ensure robust stability and maintain an acceptable level of performance (e.g., disturbance attenuation) for bounded delays and packet loss rates. While powerful, this approach can sometimes lead to conservative solutions, as it is designed for the worst-possible-case scenario [7, 44].

The system is typically modeled as a generalized plant subject to external disturbances $w(t)$, which can represent network-induced errors, noise, or modeling uncertainties. The goal is to design a controller $u(t) = Kx(t)$ that minimizes the "energy gain" from the disturbance $w(t)$ to a performance output $z(t)$. This is formulated as an H_∞ norm constraint on the closed-loop transfer function T_{zw} from w

to z:

$$\sup_{\|w(t)\|_2 \neq 0} \frac{\|z(t)\|_2}{\|w(t)\|_2} = \|T_{zw}\|_\infty < \gamma \tag{6}$$

,

where $\|\cdot\|_2$ is the L2-norm, representing the total energy of a signal over time. The H_∞ norm, $\|T_{zw}\|_\infty$, therefore represents the system's L2-gain: the worst-case amplification of energy from any possible disturbance signal $w(t)$ to the performance output $z(t)$. In the frequency domain, this value is equivalent to the peak magnitude of the system's frequency response across all frequencies. The objective is to find a controller K that satisfies this condition for the smallest possible performance bound γ. This problem is often solved using LMI-based techniques or by solving algebraic Riccati equations.

7.1.2 Lyapunov-Based Stability Analysis

A foundational and central approach for the analysis of NCS involves the use of Lyapunov stability theory, extended to systems with delays. This methodology is at the core of the work presented in this thesis.

For systems with time-varying delays, the construction of Lyapunov-Krasovskii Functionals (LKFs) is the benchmark technique. By choosing an appropriate LKF that incorporates information about the system's state history, it is possible to derive sufficient conditions for stability. A major advantage of this method is that these conditions can often be formulated as Linear Matrix Inequalities (LMIs) [23].

Solving these LMIs not only certifies the system's stability but also allows for the co-design of the controller gain (K) and the calculation of the Maximum Allowable Delay Bound (MADB) which the critical delay threshold beyond which stability can no longer be guaranteed. This is precisely the methodology adopted in our research to analyze the stability of multi-source energy systems under stochastic delays modeled by MRS-GARCH processes [10].

Consider an NCS governed by the state-feedback controller

$$u(t) = Kx(t - \tau(t)),$$

where $\tau(t)$ is a bounded, time-varying delay. The closed-loop system can be described as

$$\dot{x}(t) = Ax(t) + Bu(t) = Ax(t) + BKx(t - \tau(t)), \tag{7}$$

with $x(t) \in \mathbb{R}^n$. The delay is assumed to satisfy

$$0 \leq \tau(t) \leq h,$$

where h denotes the MADB to be determined.

To account for the effect of delays, an LKF is employed. Unlike a conventional Lyapunov function $V(x(t))$, an LKF depends on the whole trajectory segment

$$x_t = \{x(t+\theta) \,|\, \theta \in [-h, 0]\}.$$

A typical candidate functional is stated in eq (4).

The system is asymptotically stable if $V(x_t)$ is positive definite and its derivative along system trajectories satisfies $\dot{V}(x_t) < 0$. Differentiating the LKF gives eq (5). The resulting expression involves delayed terms such as $x(t - \tau(t))$, which are challenging to handle directly.

To make the conditions tractable, integral inequalities (e.g., Jensen's inequality) are applied to bound cross-terms and delay-dependent integrals. This transforms the inequality $\dot{V}(x_t) < 0$ into a matrix condition of the form

$$\zeta(t)^T \Phi \, \zeta(t) < 0,$$

where the augmented vector is defined as

$$\zeta(t) = \begin{bmatrix} x(t)^T & x(t-h)^T & x(t-\tau(t))^T \end{bmatrix}^T.$$

Stability is then ensured if there exist matrices $P, Q, R \succ 0$ such that Φ is negative definite. Introducing the change of variables $Y = KP^{-1}$, the simultaneous design of the controller gain K and the computation of the MADB h can be formulated as an LMI problem:

$$\text{Find } P, Q, R \succ 0, \, Y \quad \text{such that} \quad \Phi(P, Q, R, Y, A, B, h) < 0. \tag{8}$$

This LMI-based framework provides a constructive tool to guarantee stability while explicitly accounting for time-varying delays. Further details on its application will be developed in the next chapters.

7.2 Optimal Stochastic Control Strategies

When network imperfections are better described by probabilistic models, stochastic control strategies offer a natural framework. They aim to optimize the average

performance (i.e., the mathematical expectation) of the system. The optimal stochastic control methodology treats the effects of random network delays in an NCS as a *Linear–Quadratic–Gaussian* (LQG) problem.

The LQG approach is adapted for NCS by modeling uncertainties as stochastic processes. For a discrete-time system with process noise w_k and measurement noise v_k, and considering packet dropouts modeled by a Bernoulli process $\gamma_k \in \{0, 1\}$, the objective is to find a control law $u_k = K\hat{x}_k$ that minimizes a quadratic cost function in expectation:

$$\min_K J = \mathbb{E}\left[\sum_{k=0}^{\infty}(x_k^T Q x_k + u_k^T R u_k)\right] \tag{9}$$

The solution involves a Kalman filter to generate the state estimate $\hat{x}_k$ based on potentially missing measurements, and the controller gain K is found by solving a modified algebraic Riccati equation that accounts for the packet loss probability $p = \mathbb{P}(\gamma_k = 0)$ [24].

When measurements y_k are lost due to packet dropouts, the standard Kalman filter must be adapted. Let γ_k be a Bernoulli variable indicating if the measurement at step k is received ($\gamma_k = 1$) or lost ($\gamma_k = 0$). The update step of the Kalman filter becomes conditional:

$$\hat{x}_{k|k} = \hat{x}_{k|k-1} + \gamma_k K_k(y_k - C\hat{x}_{k|k-1}) \tag{10}$$

If the packet is lost ($\gamma_k = 0$), no update occurs, and the estimate simply propagates based on the model. This ensures an optimal estimate in a mean-squared error sense, even with intermittent data [45].

7.3 Resource-Aware Control Strategies

Resource-Aware Control Strategies focus on minimizing communication, computation, and energy use while preserving stability and performance. These strategies address resource constraints like limited bandwidth in shared networks by shifting from periodic *time-triggered control (TTC)* to aperiodic schemes.

7.3.1 Event-Triggered Control (ETC):

Event-Triggered Control (ETC) reactively triggers updates when a condition, such as state deviation exceeding a threshold, is met. This reduces transmissions compared to periodic sampling, saving bandwidth in NCS with packet loss or delays. ETC

ensures stability via input-to-state stability analysis and integrates with scheduling for multi-loop systems [46].

In ETC, data is transmitted not periodically, but only when a state-dependent triggering condition is violated. Let t_k be the last transmission instant. The measurement error is defined as $e(t) = x(t_k) - x(t)$. A new transmission is triggered at the next instant t_{k+1} defined by:

$$t_{k+1} = \inf\{t > t_k \mid \|e(t)\|^2 \geq \sigma \|x(t)\|^2\} \tag{11}$$

where $\sigma \in (0, 1)$ is a designer-specified threshold. This condition ensures that communication occurs only when the error due to holding the old value becomes significant relative to the current state's magnitude, thus saving network resources while guaranteeing stability [47, 48].

7.3.2 Self-Triggered Control (STC):

Self-Triggered Control (STC) proactively predicts the next update time using a model of system dynamics at the last update. Therefore, When the sensor transmits a measurement at time t_k, the controller (or the smart sensor itself) calculates the deadline for the next transmission t_{k+1} based on the system evolution. The fundamental principle is that $t_{k+1} = t_k + \tau_k$, where τ_k is the inter-sampling interval computed at t_k. This interval is selected to guarantee stability and a predefined level of performance until the next update. Moreover, it allows sensor shutdown between updates, further conserving energy in battery-powered NCS. STC provides a priori performance guarantees, like quadratic costs close to LQR, through co-design of feedback and triggering [49].

7.4 Predictive and Optimization-Based Strategies

Predictive and optimization-based strategies address key challenges in Networked Control Systems (NCS), such as network-induced delays, packet losses, uncertainties, and constraints, by forecasting future states and optimizing control actions accordingly.

7.4.1 Model Predictive Control (MPC)

Model Predictive Control is particularly well-suited for the challenges of NCS. It uses a system model to predict its future evolution over a given time horizon. At each step, it calculates an optimal sequence of control inputs by solving an optimization problem, and then applies the first input in the sequence.

At each sampling instant k, MPC solves a finite-horizon optimal control problem for a prediction horizon N. Given the current state x_k, it finds a control sequence $U_k^* = \{u_{k|k}^*, \ldots, u_{k+N-1|k}^*\}$ that minimizes a cost function:

$$\min_{U_k} J = \sum_{i=0}^{N-1} (x_{k+i|k}^T Q x_{k+i|k} + u_{k+i|k}^T R u_{k+i|k}) + x_{k+N|k}^T P x_{k+N|k} \tag{12}$$

subject to the system dynamics model and constraints:

$$x_{k+i+1|k} = A x_{k+i|k} + B u_{k+i|k} \tag{13}$$

$$u_{\min} \leq u_{k+i|k} \leq u_{\max} \tag{14}$$

$$x_{\min} \leq x_{k+i+1|k} \leq x_{\max} \tag{15}$$

where $x_{k+i|k}$ is the predicted state at time $k+i$ based on information at time k. Once the optimal sequence U_k^* is found, only the first element, $u_k^* = u_{k|k}^*$, is applied to the system. The entire process is repeated at the next time step, $k+1$, using the new measured state. This receding horizon principle allows MPC to handle delays, packet loss (by using predictions), and constraints effectively [50, 51].

The choice of a control strategy for an NCS is highly dependent on the application's requirements, the characteristics of the communication network, and the performance objectives. No single solution is universally optimal; often, a hybrid combination of several approaches is required.

Within the scope of this thesis, the emphasis has been placed on stability approaches based on Lyapunov theory. This choice is motivated by their theoretical rigor and their ability to provide quantifiable stability guarantees (MADB) for systems subject to complex stochastic delays, which is a central challenge for the reliable management of networked energy systems.

8 Summary

This chapter has presented a comprehensive overview of Networked Control Systems (NCSs), establishing the theoretical foundation for this thesis. The fundamental components—sensors, controllers, actuators, and communication networks—were examined alongside various NCS structures, including centralized, decentralized, and distributed configurations. Particular attention was given to network-induced imperfections, namely time delays, packet dropouts, quantization errors, and variable

sampling intervals, which distinguish NCSs from conventional control systems and pose significant challenges to stability and performance.

The stability analysis methods relevant to this work were developed in detail, progressing from classical Lyapunov theory to the Lyapunov-Krasovskii (LKF) approach for time-delay systems. The formulation of LKF functionals and their conversion to linear matrix inequality (LMI) conditions through discretization techniques was presented as the primary analytical framework adopted in this thesis. Furthermore, various control strategies for NCSs were reviewed, with emphasis on delay-dependent stability analysis and maximum allowable delay bound (MADB) computation—the methodologies that will be employed to address stochastic communication delays in multi-source energy systems.

Overall, the chapter establishes the theoretical and practical background necessary for the remainder of the thesis, motivating the development of advanced control strategies capable of ensuring stability, performance, and efficient resource utilization in networked environments.

Chapter II: Multi-sources Energy Systems

The preceding chapter established the theoretical framework of Networked Control Systems (NCSs), highlighting the challenges and strategies for managing systems where control loops are closed over a communication network [8]. This chapter transitions from theory to application, focusing on the *physical plant* to be controlled: a multi-source energy system centered around a photovoltaic (PV) prosumer.

The global energy landscape is undergoing a profound transformation, shifting from centralized, fossil-fuel-based generation towards a decentralized, digitalized, and renewable-based paradigm [3, 4]. This transition is enabled by the integration of Distributed Energy Resources (DERs)—such as solar PV, wind turbines, and energy storage systems—into localized networks known as microgrids. A microgrid is a cluster of interconnected loads and DERs within clearly defined electrical boundaries that acts as a single controllable entity with respect to the main grid. It can operate both in grid-connected mode and, crucially, in isolated *island mode* [5].

Within this architecture, the *prosumer*—an entity that both produces and consumes energy—becomes a fundamental building block. Residential and commercial buildings equipped with rooftop PV systems are prime examples. The effective coordination of these prosumers within a networked microgrid, as illustrated in Figure 3, is critical for achieving goals such as optimal energy sharing, enhanced resilience, and improved power quality [6].

However, the integration of these inherently variable resources introduces significant control challenges. The core objective of this thesis is to address one of the most critical of these challenges: maintaining system stability and performance in the presence of stochastic communication delays inherent in the NCS framework. To rigorously analyze this problem using the Lyapunov-Krasovskii methodology outlined in Chapter 1, a

precise mathematical model of the prosumer system is indispensable.

This chapter, therefore, is dedicated to deriving a control-oriented model of a PV prosumer node. We begin with the fundamental physics of a PV cell, develop its non-linear electrical model, and scale it to a full array. We then integrate this with its essential power electronics interface, applying averaging and linearization techniques to obtain a linear state-space model. This model, representing the "Prosumer" block in Figure 3, will serve as the foundation for the networked stability analysis and controller synthesis in the subsequent chapters.

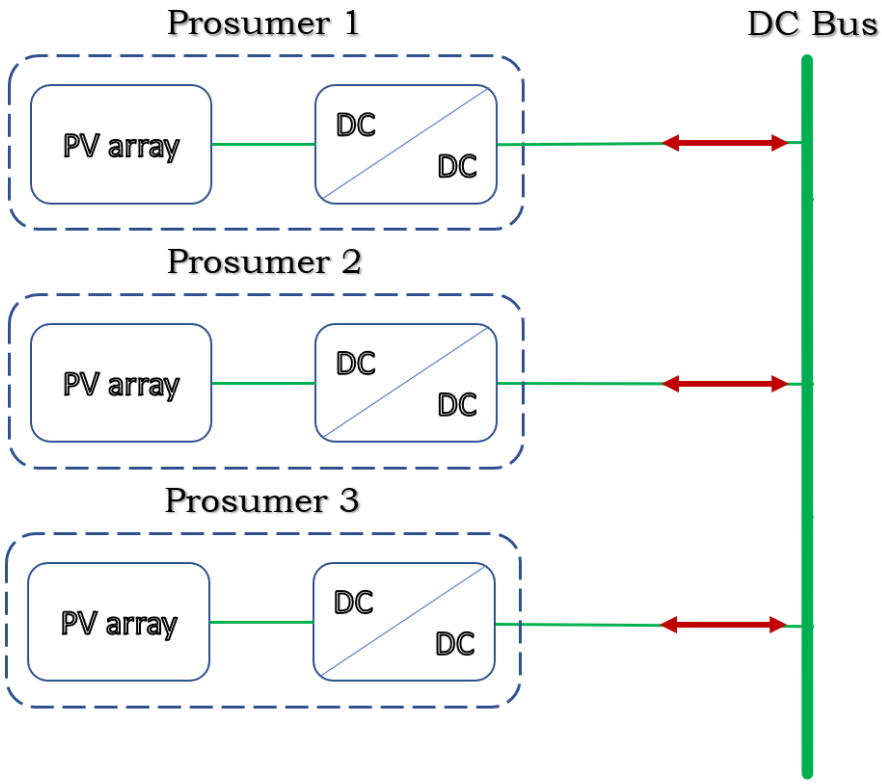

Figure 3: Multi-sources energy system including three prosumers

1 Modeling the Photovoltaic Generator

1.1 Fundamental Principles and Characteristics

The operation of a photovoltaic cell is governed by the photovoltaic effect, where photon energy from sunlight is absorbed by a semiconductor material (typically silicon), exciting electrons and creating electron-hole pairs. The inherent electric field of a p-n junction separates these charges, generating a direct current (DC) when the cell is connected to an external load [52].

The electrical behavior of a PV cell is non-linear and is most commonly represented by its current-voltage (I-V) and power-voltage (P-V) characteristic curves, as shown in Figure 4. These curves are highly sensitive to two primary environmental variables:

- **Solar Irradiance (G):** Primarily affects the short-circuit current (I_{sc}). Higher irradiance leads to a proportional increase in I_{sc} and consequently the generated power.
- **Cell Temperature (T):** Primarily affects the open-circuit voltage (V_{oc}). Higher temperatures lead to a decrease in V_{oc}, reducing the maximum available power.

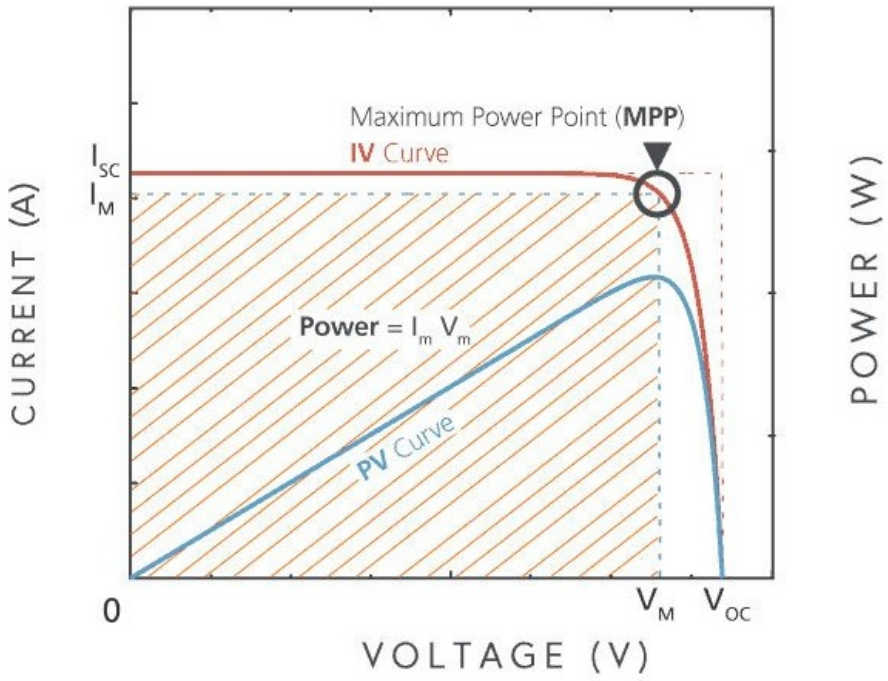

Figure 4: I-V and P-V characteristics curves

A key feature of the P-V curve is the **Maximum Power Point (MPP)**, the unique point (V_{mp}, I_{mp}) where the power output is maximized. The goal of any PV control system is to maintain operation at this point despite changing environmental conditions.

1.2 PV Modeling Techniques

Accurate mathematical modeling of photovoltaic (PV) cells and modules is a fundamental prerequisite for the simulation, analysis, design, and optimization of any PV system. The primary objective of a PV model is to faithfully replicate the non-linear

current-voltage ($I-V$) characteristic of a solar device under varying environmental conditions of solar irradiance (G) and cell temperature (T_c). The choice of modeling technique involves a critical trade-off between computational simplicity, numerical accuracy, and the physical representation of the cell's internal processes.

PV modeling approaches can be broadly categorized into three groups:

1. ***Analytical Models (Equivalent Circuit Models):*** These are the most widely adopted techniques, representing the PV cell as an electrical circuit. Their popularity stems from a strong physical basis and a good balance between accuracy and computational demand.
    - *The Single-Diode Model (SDM)* is the cornerstone of PV modeling, comprising a current source, a diode, a series resistance (R_s), and occasionally a shunt resistance (R_{sh}). It offers a robust compromise for most system-level studies.
    - *The Double-Diode Model (DDM)* adds a second diode to better account for recombination losses in the depletion region, yielding higher accuracy, particularly at low irradiance levels, at the cost of increased complexity and two additional parameters to identify.
    - *The Triple-Diode Model (TDM)* provides even greater physical detail but is often reserved for specialized cell research due to its high parameterization complexity.
2. ***Empirical Models:*** These models prioritize simplicity and computational speed by using mathematical equations that directly curve-fit the I-V data from manufacturer datasheets. While fast and easy to implement, they lack a direct physical basis and may have limited extrapolation capability beyond the provided data points.
3. ***Intelligent and Data-Driven Models:*** With the advent of artificial intelligence, techniques such as Artificial Neural Networks (ANNs), Fuzzy Logic (FL), and Adaptive Neuro-Fuzzy Inference Systems (ANFIS) have been successfully applied. These models are exceptionally powerful for capturing complex, non-linear relationships when abundant operational data is available, making them ideal for performance prediction and fault diagnosis in existing systems. However, they require extensive training data and function as

"black-box" models.

1.3 Single-Diode Model: Mathematical Formulation

The most widely adopted equivalent circuit for modeling a PV cell is the single-diode model (also known as the 1D2R model), which effectively balances accuracy and complexity for system-level studies [20]. Its circuit diagram is presented in Figure 5.

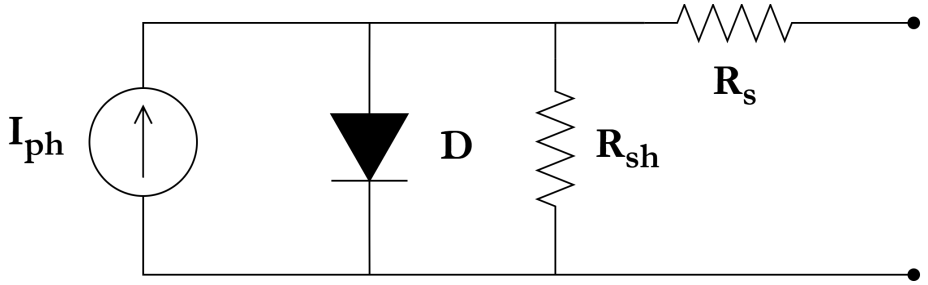

Figure 5: Single-diode equivalent circuit model (1D2R) of a photovoltaic cell.

Applying Kirchhoff's current law to the node where the current source, diode, and shunt resistor meet, the output current I of the cell is given by:

$$I = I_{ph} - I_d - I_{sh} = I_{ph} - I_s \left[\exp\left(\frac{q(V + IR_s)}{nkT} \right) - 1 \right] - \frac{V + IR_s}{R_{sh}} \tag{16}$$

where:

- I_{ph}: Photocurrent, directly proportional to irradiance (A)
- I_s: Reverse saturation current of the diode (A)
- q: Electron charge (1.602×10^{-19} C)
- k: Boltzmann constant (1.381×10^{-23} J/K)
- T: Cell junction temperature (K)
- n: Diode ideality factor (dimensionless, typically between 1 and 2)
- R_s: Series resistance (Ω)
- R_{sh}: Shunt resistance (Ω)

The photocurrent I_{ph} and saturation current I_s are temperature-dependent. They can be calculated using the following empirical relations, which are crucial for adapting

the model to real-world conditions [21]:

$$I_{ph} = [I_{sc} + K_i(T - T_{\text{ref}})] \cdot \frac{G}{G_{\text{ref}}} \tag{17}$$

$$I_s = I_{rs} \left(\frac{T}{T_{\text{ref}}}\right)^3 \exp\left[\frac{qE_g}{nk}\left(\frac{1}{T_{\text{ref}}} - \frac{1}{T}\right)\right] \tag{18}$$

$$I_{rs} = \frac{I_{sc}}{\exp\left(\frac{q\,V_{oc}}{n\,N_s\,k\,T}\right) - 1} \tag{19}$$

where I_{sc} is the short-circuit current, V_{oc} is the open-circuit voltage, K_i is the current temperature coefficient, E_g is the bandgap energy of the semiconductor ($\sim$1.12 eV for Si), T_{ref} and G_{ref} are reference conditions (typically Standard Test Conditions: 25°C, 1000 W/m^2), I_{sc} is short-circuit current of the **module** under reference conditions, V_{oc} is the open-circuit voltage of the **module** under reference conditions, N_s is the number of cells connected in series within a module, and n is the diode ideality factor per cell (1–2). The thermal voltage "seen" by the module is $N_s kT/q$.

1.4 Parameter Scaling from Cell to Array

A single PV cell produces low voltage and power. To achieve useful voltage and power levels, cells are connected in series to form a module, and modules are connected in series and parallel to form an array. Assuming uniform illumination and identical cells, the parameters in Equation 16 are scaled for an array with N_{ms} modules in series and N_{mp} modules in parallel:

$$\begin{aligned}
I_{ph,\text{array}} &= N_{mp}\, I_{ph}, & I_{s,\text{array}} &= N_{mp}\, I_s, \\
R_{s,\text{array}} &= \frac{N_{ms}}{N_{mp}}\, R_s, & R_{sh,\text{array}} &= \frac{N_{ms}}{N_{mp}}\, R_{sh}, \\
n_{\text{array}} &= n, & N_{s,\text{tot}} &= N_{ms}\, N_s.
\end{aligned} \tag{20}$$

The characteristic equation for the entire array is then the following:

$$I = I_{ph,\text{array}} - I_{s,\text{array}} \left[\exp\left(\frac{q\,(V + IR_{s,\text{array}})}{n\,N_{s,\text{tot}}\,k\,T}\right) - 1\right] - \frac{V + IR_{s,\text{array}}}{R_{sh,\text{array}}} \tag{21}$$

This equation describes the non-linear relationship between the array's terminal voltage V and current I.

2 Power Electronics Interface

The integration of photovoltaic (PV) arrays with electrical loads or the utility grid is fundamentally enabled by power electronics converters. These interfaces are critical for overcoming the inherent limitations of solar energy generation, namely its variable, weather-dependent nature and the mismatch between the output of the PV modules and the requirements of most applications. The primary functions of the power electronics interface are threefold: *Power Extraction*, *Power Conditioning*, and *System Control*.

However, modern systems often employ a multi-stage architecture for enhanced performance:

1. *DC-DC Converter Stage:* Often placed between the PV array and the inverter, this stage is responsible for Maximum Power Point Tracking (MPPT). By adjusting the operating voltage of the PV array, it ensures maximum energy harvest under varying irradiance and temperature conditions. Common topologies include buck, boost, and buck-boost converters, with the latter being particularly useful for accommodating a wide range of PV voltages.

2. *DC-AC Inverter Stage:* This is the central component that converts the controlled DC power into grid-compliant AC power. Inverter topologies have evolved significantly, ranging from simple single-phase H-bridge inverters for residential applications to complex three-level or multilevel inverters for large-scale utility systems, which offer improved efficiency and power quality. A key classification is between voltage-source inverters (VSI), which are dominant in grid-connected systems, and current-source inverters (CSI).

3. *Grid Synchronization and Control:* Advanced control algorithms, such as Phase-Locked Loops (PLL), ensure the inverter's output is perfectly synchronized with the grid's voltage and frequency. Furthermore, grid-feeding inverters are increasingly being equipped with grid-supporting capabilities (e.g., reactive power support, frequency regulation) to enhance grid stability and facilitate high penetration of renewable energy.

The power electronics interface is not merely a converter but an intelligent energy processing unit. Its topology and control strategy are paramount for determining the overall efficiency, reliability, and functionality of the PV system.

2.1 DC-DC Converter

A DC–DC converter acts as an impedance-matching interface between the PV array and the load or the DC bus. By adjusting its duty cycle d, the converter effectively shifts the PV array's operating point along the I–V curve, thereby enabling maximum power extraction while regulating the output to the required voltage level. The fundamental roles of a DC–DC converter in PV systems include: ***(i) voltage and current regulation***, ensuring stable operation under varying environmental conditions; **(ii) implementation of maximum power point tracking (MPPT) algorithms**, which optimize energy harvesting to maximize power extraction; and **(iii) providing isolation and protection**, particularly in topologies designed with galvanic isolation and safety features.

The table 4 summarizes the common types of DC-DC converters used in PV applications.

2.2 The Push-Pull Converter Topology

The push–pull converter is an isolated DC–DC topology frequently applied in medium- to high-power PV systems. It employs a center-tapped transformer and two active switches (e.g., MOSFETs or IGBTs) that are alternately driven, producing bidirectional flux in the transformer core. This allows efficient utilization of the magnetic core and provides *galvanic isolation* while enabling both *step-up* and *step-down* operation.

The push–pull converter operates in three main modes as illustrated in Figure 6. It alternates two switches Q_1 and Q_2 in a phase shift of $T/2$ with the same duty ratio D: when both switches conduct, the inductor L charges and the load is fed by the capacitor C_H. When only one switch conducts, the PV source and inductor L transfer energy through one half of the transformer's primary winding to feed the load and recharge C_H. This cycle ensures continuous and regulated power transfer.

The output voltage is related to the input voltage, transformer turns ratio, and duty cycle, governed by the equation:

$$V_{out} = n \times D \times V_{in}$$

where V_{out} is output voltage, V_{in} is input voltage, $n = \frac{N_2}{N_1}$ are transformer turns

Table 4: Common DC-DC converter types used in PV applications

Converter type	Function	Circuit diagram	Output equation
Boost (Step-Up)	Steps up the input voltage from the PV array to a desired higher output voltage.	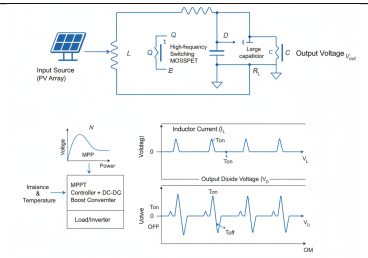	$V_{out} = \frac{V_{in}}{1-D}$
Buck (Step-Down)	Steps down the input voltage from the PV array to a voltage level that matches the battery's charging requirement or the load voltage.	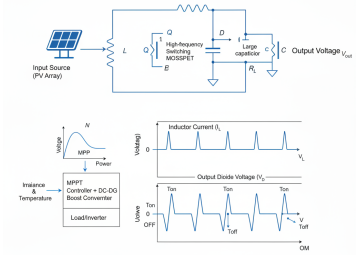	$V_{out} = DV_{in}$
Buck-Boost	Provides flexible voltage regulation, allowing for either step-up or step-down of the PV voltage. Useful for systems where the PV voltage may vary above or below the required load voltage.	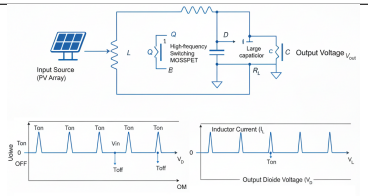	$V_{out} = V_{in}\frac{D}{1-D}$

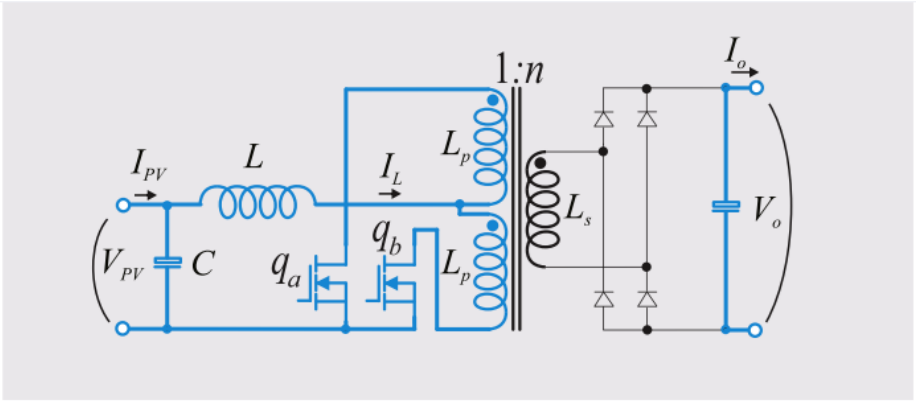

(a)

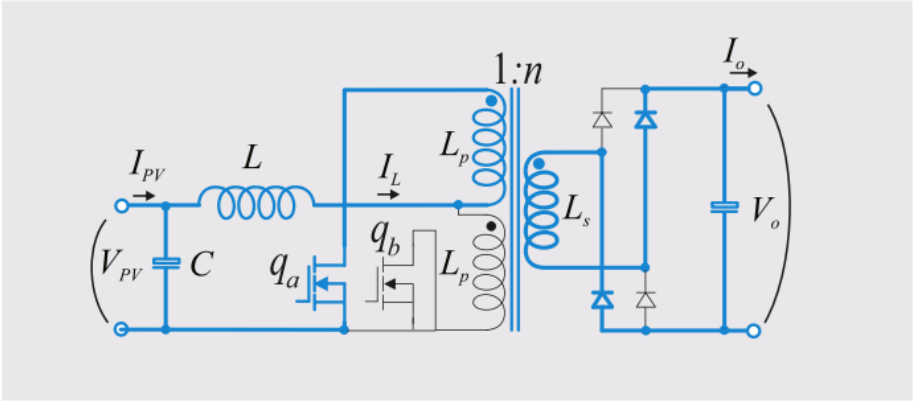

(b)

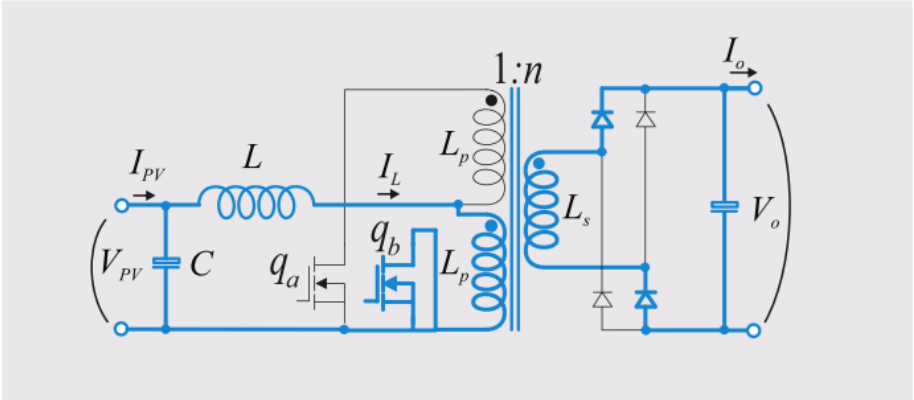

(c)

Figure 6: Operation modes of the push-pull conveter

ratio, and D is the duty cycle.

2.3 Maximum Power Point Tracking (MPPT)

The continuous movement of the MPP with changing G and T necessitates an active control strategy known as Maximum Power Point Tracking (MPPT). The MPPT algorithm is a feedback controller that adjusts the converter's duty cycle d to seek the MPP. Common techniques include Perturb and Observe (P&O) and Incremental Conductance (IC) [22]. The control variable is d, and the measured input is typically the PV array voltage V_{pv} and/or current I_{pv}.

The Maximum Power Point (MPP) of a photovoltaic (PV) array continuously shifts in response to changes in environmental conditions, such as solar irradiance (G) and temperature (T). To maximize the power extracted from the PV system under these dynamic conditions, an active control strategy known as *Maximum Power Point Tracking* (MPPT) is implemented. MPPT algorithms act as feedback controllers that adjust the duty cycle d of the power converter, typically based on measurements of the PV array voltage V_PV and/or current I_PV. The fundamental goal of MPPT algorithms is to ensure the operating point of the PV system continuously aligns with the MPP, thereby maximizing energy harvest. MPPT algorithms can be broadly classified into three categories: conventional methods, Artificial Intelligence (AI)-based methods, and metaheuristic optimization techniques [53]. A comparative summary is presented in Table 5. Each MPPT category has its own trade-offs between tracking speed, accuracy, complexity, robustness, and cost. Balancing these metrics is central to the design of practical MPPT controllers.

For this study, we will focus on the Perturb and Observe (P&O) MPPT method due to its widespread adoption, simplicity, and ease of implementation. The *P&O algorithm* operates on a straightforward principle: it systematically perturbs (slightly increases or decreases) the operating voltage (or duty cycle) of the PV array and observes the resulting change in output power.

- If the perturbation leads to an increase in power, the algorithm continues to perturb in the same direction, assuming it is moving closer to the MPP.
- If the perturbation results in a decrease in power, the algorithm reverses the direction of the perturbation, indicating that it has moved past the MPP or is moving away from it.

This iterative process drives the operating point toward the maximum power point.

Table 5: Comparison of MPPT Algorithm Categories

Algorithm Type	Key Methods	Strengths	Weaknesses
Conventional	Perturb and Observe (P&O), Incremental Conductance (INC)	Simple implementation, low computational cost, proven reliability.	Steady-state oscillations around the MPP, poor performance under partial shading conditions.
Artificial Intelligence (AI)	Fuzzy Logic Control (FLC), Artificial Neural Networks (ANN)	High accuracy, fast dynamic response, can handle non-linearities effectively.	Complex design and tuning, requires extensive training data and expert knowledge.
Metaheuristic	Particle Swarm Optimization (PSO), Firefly Algorithm	Global peak tracking, highly robust under partial shading and complex P-V curves.	Very high computational cost, slow convergence, complex implementation.

However, despite its simplicity and ease of implementation, the P&O method has inherent limitations, including steady-state oscillations, poor dynamic response, a trade-off between tracking speed and accuracy, and reduced effectiveness under partial shading conditions.

To illustrate the concept of MPPT, Figure

3 Modeling of a Photovoltaic System with DC Interface

The PV system under consideration consists of PV panels connected to a push-pull DC-DC converter, as illustrated in Figure 8. The PV array is represented by its linearized equivalent circuit at the maximum power point, characterized by an equivalent voltage source V_{eq} in series with resistance R_{eq}. The push-pull converter incorporates essential energy storage elements: an input capacitor C and an inductor L.

The state-space model is derived through the application of Kirchhoff's laws to the system circuit. The state variables are selected as the capacitor voltage V_{PV} and inductor current I_L, forming the state vector:

$$\mathbf{x} = \begin{bmatrix} x_1 \\ x_2 \end{bmatrix} = \begin{bmatrix} V_{PV} \\ I_L \end{bmatrix}$$

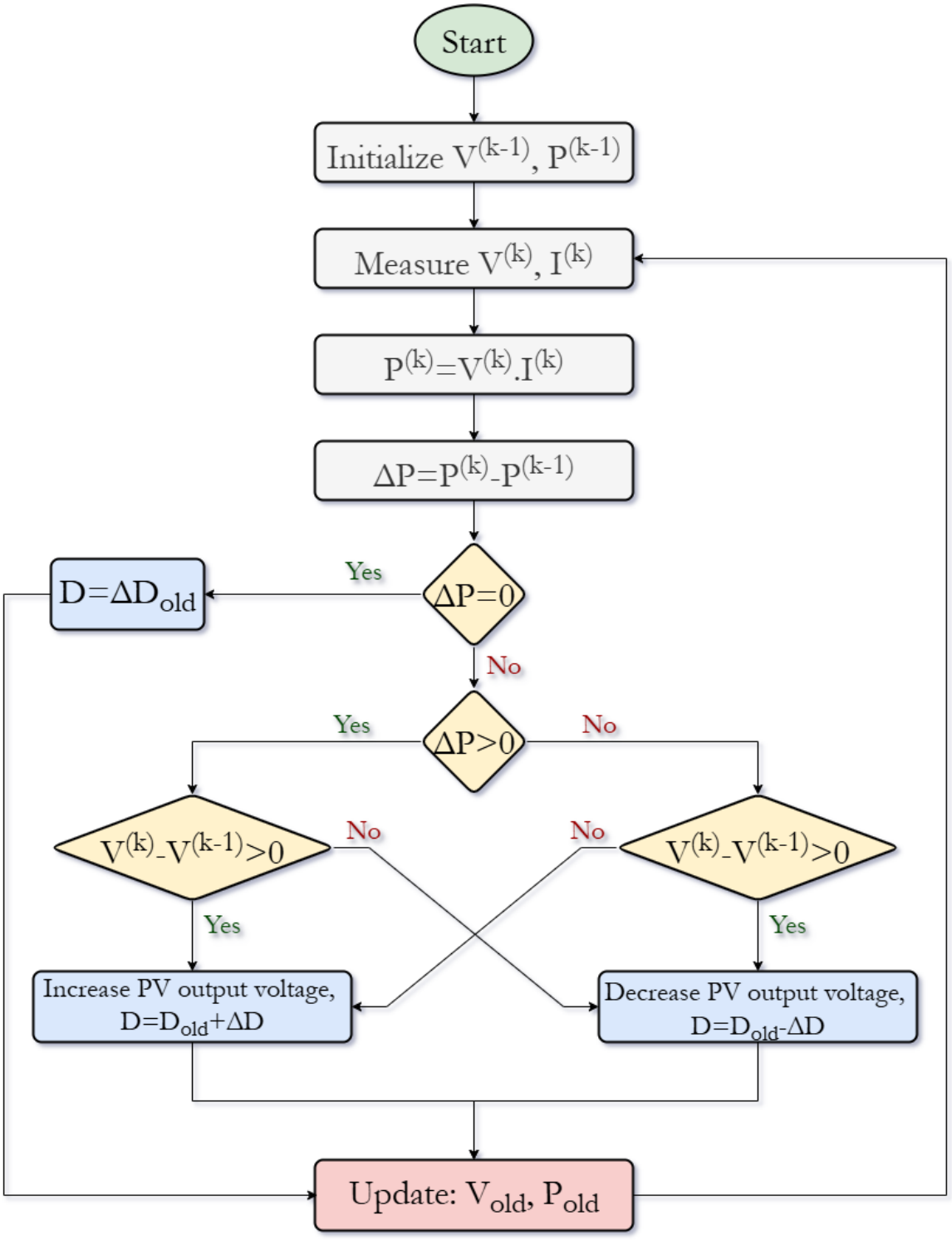

Figure 7: Perturb and Observe (P&O) MPPT algorithm

The control input is defined as the complementary duty cycle $d = 1 - D$, where D represents the duty cycle of the power switches. The system output is the PV voltage V_{PV}, which serves as the controlled variable.

Let us consider the continuous operation mode.

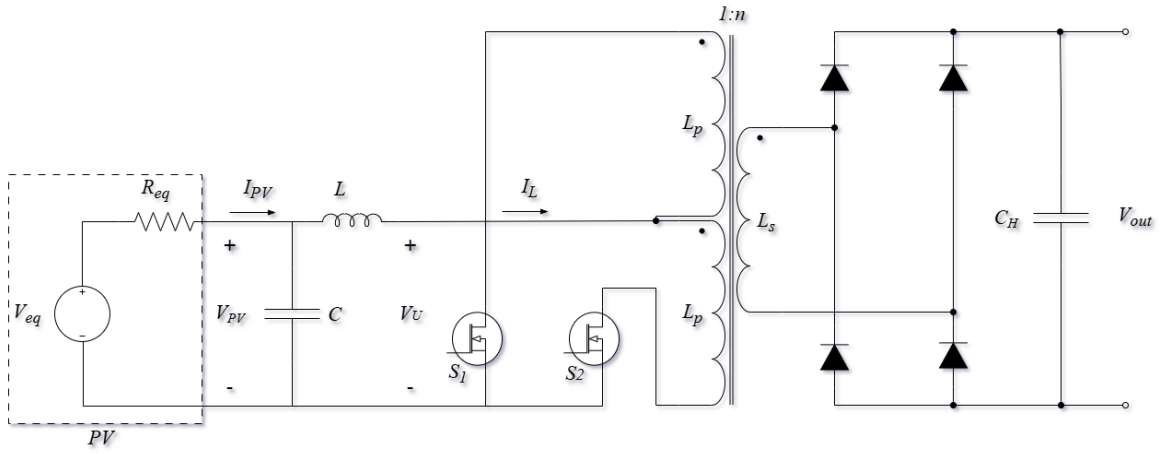

Figure 8: PV system with push-pull DC-DC converter interface circuit model

Apply Kirchhoff's Current Law (KCL) at the PV terminal:

$$I_{PV} = I_L + I_C$$

The current through the capacitor is $I_C = C\frac{dV_{PV}}{dt}$. From the PV equivalent model, the PV current is $I_{PV} = \frac{V_{eq}-V_{PV}}{R_{eq}}$.

Substitute and solve for $\dot{V_{PV}}$:

$$\frac{V_{eq} - V_{PV}}{R_{eq}} = C\frac{dV_{PV}}{dt} + I_L$$
$$\frac{dV_{PV}}{dt} = -\frac{1}{R_{eq}C}V_{PV} - \frac{1}{C}I_L + \frac{V_{eq}}{R_{eq}C}$$

This is the first state equation. For control design, V_{eq} is often considered a disturbance or its average is assumed to be zero over a switching period, simplifying the equation to:

$$\dot{V_{PV}} = -\frac{1}{R_{eq}C}V_{PV} - \frac{1}{C}I_L$$

Apply Kirchhoff's Voltage Law (KVL) to the loop containing the inductor:

Inductor voltage relates to load voltage and input voltage:

$$V_{PV} = V_L + V_U$$

The voltage across the inductor is $V_L = L\frac{dI_L}{dt}$. The input voltage to the push-pull converter V_U is given by the converter's input-output relationship: $V_U = d\frac{V_o}{n}$, where V_o is the constant output voltage and n is the transformer turns ratio.

Substitute and solve for :

$$V_{PV} = L\frac{dI_L}{dt} + d\frac{V_o}{n}$$
$$\frac{dI_L}{dt} = \frac{1}{L}V_{PV} - \frac{V_o}{nL}d$$

This is the second state equation.

The standard state-space form is:

$$\dot{\mathbf{x}} = \mathbf{A}\mathbf{x} + \mathbf{B}u$$
$$y = \mathbf{C}\mathbf{x}$$

Substitute the derived state equations x and x into this matrix form:

$$\begin{bmatrix} \dot{V}_{PV} \\ \dot{I}_L \end{bmatrix} = \begin{bmatrix} -\frac{1}{R_{eq}C} & -\frac{1}{C} \\ \frac{1}{L} & 0 \end{bmatrix} \begin{bmatrix} V_{PV} \\ I_L \end{bmatrix} + \begin{bmatrix} 0 \\ -\frac{V_o}{nL} \end{bmatrix} d$$
$$y = \begin{bmatrix} 1 & 0 \end{bmatrix} \begin{bmatrix} V_{PV} \\ I_L \end{bmatrix}$$

Where: $\mathbf{A} = \begin{bmatrix} -\frac{1}{R_{eq}C} & -\frac{1}{C} \\ \frac{1}{L} & 0 \end{bmatrix}$ is the state Matrix; $\mathbf{B} = \begin{bmatrix} 0 \\ -\frac{V_o}{nL} \end{bmatrix}$ is the input Matrix; $\mathbf{C} = \begin{bmatrix} 1 & 0 \end{bmatrix}$ is the output Matrix.

4 State-space feedback controller design

This section details the design methodology for the state-space feedback controller applied to the photovoltaic (PV) system with a push-pull DC-DC converter as illustrated in Figure 9. The primary objective of this controller is to ensure robust regulation of the PV panel voltage (V_{PV}) at a predefined reference, while simultaneously achieving desired transient performance and guaranteeing zero steady-state error.

To eliminate steady-state error for constant reference inputs, an integral control action is incorporated into the feedback loop. This necessitates augmenting the plant's state-space model by introducing a new state variable, x_N, which represents the integral

of the error between the reference voltage (r) and the actual PV voltage (V_{pv}), defined as:

$$x_N = \int (r - y)dt$$

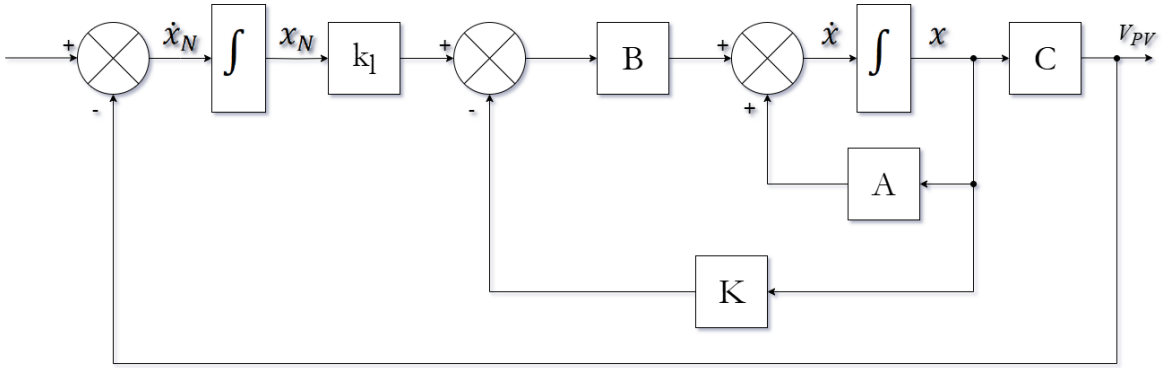

Figure 9: PV system with push-pull DC-DC converter interface circuit model

The complete state-space augmented system can then be expressed in the form:

$$\begin{aligned} \begin{bmatrix} \dot{x} \\ \dot{x}_N \end{bmatrix} &= \begin{bmatrix} A & 0 \\ -C & 0 \end{bmatrix} \begin{bmatrix} x \\ x_N \end{bmatrix} + \begin{bmatrix} B \\ 0 \end{bmatrix} u + \begin{bmatrix} 0 \\ 1 \end{bmatrix} r \\ y &= \begin{bmatrix} C & 0 \end{bmatrix} \begin{bmatrix} x \\ x_N \end{bmatrix} \end{aligned} \tag{22}$$

Where the augmented matrices are: $\mathbf{A_a} = \begin{bmatrix} -\frac{1}{R_{eq}C} & -\frac{1}{C} & 0 \\ \frac{1}{L} & 0 & 0 \\ -1 & 0 & 0 \end{bmatrix}$; $\mathbf{B_a} = \begin{bmatrix} 0 \\ -\frac{V_o}{nL} \\ 0 \end{bmatrix}$; $\mathbf{C_a} = \begin{bmatrix} 1 & 0 & 0 \end{bmatrix}$; $\mathbf{K_a} = \begin{bmatrix} k_1 & k_2 & k_l \end{bmatrix}$.

The design objective is to select such that the closed-loop poles achieve a prescribed transient behavior. The following performance specifications are adopted: settling time ($e.g., 3ms$), maximum overshoot OS ($e.g., 5\%$), zero steady-state error.

The dominant poles are determined from the classical second-order system relations:

$$\zeta = -\frac{\ln(OS)}{\sqrt{\pi^2 + \ln^2(OS)}}, \quad \omega_n = \frac{4}{\zeta t_s}$$

yielding complex conjugate poles:

$$p_{1,2} = -\zeta\omega_n \pm j\omega_n\sqrt{1-\zeta^2}$$

An additional auxiliary real pole α is placed at least five times further into the left-half plane to minimally affect the dominant dynamics:

$$p_3 = -\alpha, \quad \alpha \geq 5\,|\Re\,(p_{1,2})|$$

The desired closed-loop characteristic polynomial is then:

$$P_{des}(s) = (s-p_1)\,(s-p_2)\,(s-p_3)$$

Ackerman's method requires the inverse of the matrix of controllability ($\mathcal{C}$) calculated with the following equation:

$$\mathcal{C} = \left[\begin{array}{ccccc} B_a & A_aB_a & A_a^2B_a & \ldots & A_a^{n-2}B_a & A_a^{n-1}B_a \end{array}\right]$$

where $\mathcal{C} \in \mathbb{R}^{n\times mn}$.

Using Ackermann's formula, the feedback gain vector is obtained as:

$$K_a = \left[\begin{array}{ccccc} 0 & 0 & ... & 0 & 1 \end{array}\right].\mathcal{C}^{-1}.P_{des}(A_a) = \left[\begin{array}{ccc} k_1 & k_2 & k_I \end{array}\right]$$

5 Multi-sources Photovoltaic Energy System

In this section, we present a DC microgrid comprising three midrange residential photovoltaic (PV) prosumer systems [11]. The system configurations, including component specifications and operational parameters, are detailed in Tables 6 and 7.

To illustrate the proposed approach, we consider a multi-source energy system composed of three prosumers, each equipped with a Solar Photovoltaic Energy Source (SPVES). The corresponding state-space models are summarized in Table 8, derived from the circuit parameters listed in Table 7.

To achieve stable and efficient operation under varying irradiance conditions, the closed-loop system must meet specific transient performance objectives. Table 9

Table 6: Specifications of Prosumers systems

Specifications	Total Power (kW)	Panel Model	V_{mp} (V)	I_{mp} (A)	Panels configuration ($N_p \times N_s$)
Prosumer 1	7.83	Q.PEAK DUO L-G6 (435W)	41.81	10.41	2×9
Prosumer 2	7.74	REC AlphaPure2 (430W)	41.8	10.29	2×9
Prosumer 3	8.19	SunPower Maxeon 7 (455W)	37.42	12.16	2×9

Table 7: Parameters of the circuit models.

Parameters	$L\ (\mu H)$	$C\ (\mu F)$	$R_{eq}\ (\Omega)$	n	$I_{PV}\ (A)$	$V_{PV}\ (V)$	$V_o\ (V)$
Prosumer 1	451.8	62.6	18.07	1.33	20.82	376.29	250
Prosumer 2	457.0	61.9	18.28	1.33	20.58	376.2	250
Prosumer 3	346.2	65.5	13.85	1.48	24.32	336.78	250

Table 8: State space of the prosumers systems.

	Prosumer 01	Prosumer 02	Prosumer 03
$A_{a(i)}$	$\begin{bmatrix} -884.03 & -15974.44 & 0 \\ 2213.37 & 0 & 0 \\ -1 & 0 & 0 \end{bmatrix}$	$\begin{bmatrix} -883.76 & -16155.09 & 0 \\ 2188.18 & 0 & 0 \\ -1 & 0 & 0 \end{bmatrix}$	$\begin{bmatrix} -1102.32 & -15267.18 & 0 \\ 2888.50 & 0 & 0 \\ -1 & 0 & 0 \end{bmatrix}$
$B_{a(i)}$	$\begin{bmatrix} 0 \\ -416046.76 \\ 0 \end{bmatrix}$	$\begin{bmatrix} 0 \\ -411312.75 \\ 0 \end{bmatrix}$	$\begin{bmatrix} 0 \\ -487922.93 \\ 0 \end{bmatrix}$

defines these control response specifications, which include settling time t_s, overshoot O_s, that are used for deriving the damping ratio ζ and the natural frequency ω_n. These parameters determine the desired locations of the closed-loop dominant complex conjugate poles $p_{1,2}$ and thus directly guide the design of the feedback controller.

Table 9: Control response specifications.

Parameters	Prosumer 1	Prosumer 2	Prosumer 3
$t_s(ms)$	3	5	4
$O_s(\%)$	11	1	7
$p_{1,2}$	-1333.33 $\pm j$1897.72	-800 $\pm j$545.75	-1000 $\pm j$1181.38
p_3	-9333.33	-5600	-8269.66

Based on the desired response characteristics from Table 9, Table 10 presents the feedback gain values computed using *Ackermann's pole-placement formulation*. These

gains correspond to the augmented state-space system with integral action and are tuned to achieve the specified transient response and ensure zero steady-state error as illustrated in Figure 10.

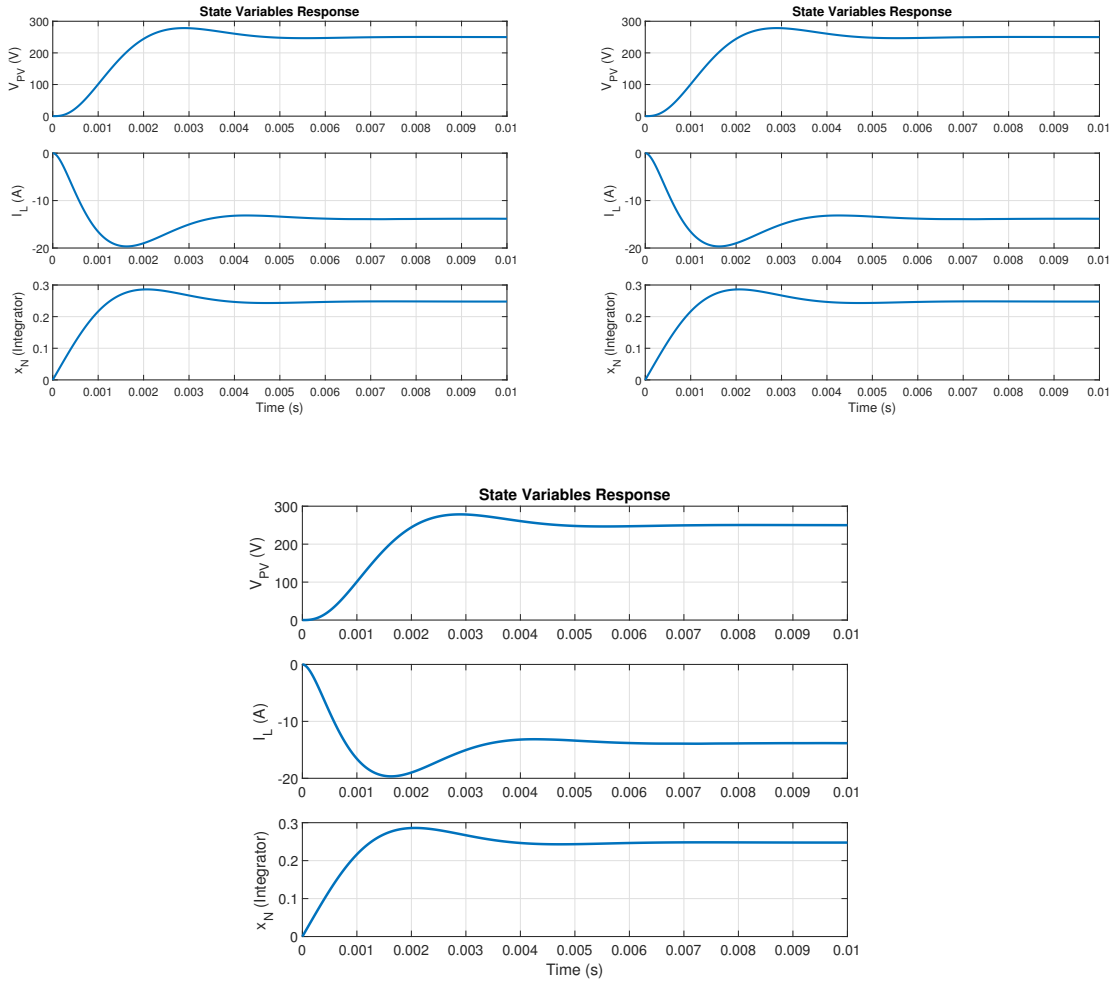

Figure 10: State Variables Responses: (a) Prosumer 01, (b) Prosumer 02, (c) Prosumer 03

Table 10: Controller gains.

Parameters	Prosumer 1	Prosumer 2	Prosumer 3
$\begin{bmatrix} k_1 & k_2 \end{bmatrix}$	$\begin{bmatrix} -0.0022 & -0.0267 \end{bmatrix}$	$\begin{bmatrix} -0.0047 & -0.0154 \end{bmatrix}$	$\begin{bmatrix} -0.0047 & -0.0188 \end{bmatrix}$
k_I	-7.5540	-0.7904	-2.6595

6 Conclusion

This chapter has established the necessary foundation for the control-oriented analysis of a multi-source energy system, focusing on its primary generating unit, the photovoltaic prosumer.

The process began with the fundamental principles of the photovoltaic effect, establishing the non-linear I-V and P-V characteristics of a semiconductor junction. The Single-Diode Model was selected and formulated as it provides an optimal balance between physical accuracy and mathematical tractability. Its parameters were then scaled from a single cell to a full array, capturing the collective behavior of the primary energy source.

Recognizing that a PV array cannot directly interface with a load or a network, the critical role of power electronics was addressed. The Push-Pull DC-DC converter topology was introduced as the key interface, responsible for regulating the energy flow. To ensure maximum energy harvest from the PV source under varying environmental conditions, the integration of a Perturb and Observe (P&O) Maximum Power Point Tracking (MPPT) algorithm was detailed. This established the core operational principle of the prosumer's generation side.

Through averaging and linearization techniques, a tractable yet precise state-space representation was derived, forming the core mathematical model of the prosumer node, representing the pivotal outcome of this chapter.

Building on this foundation, a state-space feedback controller was designed to ensure stable regulation of the PV system under dynamic operating conditions. This controller synthesis demonstrated how theoretical control principles can be translated into practical regulation strategies for renewable-based systems.

Furthermore, the analysis was further extended to a multi-source photovoltaic energy system, underscoring the flexibility of the modeling approach to encompass multiple prosumers operating within a microgrid environment, setting the stage for the networked stability analysis and sophisticated controller strategies to be developed in upcoming chapters.

PART TWO: SCIENTIFIC CONTRIBUTIONS

Chapter III: Network-Induced Delay Modeling

Chapter IV: NCS Stability Analysis

Chapter V: Networked Multi-source Energy System Controller Design

Chapter III: Network-Induced Delay Modeling

1 Introduction

Modeling Networked Control Systems (NCSs) presents critical challenges for control system design, as such systems inherently inherit imperfections and constraints from the underlying communication networks. These challenges include network-induced delays, packet dropouts, quantization errors, variable sampling and transmission intervals, and limited communication resources [31, 54]. If not properly addressed, these phenomena may significantly degrade system performance or even lead to instability.

This raises a fundamental question: how can the challenges posed by network imperfections be effectively addressed in NCS modeling to ensure robust and stable system performance?

To answer this question, it is important to recognize that the aforementioned imperfections collectively manifest themselves as communication delays, which can be regarded as a single global network-induced delay [14, 55]. Consequently, accurate delay modeling becomes mandatory, as it directly influences subsequent stages such as control design, state estimation, monitoring, and fault diagnosis. Several approaches for modeling network-induced delays in NCSs have been proposed in the literature [56], as discussed in Chapter 2.

Over the last decade, considerable research efforts have focused on the stability analysis of NCSs subject to network-induced delays, whose time-varying and random nature can severely degrade performance or destabilize closed-loop systems [57]. For instance, in [51], stability criteria were derived for closed-loop networked predictive control systems with constant delays, while [58] addressed NCS stability using a Lyapunov-based approach under unit time delay. Other works, such as [17, 18], developed linear matrix inequality (LMI)–based stability conditions relying

on distribution-dependent delay modeling and the Lyapunov–Krasovskii functional.

Alternative approaches incorporate Markov chain–based delay modeling. For example, [59] proposed an NCS model with Markovian delays, packet dropouts, disorder, and external disturbances using a CMAC neural network, while [60] extended stability analysis to develop a mode-dependent robust H_∞ controller for NCSs with Markovian jump delays. Although these methods provide satisfactory results, their effectiveness is intrinsically linked to the accuracy of the adopted delay model. In general, the more realistic the delay modeling, the more precise and reliable the resulting stability analysis.

In this study, a stochastic volatility–based modeling approach is adopted to characterize network-induced delays, due to its strong ability to emulate the inherent variability and temporal dependence of communication delays. Such modeling is expected to significantly enhance the accuracy of NCS stability analysis.

The foundations of stochastic control methodologies can be traced back to early works on signal transmission in communication systems. In this context, Claude E. Shannon, the pioneer of information theory, introduced a quantitative measure of information transmission and demonstrated the possibility of mitigating the effects of disturbances affecting transmitted signals [61]. Building on these ideas, Schützenberger [62] explored links between communication theory and game theory, proposing information measures based on linear operators for binary random variables. With the development of inferential statistics, the notion that observed variables can be modeled as realizations of stochastic processes governed by probabilistic laws became central to communication and network research [63].

Since random delays constitute one of the principal challenges in NCSs, numerous advanced techniques have been proposed to address stochastic network delays. Early approaches relied on optimal stochastic control methods, such as linear–quadratic–Gaussian (LQG) techniques based on delay statistics [24]. Other studies investigated NCS stability under long random delays [16, 64]. In recent years, further methods have been developed to cope with stochastic delays, particularly in Internet Protocol (IP)–based communication environments.

These approaches can generally be classified into two categories: models in which delays are probabilistically dependent and those assuming mutually independent delays. In the first category, probabilistic dependencies are often represented using

Bernoulli distributions or Markov chains [65, 66, 67]. When the probabilistic dependence is unknown, mutually independent delay models are typically employed within optimal stochastic control frameworks [68, 69, 70].

However, in real-time networked environments, stochastic delays cannot always be assumed to be mutually independent. Moreover, Markov-based models have been shown to exhibit limited real-time performance and may fail to accurately capture the statistical behavior of random delays in NCSs [71]. Empirical studies of network delays indicate non-uniform distributions characterized by right-skewness, excess kurtosis, and volatility clustering—where large delays tend to follow large delays and small delays tend to follow small delays. For example, most round-trip time (RTT) delays fall within a lower interval $[\tau_1; \tau_2)$, while only a small fraction occurs in an upper interval $[\tau_2; \tau_3)$, indicating that short delays dominate, whereas long delays occur with lower probability [18]. This behavior suggests the existence of two distinct delay regimes, which can be effectively modeled using regime-switching stochastic processes.

Such models have attracted significant attention in various scientific fields, including financial markets, speech recognition, population dynamics, traffic modeling, hydrology, and energy economics [72, 73, 74, 75]. Motivated by these findings, this chapter proposes the use of a Markov Regime-Switching GARCH (MRS-GARCH) model to capture the temporal dependence and volatility dynamics of network-induced delays. This framework allows different volatility regimes with distinct mean-reversion speeds and enables abrupt transitions between regimes while preserving a coherent volatility structure. To the best of our knowledge, the application of MRS-GARCH models to network-induced delay modeling in NCSs has not been previously reported, making this contribution novel and original.

Historically, GARCH models were developed within the context of time-series analysis to describe, predict, and control systems exhibiting time-varying variance. Their key principle lies in modeling conditional variance as a function of past observations. Several extensions have been proposed, including asymmetric models such as the Exponential GARCH (EGARCH) introduced by Nelson [76] and the Glosten–Jagannathan–Runkle (GJR-GARCH) model, which capture asymmetric responses of volatility to positive and negative shocks. The integration of GARCH models into a regime-switching framework led to the development of MRS-GARCH models by Gray [77] and Klaassen [78], which have demonstrated superior performance

over single-regime GARCH models in fitting financial time series.

The main contributions of this chapter can be summarized as follows:

- Introduction of stochastic volatility models, particularly GARCH-type models, as a novel framework for modeling network-induced random delays in NCSs.
- Adoption of an MRS-GARCH modeling approach to enable the development of more effective delay compensation and control strategies.

To address practical challenges related to data availability and reliability, real network delay measurements are obtained using the *Ping* utility, enabling an empirical characterization of delay behavior. This research contributes to the advancement of NCS modeling by providing a realistic representation of communication-induced delays and enhancing stability analysis through the proposed MRS-GARCH framework.

The implementation procedure adopted in this chapter is summarized as follows:

1. **Data Collection and Analysis:** Acquisition of real-world latency measurements and statistical analysis to identify key delay characteristics.
2. **Model Development:** Construction and estimation of MRS-GARCH–based stochastic volatility models and validation against empirical data.
3. **Numerical Validation:** Simulation-based evaluation of the proposed approach using real delay data samples.

The remainder of this chapter is organized as follows. Section 2 presents the theoretical background of GARCH(1,1), EGARCH, GJR-GARCH, and MRS-GARCH models, along with their estimation procedures. Section 3 applies these models to a real dataset of IP communication delays collected from an Algerian ADSL network and provides a comparative empirical analysis. The objective is to identify the most suitable model for capturing the statistical properties of network delays, thereby establishing a solid foundation for subsequent stability analysis and controller synthesis in NCSs.

2 GARCH-type models

In this section, we take a brief look at various GARCH-type models used in this study to model network-induced discrete-time delays. Formally, a GARCH $(1, 1)$ model of Bollerslev [79] for the series $\tau(k)$ with constant mean τ and conditional variance $\sigma(k)$ can be written as

$$\begin{cases} \tau(k) = \tau + u(k) = \tau + \sqrt{\sigma(k)}\varepsilon(k) \\ \sigma(k) = \omega + \alpha u^2(k-1) + \beta\sigma(k-1) \end{cases} \tag{23}$$

where $\varepsilon(t)$ are zero-mean independent random variables (possibly Gaussian) with unit variance, $\omega > 0$, $\alpha \geq 0$, $\beta \geq 0$, The weak stationarity condition for the model defined by Equations (23) is approximately given by $\alpha + \beta < 1$.
Nelson (1991) [76] dealt with the asymmetry effect and external shocks in volatility by introducing the (EGARCH) model defined as:

$$\begin{cases} \tau(k) & = \tau + u(k) = \tau + \sqrt{\sigma(k)}\varepsilon(k) \\ \log\sigma(k) & = \omega + \alpha\left|\frac{u(k-1)}{\sigma(k-1)}\right| + \zeta\frac{u(k-1)}{\sigma(k-1)} \\ & \quad +\beta\log\sigma(k-1) \end{cases} \tag{24}$$

with no constraints on parameters.

To take into account the effect of negative shocks on volatility, the GJR GARCH model of Glosten, Jagannathan, and Runkle (1993) [80] has seen the light with the following specification,

$$\begin{cases} \tau(k) & = \tau + u(k) = \tau + \sigma(k)\varepsilon(k) \\ \sigma^2(k) & = \omega + \alpha u^2(k-1) + \gamma I(k-1)u^2(k-1) \\ & \quad +\beta\sigma^2(k-1) \end{cases} \tag{25}$$

where $\omega > 0$, $\alpha \geq 0$, $\beta \geq 0$, $\gamma \geq 0$ and

$$I(k-1) = \begin{cases} 0 & if \quad u(k-1) \geq 0, \\ 1 & if \quad u(k-1) < 0, \end{cases}$$

However, estimates of the above GARCH models have been shown to be biased due to structural breaks in the dynamics of volatility [81]. One possible solution is to allow the conditional variance to move in time from one GARCH process to another. This led to the Markov Regime-Switching GARCH (MRS-GARCH) model developed by Gray (1996) [77] and Klaassen (2002) [78]. In this framework, a state variable s_k following a first-order Markov chain is assumed to be an unobserved latent random variable affecting the observed variables.

Such an approach is attractive because it enables the use of a mixture of distributions with different characteristics, wherein the current value of the variable is obtained,

depending on the more likely state that could have been the source of such observation. The state variable is governed by a first-order stationary and irreducible Markov chain, with transition probability

$$Pr\left(s_k = j \backslash s_{k-1} = i\right) = p_{ij}$$

which is the probability of switching from state i at time $k-1$ into state j at time k. The initial non-conditional probability of being in state 1 is given by $Pr\left(s_0 = 1\right) = \pi_0 = \frac{1-p_{11}}{2-p_{11}-p_{22}}$. The MRS-GARCH model $\{\tau(k)\}$, for $k = 1, \ldots, T$, can be written as,

$$\begin{cases} \tau(k) = \tau_{s_k} + u(k) = \tau_{s_k} + \sigma_k\left(s_k\right)\varepsilon(k) \\ \sigma_k^2\left(s_k\right) = \omega\left(s_k\right) + \alpha\left(s_k\right)u^2(k-1) + \beta\left(s_k\right)\sigma_{k-1}^2\left(s_k\right) \end{cases} \tag{26}$$

where $s_k \in \{1, 2\}$, $\omega(i) > 0$, $\alpha(i) \geq 0$, and $\beta(i) \geq 0$, $i = 1, 2$ for positivity of the conditional variance. The ex-ante probability $\pi_k = Pr\left(s_k = 1 \backslash \zeta_{k-1}\right)$ can be calculated from,

$$\begin{array}{l} \pi_k = p_{11}\left[\frac{f(\tau(k)\backslash s_{k-1}=1)(1-\pi_{k-1})}{f(\tau(k)\backslash s_{k-1}=1)\pi_{k-1}+f(\tau(k)\backslash s_{k-1}=2)(1-\pi_{k-1})}\right] \\ + (1-p_{22})\left[\frac{f(\tau(k)\backslash s_{k-1}=2)(1-\pi_{k-1})}{f(\tau(k)\backslash s_{k-1}=1)\pi_{k-1}+f(\tau(k)\backslash s_{k-1}=2)(1-\pi_{k-1})}\right] \end{array} \tag{27}$$

where $f\left(\cdot \backslash s_k = j\right)$ denotes the conditional distribution of $\tau(k)$ given that regime j occurs at time k and ζ_{k-1} is the information set up to time $k-1$. For the process defined by Equation (26), explicit stationarity conditions can be found in [82]. Moreover, notice that, for all time point k, the conditional mean of the observation $\tau(k)$ is $\tau_{s_k} = E\left(\tau(k) \backslash s_k\right)$ and the conditional variance is $\sigma_k^2\left(s_k\right) = Var\left(\tau(k) \backslash \tau(1), \ldots, \tau(k-1), s_k\right)$.

For all the single-regime GARCH models defined by Equations (23), (24) and (25), the model parameters can be estimated using maximum likelihood estimation (MLE) by maximizing the log-likelihood. Distributional assumptions on $\varepsilon(k)$ have to be made, so $\varepsilon(k)$ can be assumed to be *i.i.d.* $N(0, 1)$. This choice is not as restrictive as it seems because even in the case of a different distribution, the QuasiMaximum Likelihood (QML) approach can still be used to obtain a consistent estimator under pretty mild regularity conditions. In this case, $\tau(k)$ is conditionally distributed as,

$$\tau(k) \backslash \{\tau(k-1), \sigma(k-1)\} \sim \mathcal{N}\left(\tau, \sigma^2(k)\right) \tag{28}$$

For a sample $(u(1), \ldots, u(N))$, the (conditional) sample log-likelihood function is given by,

$$L(\theta) = \sum_{t=1}^{N} \frac{1}{2}\left[-\log 2\pi - \log \sigma^2(t) - \frac{u^2(t)}{\sigma^2(t)}\right].$$

Note here that $L(\theta)$ computes the volatility recursion and the log-likelihood. The (MLE) estimator of each model parameters is then obtained iteratively by solving a constrained maximization of the likelihood function with respect to the model parameter.

For the MRS-GARCH, a quasi-maximum likelihood approach in a recursive way could be undertaken using the ex-ante probability π_k given in (27). This estimation procedure is described in detail in the appendix of [78].

3 GARCH-type modeling of communication delay in IP-based NCS

The purpose of this part aims to illustrate how the GARCH-type models described in the previous section provide a suitable and flexible tool for modeling the network-induced delay. To empirically compare GARCH, EGARCH, GJR-GARCH, and MRS-GARCH models, we work on the dataset described in the next subsection. The mean and volatility structure of the considered communication delay in IP ($CD-IP$) will also be analyzed in the rest of the section.

3.1 Data description

As argued above, communication delay stands out as a crucial factor impacting overall network performance. To assess network efficiency and quality, various tools, both software-based and hardware-based, are employed. These tools offer insights into different aspects of network performance. Among these methods, the Ping utility is widely recognized and extensively utilized for measuring communication delay in IP networks.

In essence, Ping, short for Packet Internet or Inter-Network Groper, is a networking utility designed to examine a host's accessibility on an Internet Protocol (IP) network. It functions by transmitting Internet Control Message Protocol (ICMP) packets. The process involves sending an ICMP echo request to the target host, awaiting an ICMP echo reply, and subsequently measuring the round-trip time (RTT).

In Algeria, the most widely used communication technology to provide internet is the internet protocol IP network based on PPPoE, which is a protocol for encapsulating data packets over Ethernet networks for transmission over ADSL connections. PPPoE is used to establish a connection between a user's computer and an Internet Service

Provider (ISP), allowing for data transmission over an ADSL line. For a data rate of 15Mbps, a ping tool is used to measure the latency of the communication network to know the behavior of the network-induced delay phenomena. The utilized settings of the tool are illustrated in Table 11.

Table 11: SETTING OF THE TOOL

Option	value
Ping time-out	4000 ms
Delay between Pings	1000ms
Target host (address)	www.algerietelecom.dz
IP address	197.112 .0 .217
Location	Algeria

Figure 11 displays the collected $(CD - IP)$ data during the sampling period. The trajectory in Figure 11 clearly exhibits the two most prominent features, namely, volatility clustering and a time-varying mean.

The histogram related to the considered data is shown in Figure 12. It is skewed to the left revealing a probably asymmetric probability density.

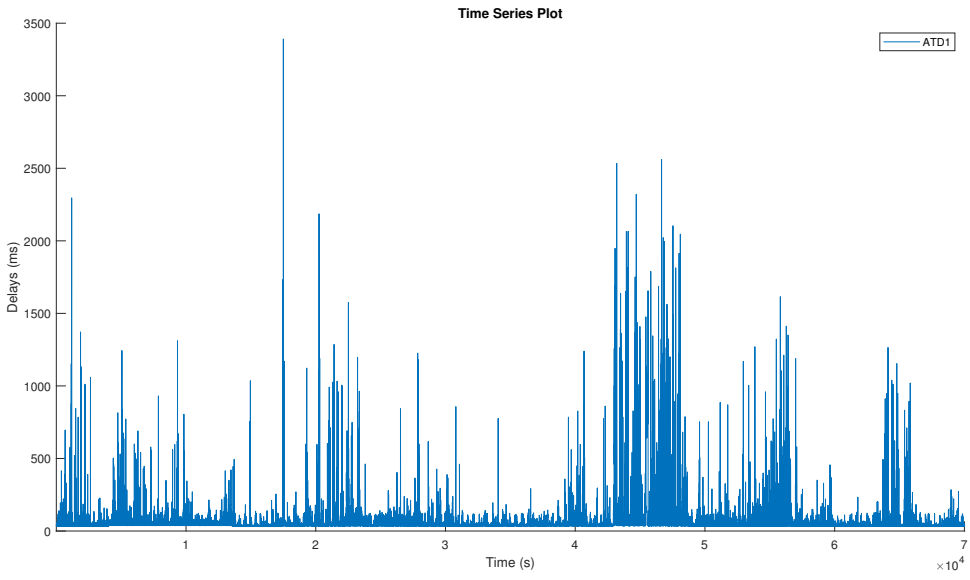

Figure 11: Communication delay in IP (CD-IP)

Some descriptive statistics of the above data are shown in Table 12.

We can notice that:

- As expected, the skewness is significantly high and positive, indicating that small values of the observed delays are more frequent than higher values.

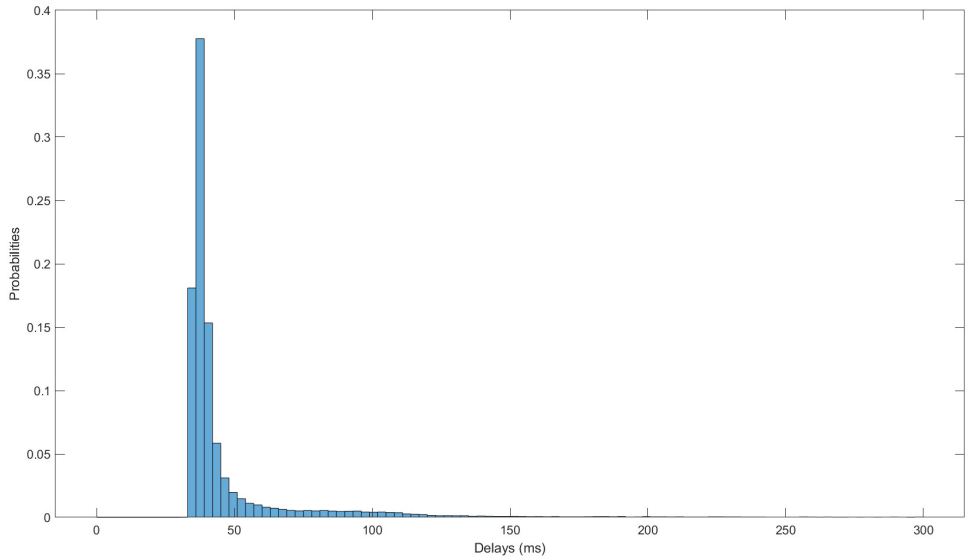

Figure 12: Histogram of the network delay shown in figure 11

Table 12: Descriptive statistics of the data

Min	Max	Mean	Std	Kurtosis	Skewness
32	3391	$59,3$	$101,5$	129.5	9.5

- The kurtosis is significantly higher than the normal value of 3, indicating that fat-tailed distributions are necessary to correctly describe the distribution of the current data.

To assess the presence of conditional heteroscedasticity in our series, we conducted Engle's ARCH test. The test is run assuming an ARCH(1) alternative model; then it is run again assuming an ARCH(2) alternative model. An overall significance level of 0.05 is maintained by decreasing the significance level of each test to $0.05/2 = 0.025$. The test results appear in Table 13.

Table 13: Results of Engle's ARCH test

Null hypothesis: no ARCH effect					
Null rejected	P-value	Test statistic	Critical value	Lags	Significance level
true	0	$7,8964e^{+3}$	$5,0239$	1	0.025
true	0	$9,3250e^{+3}$	$7,3778$	2	0.025

The null hypothesis of no ARCH effects is rejected by the tests against the alternative models. Specifying a conditional variance model for the data with at least two ARCH lags is strongly recommended in view of this result. For this, models with

one ARCH and one GARCH lag are considered for the actual (CD-IP) data, namely, GARCH(1,1), EGARCH(1,1), GJR(1,1), and first-order MRS-GARCH-type models.

Remark 2 *The initialization parameters of all GARCH-type models presented in this section are very important to the accuracy of modeling and predicting random communication delays. An entropy or cluster-based initialization method can be used to obtain the optimal initialization of these parameters.*

3.2 Analysis and model selection

Based on the aforementioned data description, we first analyze one regime model (GARCH, EGARCH, GJR-GARCH), and then we use MRS-GARCH-type models to take regime switching into account.

Hence, we fit GARCH(1,1), EGARCH(1,1), GJR-GARCH(1,1) models to our data. Next, first order two regimes MRS-GARCH\GARCH, EGARCH\ EGARCH, GJR-GARCH\GJR-GARCH, GARCH\GJR-GARCH, GARCH\ EGARCH, and GJR-GARCH\EGARCH models are fitted. The set of competing GARCH-type models is estimated using quasi-maximum likelihood with jointly the normal and the Student's-t distributions. Particularly, for each GARCH-type model, the likelihood function is defined based on the model's structure and assumptions, such as the conditional mean and variance equations. The optimization algorithm, often a numerical optimization technique like the Newton-Raphson method or the Broyden-Fletcher-Goldfarb-Shanno (BFGS) algorithm, is then employed to find the parameter values that maximize this likelihood function.

Once the parameters are estimated, model evaluation criteria are used to assess the model's goodness-of-fit with the observed data. The log-likelihood (LL), Akaike information criterion (AIC), and Bayesian information criterion (BIC) criteria are used to quantify the improvement to the modeling brought by the best model compared to the others. As can be seen in Table 14, MRS-GARCH(1,1)\GARCH(1,1) model with normal and Student-t conditional distribution for the first and the second regime, respectively, outperforms all alternative models for the aforementioned criteria (it has the largest log-likelihood and the lowest AIC and BIC among competitive models).

To conclude this section, we can tell that among the thirty-three models, MRS GARCH-norm \ GARCH-t outperforms other alternatives. The proposed modeling could be seen as an important contribution to determining accurate volatility models in

Table 14: Alternative Garch models comparison

Conditional distributions	Regimes	Conditional volatility models	AIC	BIC	LL
Normal distribution	Single regime	Garch	784905.6170	784933.0867	-392449.8085
		EGarch	784822.0991	784858.7254	-392407.0495
		GJRGarch	784908.7478	784945.3741	-392450.3739
	2-regime Markov-switching	MRS(Garch)	760060.5657	760133.8182	-380022.2829
		MRS(eGarch)	759583.6543	759675.2199	-379781.8271
		MRS(GJRGarch)	760424.7593	760516.3249	-380202.3796
		MRS(Garch, EGarch)	759609.5331	759691.9421	-379795.7665
		MRS(Garch, GJRGarch)	760081.8428	760164.2519	-380031.9214
		MRS(EGarch, GJRGarch)	759730.2988	759821.8644	-379855.1494
Student-t distribution	Single regime	Garch	765169.7622	765206.3885	-382580.8811
		EGarch	766122.8693	766168.6521	-383056.4346
		GJRGarch	765172.2513	765218.0341	-382581.1256
	2-regime Markov-switching	MRS(Garch)	758550.4368	758642.0024	-379265.2184
		MRS(eGarch)	758674.0382	758783.9170	-379325.0191
		MRS(GJRGarch)	758555.2479	758665.1267	-379265.6240
		MRS(Garch, EGarch)	758646.9212	758747.6434	-379312.4606
		MRS(Garch, GJRGarch)	759089.7466	759190.4688	-379533.8733
		MRS(EGarch, GJRGarch)	758688.5651	758798.4439	-379332.2826
Mixture	2-regime Markov-switching	MRS($EGarch_{norm}, Garch_{std}$)	758316.4963	758408.0620	-379148.2482
		MRS($EGarch_{std}, Garch_{norm}$)	759869.6448	759961.2105	-379924.8224
		MRS($Garch_{norm}, Garch_{std}$)	758310.1821	758392.5912	-379146.0910
		MRS($EGarch_{norm}, EGarch_{std}$)	758476.3340	758577.0562	-379227.1670
		MRS($GJRGarch_{std}, GJRGarch_{norm}$)	759807.3001	759908.0223	-379892.6500

communication delay. Finally, this study revealed that regime-switching characteristics of the volatility in $(CD - IP)$ data are also critical features to be considered.

4 Conclusion

This chapter has presented a novel and robust framework for modeling network-induced delays by leveraging the power of GARCH-type econometric models. The empirical investigation of a real-world IP communication delay dataset confirmed the presence of significant volatility clustering, asymmetry, and structural breaks—features that necessitate a sophisticated modeling approach beyond conventional time-series methods.

Our comprehensive model comparison, evaluated using log-likelihood, AIC, and BIC criteria, yielded a clear and significant result: the Markov Regime-Switching GARCH model with a mixed conditional distribution (specifically, MRS-GARCH-norm GARCH-t) outperformed all competing single-regime and homogeneous regime-switching models. This finding is pivotal. It demonstrates that the volatility of network delays is not only time-varying but also subject to discrete shifts between distinct regimes, likely corresponding to different network states such as normal operation and congested periods. The superior fit of the mixed-distribution MRS model underscores the importance of allowing for different error distributions (e.g., Normal vs. Student-t) in different regimes to capture the fat-tailed behavior observed in the data.

In conclusion, this study makes a substantive contribution to the field of networked control systems by introducing and validating a highly accurate and flexible modeling paradigm for stochastic delays. The proposed MRS-GARCH methodology successfully captures the key stylized facts of network delay data, including volatility clustering, asymmetry, and regime-dependent behavior. This accurate stochastic model is not an end in itself; it serves as a critical prerequisite for the subsequent development of advanced control strategies. By providing a more realistic characterization of delay uncertainty, the model established in this chapter forms an essential foundation for the design of resilient, high-performance controllers that can explicitly account for the complex stochastic nature of network environments, which will be explored in the following chapters.

Chapter IV: NCS Stability Analysis

Using the stochastic delay model developed in the previous chapter—where network-induced delays are characterized by an MRS-GARCH process—this chapter concentrates on the stability analysis of Networked Control Systems (NCSs). Leveraging the time-varying, regime-switching delay description already introduced, we derive Lyapunov–Krasovskii–based stability conditions and cast them as Linear Matrix Inequalities (LMIs) suitable for practical verification and controller synthesis. The analysis quantifies the Maximum Allowable Upper Delay Bound (MAUDB) and demonstrates reduced conservatism relative to conventional deterministic or simplified stochastic models, thereby providing a more realistic and less conservative stability assessment for NCSs operating under volatile communication conditions.

1 Introduction

The integration of communication networks into control loops has given rise to *Networked Control Systems* (NCSs), offering numerous advantages such as reduced wiring, lower costs, and simplified maintenance. However, this architecture introduces network-induced phenomena, with time-varying communication delays being a primary concern for system stability and performance.

This chapter addresses this challenge by presenting a novel stability analysis framework for NCSs that leverages a sophisticated *Markov-Regime-Switching GARCH* (MRS-GARCH) model to characterize network-induced delays. The MRS-GARCH model is particularly well-suited for this task, as it can capture both the time-varying volatility and the regime-switching behavior often observed in network traffic. By integrating this realistic delay model into the control system description, we move beyond conventional approaches to derive less conservative stability conditions. The

core contribution of this chapter is the formulation of a delay-dependent stability criterion using a Lyapunov-Krasovskii functional. This criterion is cast as a set of *Linear Matrix Inequalities* (LMIs), which are computationally tractable and allow for the determination of a *Maximum Allowable Delay Bound* (MADB) that guarantees the mean-square stability of the closed-loop system. The proposed method not only provides a more accurate stability assessment but also offers valuable insights into how the parameters of the MRS-GARCH model, such as transition probabilities and volatility coefficients, influence the system's robustness. The theoretical findings are validated through numerical examples, demonstrating the reduced conservatism and practical applicability of the proposed approach.

The remainder of this chapter is organized as follows. Section 2 presents the problem formulation, beginning with the continuous-time plant model and the assumptions for the NCS. It details the proposed MRS-GARCH-based delay characterization and introduces the mode-dependent feedback control law that accounts for the delay's regime-switching behavior. Section 3 contains the main theoretical results, where a Lyapunov-Krasovskii functional is employed to derive delay-dependent stability conditions. These conditions are then cast as Linear Matrix Inequalities (LMIs) in Theorem 5, providing a computationally verifiable criterion for mean-square stability. Finally, Section 4 presents numerical examples to validate the theoretical findings. These examples demonstrate the reduced conservatism of the proposed method compared to existing approaches and investigate the impact of the MRS-GARCH model parameters, including transition probabilities and volatility coefficients, on the Maximum Allowable Upper Delay Bound (MAUDB). Section 5 concludes the chapter.

2 NCSs stability analysis based on MS-GARCH delay modeling

The application of the Markov-Regime-Switching GARCH (MRS-GARCH) model to Networked Control Systems (NCSs) offers several key advantages. Firstly, it effectively captures the temporal dependence of random delays inherent in IP-based networks, accommodating the complex dynamics of delay behavior. Secondly, the MRS-GARCH model identifies different volatility regimes within delay dynamics, providing a nuanced understanding of variability in delay behavior compared to traditional models.

The main theorem in this section enables the determination of a Maximum Allowable Delay-Bound (MADB) that guarantees the stability of the networked system, allowing more knowledge about its effectiveness and practical applicability in real-world scenarios.

2.1 Control strategy

Consider a plant governed by the following continuous-time linear model,

$$\dot{x}(t) = Ax(t) + B\mathcal{U}(t) \tag{29}$$

with the given initial condition of the system

$$x(t) = \eta(t), \quad t \in [-\tau_3, -\tau_1]$$

where $x(t) \in \mathbb{R}^n$ and $\mathcal{U}(t) \in \mathbb{R}^m$ are state and control vectors, respectively, $A \in \mathbb{R}^{n\times n}, B \in \mathbb{R}^{n\times m}$ are constant matrices. $\eta(t)$ is the associated function of the initial state.

Some common assumptions in NCSs open literature are made as follows:

1. The controller and the actuator are event-driven, and the sensor is clock-driven.
2. The data are transmitted with a single packet, and all the state variables are available for measurement.
3. Only the round trip delay $\tau(t)$, at time t, is of interest and it is assumed to be the key reason for IP network quality-of-service (QoS). Denote $\tau_1 = \inf_t(\tau(t))$ and $\tau_3 = \sup_t(\tau(t))$.
4. We employ a piecewise continuous feedback controller, constructed by a zero-order-hold (ZOH), given by,

$$\begin{gathered}\mathcal{U}(t) = Kx(t - \tau(t)), \quad t \in [kT, (k+1)T[, \\ k = 1, 2 \ldots, \mathcal{N}\end{gathered} \tag{30}$$

   where K is fixed feedback gain for all the network controller, $\mathcal{N} \in \mathbb{N}^*$ is a given finite number, $\tau(t) \in [\tau_1, \tau_3]$ and T is the sampling period.

Remark 3 *Assumption (iv) means that the sensor acts in a time-driven way, that is sampling at the times $kT, T \in \mathbb{N}$ and $k = 1, 2 \ldots, \mathcal{N}$*

Now, assume that $(\tau(kT))_k$ is the fitted stochastic MRS-GARCH $(1,1)$ (norm, std) model defined in Section 2. Then the behavior of the network induced delay $\tau(t)$ for $t \in [kT, (k+1)T[,\ k = 1, 2 \ldots, \mathcal{N}$, can be described as follows:

$$\begin{cases} \tau_1 \leq \tau(t) \leq \tau_3 < \infty, \quad \forall\, t \geq 0 \\ \text{Prob}\left(\tau(t) \in [\tau_1, \tau_2]\right) = \pi_k, \forall\, kT \leq t < (k+1)T \\ \text{Prob}\left(\tau(t) \in [\tau_2, \tau_3]\right) = 1 - \pi_k, \forall\, kT \leq t < (k+1)T \end{cases} \tag{31}$$

where τ_2 is the bound separating the lower and the upper intervals in which the delays vary, $\{\tau(t) \in [\tau_1, \tau_2]\}$ and $\{\tau(t) \in [\tau_2, \tau_3]\}$ represent the first and the second state of the delay, respectively, π_k as defined in (32), with $\sigma(kT)$ recursively calculated using (26).

Define the white sequence $\delta(t)$ as

$$\delta_k(t) = \begin{cases} 1, & t \in \Phi_1(k) \\ 0, & t \in \Phi_2(k) \end{cases} \tag{32}$$

Where $\Phi_1(k) = \{t \in [kT, (k+1)T[: \tau(t) \in [\tau_1, \tau_2)\}$,

$\Phi_2(k) = \{t \in [kT, (k+1)T[: \tau(t) \in [\tau_2, \tau_3)\}$.

Hence, for all $k = 1, 2 \ldots, \mathcal{N}$

$$\begin{cases} \text{Prob}\left[\delta_k(t) = 1\right] = \pi_k, & for\ kT \leq t < (k+1)T \\ \text{Prob}\left[\delta_k(t) = 0\right] = 1 - \pi_k, & for\ kT \leq t < (k+1)T \end{cases} \tag{33}$$

To take into account the delay distribution information proposed in (31) and using (32), the feedback control law (30) is replaced by the following one,

$$\mathcal{U}(t) = \sum_{k=1}^{\mathcal{N}} I_{[kT,(k+1)T[}(t) \left[\delta_k(t) Kx\left(t - \tau_1^k(t)\right) + (1 - \delta_k(t))\, Kx\left(t - \tau_2^k(t)\right)\right] \tag{34}$$

where $I_B(.)$ is the indicator function and $\tau_1^k(t) = \delta_k(t)\tau(t)$, $\tau_2^k(t) = (1 - \delta_k(t))\,\tau(t)$, $k = 1, 2 \ldots, \mathcal{N}$.

Remark 4 *The feedback controller (34) covers all possible states of our system and provides the necessary control actions for each state. The use of the controller (34) allows for a unified controller that handles different states or intervals within a single streamlined implementation that can simplify the control logic for the considered system.*

Using the new feedback control law (34), the closed-loop control system (29) becomes,

$$\begin{cases} \dot{x}(t) = & Ax(t) + \sum_{k=1}^{\mathcal{N}} I_{[kT,(k+1)T[}(t) \left[\delta_k(t) BKx\left(t - \tau_1^k(t)\right) + (1 - \delta_k(t)) BKx\left(t - \tau_2^k(t)\right)\right], \\ x(t) = & \eta(t), \quad t \in [-\tau_3, -\tau_1] \end{cases} \tag{35}$$

Remark 5 *A first-order MRS($GARCH_{norm}$ / $GARCH_{std}$) has been considered to model the delay in Eq. (35). When the delay volatility is reduced to a constant (i.e. $\alpha(1) = \alpha(2) = \beta(1) = \beta(2) = 0$), model (35) can be likened to model (10) of Peng et al. 2009 [18] in case of Bernouilli delay distribution having parameter $\bar{\delta} = \frac{p_{11}+p_{22}}{2}$, where p_{ii} are the transition probabilities from state i to state $i, i = 1, 2$.*

2.2 Main results

Based on the proposed stochastic time-dependent delay, a stability criterion in the mean square for the closed-loop control system (35) is obtained in the following theorem.

Theorem 5 *The closed-loop system given by (35) is asymptotically stable in the mean square if, for given $\tau_1, \tau_2, \tau_3, \mathcal{N}$, and matrix K, there exist matrices $P > 0, M_i > 0, G_i > 0, H_j > 0$ $(i = 1, 2, 3,\ j = 1, 2)$ with appropriate dimensions such that, for all $k = 1, 2 \ldots, \mathcal{N}$ the following LMIs hold,*

$$\Lambda_{=} \begin{bmatrix} \Lambda_{11} & \Lambda_{12} & \Lambda_{13} \\ * & \Lambda_{22} & 0 \\ * & * & \Lambda_{33} \end{bmatrix} < 0, \tag{36}$$

where

$$\Lambda_{11} = \begin{bmatrix} \mathcal{G}_{11} & \mathcal{G}_{12} & \mathcal{G}_{13} & 0 & \mathcal{G}_{15} & 0 \\ * & \mathcal{G}_{22} & \mathcal{G}_{23} & 0 & 0 & 0 \\ * & * & \mathcal{G}_{33} & \mathcal{G}_{34} & 0 & 0 \\ * & * & * & \mathcal{G}_{44} & \mathcal{G}_{45} & 0 \\ * & * & * & * & \mathcal{G}_{55} & \mathcal{G}_{56} \\ * & * & * & * & * & \mathcal{G}_{66} \end{bmatrix}$$

$$
\begin{aligned}
\Lambda_{12} =& diag\left(A^T, 0, \mathfrak{X}\pi_k K^T B^T, 0, \beta\left(1-\pi_k\right) K^T B^T, 0\right) \Psi \\
\Lambda_{13} =& \mathfrak{X}\pi_k(1-\pi_k) diag\left(0, 0, K^T B^T, 0, -K^T B^T, 0\right) \Psi, \\
\Lambda_{22} =& diag\left(-G_1, -G_2, -G_3, -H_1, -H_2\right), \\
\Lambda_{33} =& \mathfrak{X}\pi_k\left(1-\pi_k\right)\Lambda_{22}, \\
\Sigma =& diag\left(\tau_1 G_1, \tau_2 G_2, \tau_3 G_3, \left(\tau_2-\tau_1\right) H_1, \left(\tau_3-\tau_2\right) H_2\right) \\
\Psi =& Ones(6,5)\Sigma, \qquad \mathfrak{X} = \sum_{k=1}^{\mathcal{N}} I_{[kT,(k+1)T[},
\end{aligned}
$$

and

$$
\begin{aligned}
&\mathcal{G}_{11} = PA + A^T P + M_1 + M_2 + M_3 - G_1 - G_2 - G_3 \\
&\mathcal{G}_{12} = G_1, \quad \mathcal{G}_{13} = \mathfrak{X}\pi_k PBK + G_2, \\
&\mathcal{G}_{15} = \mathfrak{X}\left(1-\pi_k\right) PBK + G_3, \quad \mathcal{G}_{22} = -M_1 - G_1 - H_1, \\
&\mathcal{G}_{23} = H_1, \quad \mathcal{G}_{33} = -2G_2 - 2H_1, \quad \mathcal{G}_{34} = G_2 + H_1, \\
&\mathcal{G}_{44} = -M_2 - G_2 - H_1 - H_2, \quad \mathcal{G}_{45} = H_2, \\
&\mathcal{G}_{55} = -2G_3 - 2H_2, \quad \mathcal{G}_{56} = G_3 + H_2, \\
&\mathcal{G}_{66} = -M_2 - G_3 - H_2,
\end{aligned}
$$

Ones $(6,5)$ *is an* $6-by-5$ *matrix of ones.*

Proof 1 *Define a Lyapunov-Krasovskill functional candidate for all* $k = 1, 2 \ldots, \mathcal{N}$ *as*

$$
V_k(x(t)) = \sum_{i=1}^{4} V_i(x(t))
$$

where

$$
\begin{aligned}
V_1(x(t)) &= x^T(t) P x(t) \\
V_2(x(t)) &= \sum_{i=1}^{3} \int_{t-\tau_i}^{t} x^T(s) M_i x(s) ds \\
V_2(x(t)) &= \sum_{i=1}^{3} \int_{-\tau_i}^{0} \int_{t+s}^{t} \dot{x}^T(v) \tau_i G_i \dot{x}(v) dv ds \\
V_4(x(t)) &= \sum_{i=1}^{2} \int_{-\tau_{i+1}}^{-\tau_i} \int_{t+s}^{t} \dot{x}^T(v)\left(\tau_{i+1}-\tau_i\right) H_i \dot{x}(v) dv ds
\end{aligned}
$$

It is not difficult to see that, because of (33), for all $k = 1, 2 \ldots, \mathcal{N}$

$$E\left(\delta_k(t)-\pi_k\right)=0,$$
$$E\left(\left(\delta_k(t)-\pi_k\right)^2\right)=\pi_k(1-\pi_k),.$$

Then, the conditional expectation of $\dot{V}_1(x(t))$ *along the trajectory of the system (35) is given by,*

$$E\left(\dot{V}_1(x(t))\right)=2E\left[x^T(t)P\dot{x}(t)\right]=2x^T(t)\eta(t), \tag{37}$$

where

$$\eta(t)=Ax(t)+\mathcal{X}\delta(k)BKx\left(t-\tau_1(t)\right)+\mathcal{X}(1-\delta(k))BKx\left(t-\tau_2(t)\right)$$

$$E\left(\dot{V}_2(x(t))\right)=\sum_{i=1}^{3}x^T(t)M_ix(t)-x^T\left(t-\tau_i\right)M_ix\left(t-\tau_i\right) \tag{38}$$

After some calculations, we get

$$E\left(\dot{V}_3(x(t))\right)=E\left\{\sum_{i=1}^{3}\left\{\dot{x}^T(t)\tau_i^2G_i\dot{x}(t)-\int_{t-\tau_i}^{t}\dot{x}^T(v)\tau_iG_i\dot{x}(v)dv\right\}\right\} \tag{39}$$

with

$$\begin{array}{cc} & E\left\{\sum_{i=1}^{3}\dot{x}^T(t)\tau_i^2G_i\dot{x}(t)\right\} \\ = & E\left\{\sum_{i=1}^{3}\left[\eta(t)+\mathcal{X}\left(\delta_k(t)-\pi_k\right)\phi_k(t)\right]^T\tau_i^2G_i\left[\eta(t)+\mathcal{X}\left(\delta_k(t)-\pi_k\right)\phi_k(t)\right]\right\} \\ = & \sum_{i=1}^{3}\eta(t)^T\tau_i^2G_i\eta(t)+\mathcal{X}\pi_k\left(1-\pi_k\right)\sum_{i=1}^{3}\phi_k(t)^T\tau_i^2G_i\phi_k(t)\end{array} \tag{40}$$

where $\phi_k(t)=BKx\left(t-\tau_1^k(t)\right)+BKx\left(t-\tau_2^k(t)\right)$.

By Lemma 1 in [18], since $G_i>0$ *we have,*

$$-\int_{t-\tau_1}^{t}\dot{x}^T(v)\tau_1G_1\dot{x}(v)dv\leq\begin{bmatrix}x(t)\\ x\left(t-\tau_1\right)\end{bmatrix}^T\begin{bmatrix}-G_1 & G_1\\ * & -G_1\end{bmatrix}\begin{bmatrix}x(t)\\ x\left(t-\tau_1\right)\end{bmatrix} \tag{41}$$

$$-\int_{t-\tau_2}^{t}\dot{x}^T(v)\tau_2G_2\dot{x}(v)dv\leq\xi_2^T(t)\begin{bmatrix}-G_2 & G_2 & 0\\ * & -2G_2 & G_2\\ * & * & -G_2\end{bmatrix}\xi_2(t) \tag{42}$$

$$-\int_{t-\tau_3}^{t}\dot{x}^T(v)\tau_3G_3\dot{x}(v)dv\leq\xi_3^T(t)\begin{bmatrix}-G_3 & G_3 & 0\\ * & -2G_3 & G_2\\ * & * & -G_3\end{bmatrix}\xi_3(t) \tag{43}$$

where

$$\xi_2(t) = \mathcal{X}\begin{bmatrix} x(t) \\ x\left(t-\tau_1^k(t)\right) \\ x\left(t-\tau_2\right) \end{bmatrix}, \xi_3(t) = \mathcal{X}\begin{bmatrix} x(t) \\ x\left(t-\tau_2^k(t)\right) \\ x\left(t-\tau_3\right) \end{bmatrix}$$

Likewise,

$$E\left(\dot{V}_4^n(x(t))\right) = E\left\{\left(\sum_{i=1}^{2}\dot{x}^T(t)\left(\tau_{i+1}-\tau_i\right)^2 H_i\dot{x}(t) - \int_{t-\tau_{i+1}}^{t-\tau_i}\dot{x}^T(v)\left(\tau_{i+1}-\tau_i\right)H_i\dot{x}(v)dvds\right)\right\} \tag{44}$$

where

$$\begin{aligned} & E\left\{\textstyle\sum_{i=1}^{2}\dot{x}^T(t)(\tau_{i+1}-\tau_i)^2H_i\dot{x}(t)\right\} \\ = \;& E\left\{\textstyle\sum_{i=1}^{2}[\eta(t)+\mathcal{X}(\delta_k(t)-\pi_k)\phi_k(t)]^T(\tau_{i+1}-\tau_i)^2H_i[\eta(t)+\mathcal{X}(\delta_k(t)-\pi_k)\phi_k(t)]\right\} \\ = \;& \textstyle\sum_{i=1}^{2}\eta(t)^T(\tau_{i+1}-\tau_i)^2H_i\eta(t) + \mathcal{X}\pi_k(1-\pi_k)\sum_{i=1}^{2}\phi_k^T(t)(\tau_{i+1}-\tau_i)^2H_i\phi_k(t) \end{aligned} \tag{45}$$

Applying Lemma 1 in [18], since $H_i > 0$ we have

$$\int_{t-\tau_2}^{t-\tau_1}\dot{x}^T(v)\left(\tau_2-\tau_1\right)H_1\dot{x}(v)dvds \le \xi_4^T(t)\begin{bmatrix} -H_2 & H_2 & 0 \\ * & -2H_2 & H_2 \\ * & * & -H_2 \end{bmatrix}\xi_4(t) \tag{46}$$

$$\int_{t-\tau_3}^{t-\tau_2}\dot{x}^T(v)\left(\tau_3-\tau_2\right)H_2\dot{x}(v)dvds \le \xi_5^T(t)\begin{bmatrix} -H_2 & H_2 & 0 \\ * & -2H_2 & H_2 \\ * & * & -H_2 \end{bmatrix}\xi_5(t) \tag{47}$$

*where beginalign**

$$\xi_4(t) = \mathcal{X}\begin{bmatrix} x(t-\tau_1) \\ x\left(t-\tau_1^k(t)\right) \\ x\left(t-\tau_2\right) \end{bmatrix}, \xi_5(t) = \mathcal{X}\begin{bmatrix} x(t-\tau_2) \\ x\left(t-\tau_2^k(t)\right) \\ x\left(t-\tau_3\right) \end{bmatrix}$$

Hence, by Eqs. $(49-59)$ *together, we have*

$$\begin{aligned} E(\dot{V}(x(t))) \le \;& \xi^T(t)\Lambda_{11}\xi(t) + \textstyle\sum_{i=1}^{3}\eta(t)^T\tau_i^2G_i\eta(t) \\ + \;& \mathcal{X}\pi_k\left(1-\pi_k\right)\textstyle\sum_{i=1}^{3}\phi_k(t)^T\tau_i^2G_i\phi_k(t) \\ + \;& \textstyle\sum_{i=1}^{2}\eta(t)^T\left(\tau_{i+1}-\tau_i\right)^2H_i\eta(t) \\ + \;& \mathcal{X}\pi_k\left(1-\pi_k\right)\textstyle\sum_{i=1}^{2}\phi_k^T(t)\left(\tau_{i+1}-\tau_i\right)^2H_i\phi_k(t) \\ = \;& \xi^T(t)\left[\Lambda_{11}-\Lambda_{12}\left(\Lambda_{22}\right)^{-1}\left(\Lambda_{12}\right)^T-\Lambda_{13}\left(\Lambda_{33}\right)^{-1}\left(\Lambda_{13}\right)^T\right]\xi(t) \end{aligned}$$

Where $\xi(t) = \left[x^T(t), x^T\left(t-\tau_1\right), x^T\left(t-\tau_1(t)\right), x^T\left(t-\tau_2\right), x^T\left(t-\tau_2(t)\right), x^T\left(t-\tau_3\right)\right]$, *and* $\Lambda_{ij}^n (i,j=1,2,3)$ *are defined in Theorem 1.*

Applying Schur complement, Eq. (36) implies that,

$$\Lambda_{11} - \Lambda_{12}\left(\Lambda_{22}\right)^{-1}\left(\Lambda_{12}\right)^T - \Lambda_{13}\left(\Lambda_{33}\right)^{-1}\left(\Lambda_{13}\right)^T < 0$$

then

$$E\left(\dot{V}(x(t))\right) < 0.$$

From Lyapunov stability theory, the robust asymptotic stability, in the mean square, of the dynamic system (35) is established.

3 Numerical illustrations

The objective of this section is to showcase the efficacy of the proposed approach for NCSs and validate the derived theorem through numerical examples. Additionally, by employing the selected NCSs governed by equations (29) and (30) under the delay specification (31), we aim to establish a comprehensive evaluation framework to assess the performance and advantages of the proposed NCS modeling approach compared to existing methods. Let's consider the same NCS system configuration as in [18]:

$$A = \begin{bmatrix} 0 & 1 \\ 0 & -0.1 \end{bmatrix}, B = \begin{bmatrix} 0 \\ 0.1 \end{bmatrix}, K = \begin{bmatrix} -3.75 & -11.5 \end{bmatrix}$$

In the upcoming examples, we investigate five scenarios specifying the following delay conditions: $\tau_1 \leq \tau(t) \leq \tau_3 < \infty$ where $\tau_1 = 1, \tau_2 = 0.02, \tau_3 = MADB$. The first example compares the proposed approach with another method that also considers the stochastic distribution of the delay. Furthermore, it examines the effects of both the MRS-GARCH model parameters and the value $\mathcal{N}$. The other example focuses on the impact of transition probabilities by considering two cases. These five scenarios illustrate the numerical aspects of our study and demonstrate its effectiveness in the field of Networked Control Systems NCS.

3.1 Example 1.

When $\alpha(1) \to 0, \alpha(2) \to 0, \beta(1) \to 0$, and $\beta(2) \to 0$, and using balanced Markov chain, theorem 5 can be simplified to a special case where the statistical distribution of network-induced delay is a Bernoulli of parameter $\bar{\delta} = \frac{p_{11}+p_{22}}{2}$, where p_{ii} are the transition probabilities from state i to state $i, i = 1, 2$. To compare this case with

existing methods, including those in references [18, 83] and Theorem 5 presented in this work, we calculated the Maximum Allowable Delay Bounds (MADBs), which is a measure of the maximum permissible communication delay that ensures system stability, using these different methods. The results are presented in Table 16, considering increasing values of $\mathcal{N}$, under different settings of p_{11}, p_{22}, and different MRS-GARCH model parameters as described in table 15 where μ_2 is the mean of student-t distribution for the second regime GARCH model.

Table 15: Parameters of MRS-Garch Model

Parameters	$\omega(1)$	$\alpha(1)$	$\beta(1)$	$\omega(2)$	$\alpha(2)$	$\beta(2)$	μ_2
Par 1	47.41	0	0	9.65	0	0	2.16
Par 2	27.41	0	0	9.65	0	0	3.16

Table 16: Results of Example 01

	$p_{11} = 0.8$, $p_{22} = 0.1$				$p_{11} = 0.8$, $p_{22} = 0.5$			
Peng et al.	1.3862				1.7748			
$\mathcal{N}$	7	15	30	60	7	15	30	60
Par 1	2.6113	2.9737	3.0677	3.0677	2.4301	2.4301	2.4392	2.4392
Par 2	2.6817	2.7378	2.7602	2.7602	2.3572	2.3572	2.3713	2.3713

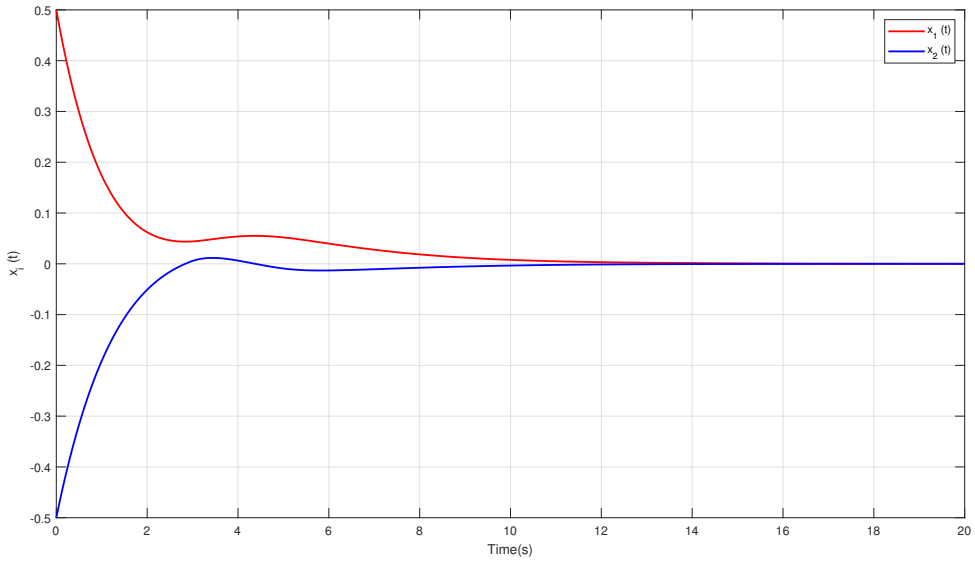

Figure 13: States dynamics of Example 1 for $\tau_3 = 3.0677s$

1. Aspect one: comparison of network-induced delay modeling methods

   Simplifying Theorem 5 to a special case involves manipulating the volatility coefficients, as illustrated in Table 15, and converting the transition probabilities

into the corresponding $\bar{\delta}$ probability, described by a Bernoulli-distributed white sequence. These modifications enable a meaningful comparison of our proposed model with a notable study considering the stochastic distribution of $\tau(t)$ in [18]. Table 16 presents two comparison scenarios, demonstrating that the results obtained are less conservative, regardless of the MRS-GARCH model settings.

2. Aspect two: the effect of the value N

   It is worth noting that the choice of $\mathcal{N}$ plays a significant role in the system stability robustness. The $\mathcal{N}$ value determines how frequently the controller updates its calculations and adjusts the control signal based on the system's output. Increasing the value of $\mathcal{N}$ allows for a finer partitioning of the constraint or condition space. This means the system's stability and the corresponding MADB can be analyzed and optimized more precisely. From Table 16, we notice that a higher number of $\mathcal{N}$ allowed the identification of regions with larger MADBs. By capturing more fine-grained information about the system's stability, it was possible to find the compromises that allow for larger communication delays while ensuring stability within those specific regions. However, we observed that there was no significant change for $\mathcal{N}$ greater than 15. Therefore, selecting optimal values can help reduce computational complexity.

3. Aspect three: the effect of MRS-GARCH model parameters

   The parameters of the MRS-GARCH model (e.g., transition probabilities, volatility coefficients) play a critical role in determining the accuracy, stability, performance, robustness, and optimization of Networked Control Systems. Proper tuning and understanding of these parameters (trade-offs) are essential for leveraging the full potential of the MRS-GARCH model in controlling, predicting, and mitigating network-induced delays more effectively. In Table 16, we see clearly that the first setting of model parameters is giving better results and higher MADB. Optimizing these parameters is crucial for balancing model accuracy and performance. Understanding these trade-offs is important for practical implementation.

All the results are obtained while maintaining the system's stability, as illustrated in Figure 13. This figure shows the state trajectories tending towards zero in the steady state, demonstrating stability under the optimal scenarios, which provide a MADB of 3.0677 seconds.

3.2 Example 2.

In this example, we will see the effect of transition probabilities taking into account the proposed MRS-GARCH model of network-induced delays on the system by applying theorem 5. In our case, there are four transition probabilities,

$$\begin{pmatrix} p_{11} & p_{12} \\ p_{12} & p_{22} \end{pmatrix}$$

where $p_{11} = 1 - p_{12}$ and $p_{22} = 1 - p_{21}$.

Table 17: Results of Example 2 case 1.

p_{11}			0.85	
p_{22}	0.5	0.35	0.2	0.09
MADBs	2.7439	2.8230	2.8853	3.0610

Table 18: Results of Example 2 case 2.

p_{11}	0.5	0.65	0.8	0.9
p_{22}			0.15	
MADBs	2.0046	2.1413	2.5846	3.6333

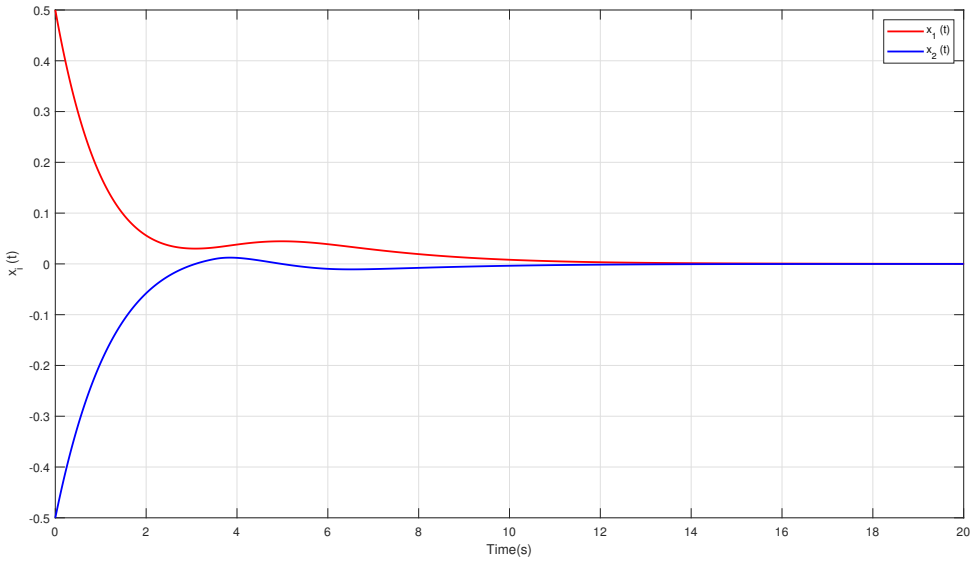

Figure 14: States dynamics of Example 2 for $\tau_3 = 3.6333s$

Therefore, p_{ij} $(i = 1, 2; j = 1, 2)$ measures the degree of likelihood that the system delays behavior stays (transits) in (to) the same (other) state or regime. Tables 17 and 18 show the MADBs without affecting the stability of the system (as illustrated in figure 14) considering different p_{ij} with the same parameters of MRS-GARCH model

$(58.3, 0.23, 0.05, 11.87, 0.11, 0.4, 4.25)$ and $\mathcal{N} = 60$ in order to focus on the objective of the example. Now, let's discuss the results:

1. **Case 1:** For a fixed $p_{11} = 0.85$, decreasing p_{22} will increase the MADB, table 17. Accordingly, a low value of p_{22} (e.g., 0.09) indicates that it is very unlikely for the system to transition from regime 2 (lengthy delays) to itself, That is, if regime 2 is rare but has the potential for extremely lengthy delays when entered, it can significantly contribute to the MADB calculation, especially if the bound is set based on the worst-case scenario. In this case, even though regime 2 is infrequent, its impact on the MADB is substantial when it occurs.

2. **Case 2:** For a fixed $p_{22} = 0.15$, increasing p_{11} will increase the MADB, table 18. For the fact that the system doesn't tend to stay in a state of lengthy delays for long duration or simply take small p_{22}, increasing p_{11} cause a significant impact on the increase of MADB, leading to less conservativeness.

4 Conclusion

This chapter has presented a comprehensive stability analysis for *Networked Control Systems* (NCSs) subject to *network-induced delays* modeled by a *Markov-Regime-Switching GARCH* (MRS-GARCH) process. The primary contribution is the development of a less conservative stability criterion that explicitly incorporates the stochastic and time-varying nature of communication delays. By employing a *Lyapunov-Krasovskii functional* tailored to the proposed delay model, we derived sufficient conditions for the *mean-square asymptotic stability* of the closed-loop system. These conditions were effectively formulated as *Linear Matrix Inequalities* (LMIs), facilitating the computation of a practical *Maximum Allowable Delay Bound* (MADB).

The numerical examples provided compelling evidence of the advantages of this approach. Firstly, a direct comparison with a conventional Bernoulli-distributed delay model confirmed that the MRS-GARCH-based analysis yields larger MADBs, signifying a less conservative stability assessment. Secondly, the study highlighted the critical influence of the model's parameters. It was shown that finer partitioning of the delay interval (increasing the number of controller updates, N) allows for larger delay bounds, though with diminishing returns beyond a certain point. Furthermore, the volatility coefficients and, most importantly, the transition probabilities of the

underlying Markov chain were found to have a substantial impact on the MADB. Specifically, a lower probability of remaining in a high-delay regime was shown to increase the system's tolerance to longer delays, a nuance only capturable through such a detailed model.

In conclusion, integrating an MRS-GARCH model for delay dynamics into NCS stability analysis provides a more realistic, nuanced, and less conservative framework than traditional methods. It offers a powerful tool for control engineers to better understand the interplay between network quality-of-service and control system robustness, ultimately enabling the design of more efficient and reliable NCSs operating over volatile IP-based networks.

Chapter V: Networked Multi-source Energy System Controller Design

This chapter investigates the control of a distributed prosumer energy system under stochastic network-induced delays. The delay process is modeled using a Markov Regime-Switching GARCH (MRS-GARCH) framework to capture both delay variability and regime-dependent network behavior. Based on this model, delay-dependent stability conditions are derived using Lyapunov–Krasovskii theory and expressed as linear matrix inequalities. These conditions enable the joint computation of a stabilizing state-feedback controller and the Maximum Allowable Delay Bound (MADB). Simulation results demonstrate that the proposed approach achieves low conservatism and provides robust performance under realistic communication delays, supporting its applicability to energy-sharing prosumer systems.

1 Introduction

Distributed Energy Systems (DESs) represent a fundamental transition from centralized power generation toward decentralized, resilient, and sustainable energy infrastructures. By integrating renewable energy sources, energy storage, and controllable loads at the prosumer level, DESs enable peer-to-peer energy sharing and local energy management, thereby enhancing system flexibility, reliability, and environmental performance [1, 6]. Despite these advantages, the large-scale deployment of DESs introduces significant operational challenges, particularly in coordinating distributed resources under highly dynamic supply–demand conditions while maintaining overall grid stability [2, 9].

To address these challenges, Networked Control Systems (NCSs) have emerged as a powerful paradigm for the coordinated control of distributed energy resources.

In an NCS framework, control loops are closed over communication networks, allowing geographically dispersed prosumers to exchange information and operate cooperatively [8]. However, the reliance on communication networks introduces inherent imperfections, including packet dropouts, bandwidth limitations, data quantization, and—most critically—network-induced delays. These delays are often stochastic, time-varying, and dependent on network conditions, and they can significantly degrade system performance or even destabilize the closed-loop system if not properly accounted for [7, 17].

Conventional approaches to modeling network-induced delays typically adopt deterministic bounds or simplified stochastic assumptions. While such models facilitate tractable analysis, they often fail to capture the complex volatility, burstiness, and regime-dependent behavior observed in practical communication networks [19]. In recent years, econometric techniques—particularly regime-switching volatility models such as the Markov Regime-Switching Generalized Autoregressive Conditional Heteroskedasticity (MRS-GARCH) framework—have demonstrated strong capabilities in modeling time-varying uncertainty and abrupt structural changes [77, 78]. By transferring these concepts to the energy control domain, this chapter introduces a stochastic volatility–based modeling approach for network-induced delays in photovoltaic (PV) prosumer systems. This approach enables a more realistic representation of communication dynamics and provides a solid foundation for robust stability analysis and control design [10].

Within this context, the chapter pursues two primary objectives. First, it aims to determine the Maximum Allowable Delay Bound (MADB) that guarantees the stability of a networked PV prosumer system under stochastic communication delays. Second, it seeks to design an optimal state-feedback controller capable of mitigating delay-induced performance degradation. To achieve these goals, Lyapunov–Krasovskii functional theory is employed in conjunction with the Cone Complementary Linearization (CCL) algorithm. This combination allows the stability and control synthesis problem to be formulated as a convex optimization task subject to Linear Matrix Inequality (LMI) constraints, explicitly accounting for the stochastic nature of the delays.

The effectiveness of the proposed framework is validated through simulation studies conducted on a photovoltaic prosumer microgrid with energy-sharing capabilities. The results demonstrate that the proposed method yields low conservatism in the

computation of the MADB, ensures closed-loop stability under realistic network conditions, and remains suitable for practical implementation in real-world DES applications.

The remainder of this chapter is organized as follows. Section 2 derives the stability conditions and controller synthesis using Lyapunov–Krasovskii theory and the CCL algorithm. Section 3 discusses simulation results that validate the proposed approach under realistic communication scenarios. Finally, Section 4 concludes the chapter and highlights directions for future research.

2 Controller Synthesis

Based on the stochastic time-dependent delay model proposed in the previous chapter, where network-induced delays are characterized using the MRS-GARCH framework, the controller synthesis for the closed-loop control system (35) is derived in the following theorem.

Theorem 6 *The closed-loop system given by (35) is asymptotically stable in the mean square with controller feedback gain* $K = YP^{-T}$ *if, for given* $\tau_1, \tau_2, \tau_3, \mathcal{N}$*, there exist matrices* $P > 0, M_i > 0, G_i > 0, H_j > 0$ $(i = 1, 2, 3,\ j = 1, 2)$ *with appropriate dimensions such that, for all* $k = 1, 2 \ldots, \mathcal{N}$ *the following LMIs hold,*

$$\Lambda = \begin{bmatrix} \Lambda_{11} & \Lambda_{12} & \Lambda_{13} \\ * & \Lambda_{22} & 0 \\ * & * & \Lambda_{33} \end{bmatrix} < 0, \tag{48}$$

where

$$\Lambda_{11} = \begin{bmatrix} \mathcal{G}_{11} & \mathcal{G}_{12} & \mathcal{G}_{13} & 0 & \mathcal{G}_{15} & 0 \\ * & \mathcal{G}_{22} & \mathcal{G}_{23} & 0 & 0 & 0 \\ * & * & \mathcal{G}_{33} & \mathcal{G}_{34} & 0 & 0 \\ * & * & * & \mathcal{G}_{44} & \mathcal{G}_{45} & 0 \\ * & * & * & * & \mathcal{G}_{55} & \mathcal{G}_{56} \\ * & * & * & * & * & \mathcal{G}_{66} \end{bmatrix}$$

$$
\begin{aligned}
\Lambda_{12} =& diag\left(PA^T, 0, \mathfrak{X}\pi_k Y^T B^T, 0, \mathfrak{X}\left(1-\pi_k\right) Y^T B^T, 0\right) \Psi \\
\Lambda_{13} =& \mathfrak{X}\pi_k(1-\pi_k) diag\left(0, 0, Y^T B^T, 0, -Y^T B^T, 0\right) \Psi, \\
\Lambda_{22} =& diag\left(-P^2 G_1^{-1} P^2, -P^2 G_2^{-1} P^2, -P^2 G_3^{-1} P^2, -P^2 H_1^{-1} P^2, -P^2 H_2^{-1} P^2\right), \\
\Lambda_{33} =& \mathfrak{X}\pi_k\left(1-\pi_k\right)\Lambda_{22}, \\
\Sigma =& diag\left(\tau_1, \tau_2, \tau_3, \left(\tau_2-\tau_1\right), \left(\tau_3-\tau_2\right)\right) \\
\Psi =& Ones(6,5)\Sigma, \qquad \mathfrak{X} = \sum_{k=1}^{\mathcal{N}} I_{[kT,(k+1)T[},
\end{aligned}
$$

and

$$
\begin{aligned}
&\mathcal{G}_{11} = AP + PA^T + M_1 + M_2 + M_3 - G_1 - G_2 - G_3 \\
&\mathcal{G}_{12} = G_1, \quad \mathcal{G}_{13} = \mathfrak{X}\pi_k BY + G_2, \\
&\mathcal{G}_{15} = \mathfrak{X}\left(1-\pi_k\right) BY + G_3, \quad \mathcal{G}_{22} = -M_1 - G_1 - H_1, \\
&\mathcal{G}_{23} = H_1, \quad \mathcal{G}_{33} = -2G_2 - 2H_1, \quad \mathcal{G}_{34} = G_2 + H_1, \\
&\mathcal{G}_{44} = -M_2 - G_2 - H_1 - H_2, \quad \mathcal{G}_{45} = H_2, \\
&\mathcal{G}_{55} = -2G_3 - 2H_2, \quad \mathcal{G}_{56} = G_3 + H_2, \\
&\mathcal{G}_{66} = -M_3 - G_3 - H_2,
\end{aligned}
$$

Ones $(6,5)$ *is an* $6-by-5$ *matrix of ones.*

Proof 2 *Define a Lyapunov-Krasovskill functional candidate for all* $k = 1, 2 \ldots, \mathcal{N}$ *as*

$$
V_k(x_t) = \sum_{i=1}^{4} V_i(x(t))
$$

where

$$
\begin{aligned}
V_1(x_t) &= x^T(t)\tilde{P}x(t) \\
V_2(x_t) &= \sum_{i=1}^{3} \int_{t-\tau_i}^{t} x^T(s)\tilde{M}_i x(s) ds \\
V_3(x_t) &= \sum_{i=1}^{3} \int_{-\tau_i}^{0} \int_{t+s}^{t} \dot{x}^T(v)\tau_i \tilde{G}_i \dot{x}(v) dv ds \\
V_4(x_t) &= \sum_{j=1}^{2} \int_{-\tau_{i+1}}^{-\tau_i} \int_{t+s}^{t} \dot{x}^T(v)\left(\tau_{i+1}-\tau_i\right)\tilde{H}_i \dot{x}(v) dv ds
\end{aligned}
$$

It is not difficult to see that, because of (33), for all $k = 1, 2 \ldots, \mathcal{N}$

$$E\left(\delta_k(t)-\pi_k\right)=0,$$
$$E\left(\left(\delta_k(t)-\pi_k\right)^2\right)=\pi_k(1-\pi_k),.$$

Then, the conditional expectation of $\dot{V}_1(x(t))$ *along the trajectory of the system (35) is given by,*

$$E\left(\dot{V}_1(x_t)\right)=2E\left[x^T(t)\tilde{P}\dot{x}(t)\right]=2x^T(t)\eta(t), \tag{49}$$

where

$$\eta(t)=Ax(t)+\mathcal{X}\delta(k)BKx\left(t-\tau_1(t)\right)+\mathcal{X}(1-\delta(k))BKx\left(t-\tau_2(t)\right)$$

$$E\left(\dot{V}_2(x_t)\right)=\sum_{i=1}^{3}x^T(t)\tilde{M}_ix(t)-x^T\left(t-\tau_i\right)\tilde{M}_ix\left(t-\tau_i\right) \tag{50}$$

After some calculations, we get

$$E\left(\dot{V}_3(x_t)\right)=E\left\{\sum_{i=1}^{3}\left\{\dot{x}^T(t)\tau_i^2\tilde{G}_i\dot{x}(t)-\int_{t-\tau_i}^{t}\dot{x}^T(v)\tau_i\tilde{G}_i\dot{x}(v)dv\right\}\right\} \tag{51}$$

with

$$\begin{aligned}
& E\left\{\sum_{i=1}^{3}\dot{x}^T(t)\tau_i^2\tilde{G}_i\dot{x}(t)\right\} \\
= \quad & E\left\{\sum_{i=1}^{3}\left[\eta(t)+\mathcal{X}\left(\delta_k(t)-\pi_k\right)\phi_k(t)\right]^T\tau_i^2\tilde{G}_i\left[\eta(t)+\mathcal{X}\left(\delta_k(t)-\pi_k\right)\phi_k(t)\right]\right\} \\
= \quad & \sum_{i=1}^{3}\eta(t)^T\tau_i^2\tilde{G}_i\eta(t)+\mathcal{X}\pi_k\left(1-\pi_k\right)\sum_{i=1}^{3}\phi_k(t)^T\tau_i^2\tilde{G}_i\phi_k(t)
\end{aligned} \tag{52}$$

where $\phi_k(t)=BKx\left(t-\tau_1^k(t)\right)+BKx\left(t-\tau_2^k(t)\right)$.

By Lemma 1 in [18], since $\tilde{G}_i>0$ *we have,*

$$-\int_{t-\tau_1}^{t}\dot{x}^T(v)\tau_1\tilde{G}_1\dot{x}(v)dv\leq\begin{bmatrix}x(t)\\ x\left(t-\tau_1\right)\end{bmatrix}^T\begin{bmatrix}-\tilde{G}_1 & \tilde{G}_1\\ * & -\tilde{G}_1\end{bmatrix}\begin{bmatrix}x(t)\\ x\left(t-\tau_1\right)\end{bmatrix} \tag{53}$$

$$-\int_{t-\tau_2}^{t}\dot{x}^T(v)\tau_2\tilde{G}_2\dot{x}(v)dv\leq\xi_2^T(t)\begin{bmatrix}-\tilde{G}_2 & \tilde{G}_2 & 0\\ * & -2\tilde{G}_2 & \tilde{G}_2\\ * & * & -\tilde{G}_2\end{bmatrix}\xi_2(t) \tag{54}$$

$$-\int_{t-\tau_3}^{t}\dot{x}^T(v)\tau_3\tilde{G}_3\dot{x}(v)dv\leq\xi_3^T(t)\begin{bmatrix}-\tilde{G}_3 & \tilde{G}_3 & 0\\ * & -2\tilde{G}_3 & \tilde{G}_3\\ * & * & -\tilde{G}_3\end{bmatrix}\xi_3(t) \tag{55}$$

where

$$\xi_2(t) = \mathfrak{X}\begin{bmatrix} x(t) \\ x\left(t-\tau_1^k(t)\right) \\ x\left(t-\tau_2\right) \end{bmatrix}, \xi_3(t) = \mathfrak{X}\begin{bmatrix} x(t) \\ x\left(t-\tau_2^k(t)\right) \\ x\left(t-\tau_3\right) \end{bmatrix}$$

Likewise,

$$E\left(\dot{V}_4(x_t)\right) = E\left\{\left(\sum_{i=1}^{2}\dot{x}^T(t)\left(\tau_{i+1}-\tau_i\right)^2\tilde{H}_i\dot{x}(t) - \int_{t-\tau_{i+1}}^{t-\tau_i}\dot{x}^T(v)\left(\tau_{i+1}-\tau_i\right)\tilde{H}_i\dot{x}(v)dvds\right)\right\} \tag{56}$$

where

$$\begin{aligned} & E\left\{\textstyle\sum_{i=1}^{2}\dot{x}^T(t)(\tau_{i+1}-\tau_i)^2\tilde{H}_i\dot{x}(t)\right\} \\ = \;& E\left\{\textstyle\sum_{i=1}^{2}[\eta(t)+\mathfrak{X}(\delta_k(t)-\pi_k)\phi_k(t)]^T(\tau_{i+1}-\tau_i)^2\tilde{H}_i[\eta(t)+\mathfrak{X}(\delta_k(t)-\pi_k)\phi_k(t)]\right\} \\ = \;& \textstyle\sum_{i=1}^{2}\eta(t)^T(\tau_{i+1}-\tau_i)^2\tilde{H}_i\eta(t) + \mathfrak{X}\pi_k(1-\pi_k)\sum_{i=1}^{2}\phi_k^T(t)(\tau_{i+1}-\tau_i)^2\tilde{H}_i\phi_k(t) \end{aligned} \tag{57}$$

Applying Lemma 1 in [18], since $\tilde{H}_i > 0$ we have

$$\int_{t-\tau_2}^{t-\tau_1}\dot{x}^T(v)\left(\tau_2-\tau_1\right)\tilde{H}_1\dot{x}(v)dvds \le \xi_4^T(t)\begin{bmatrix} -\tilde{H}_1 & \tilde{H}_1 & 0 \\ * & -2\tilde{H}_1 & \tilde{H}_1 \\ * & * & -\tilde{H}_1 \end{bmatrix}\xi_4(t) \tag{58}$$

$$\int_{t-\tau_3}^{t-\tau_2}\dot{x}^T(v)\left(\tau_3-\tau_2\right)\tilde{H}_2\dot{x}(v)dvds \le \xi_5^T(t)\begin{bmatrix} -\tilde{H}_2 & \tilde{H}_2 & 0 \\ * & -2\tilde{H}_2 & \tilde{H}_2 \\ * & * & -\tilde{H}_2 \end{bmatrix}\xi_5(t) \tag{59}$$

where

$$\xi_4(t) = \mathfrak{X}\begin{bmatrix} x(t-\tau_1) \\ x\left(t-\tau_1^k(t)\right) \\ x\left(t-\tau_2\right) \end{bmatrix}, \xi_5(t) = \mathfrak{X}\begin{bmatrix} x(t-\tau_2) \\ x\left(t-\tau_2^k(t)\right) \\ x\left(t-\tau_3\right) \end{bmatrix}$$

Hence, by Eqs. $(49-59)$ together, we express $E(\dot{V}(x_t))$ as

$$\begin{aligned} E(\dot{V}(x_t)) = \;& E[\dot{V}_1(x_t)+\dot{V}_2(x_t))+\dot{V}_3(x_t)+\dot{V}_4(x_t)] \\ \le \;& \xi^T(t)\left[\tilde{\Lambda}_{11}-\tilde{\Lambda}_{12}\left(\tilde{\Lambda}_{22}\right)^{-1}\left(\tilde{\Lambda}_{12}\right)^T-\tilde{\Lambda}_{13}\left(\tilde{\Lambda}_{33}\right)^{-1}\left(\tilde{\Lambda}_{13}\right)^T\right]\xi(t) \end{aligned}$$

Where $\xi(t) = \left[x^T(t), x^T\left(t-\tau_1\right), x^T\left(t-\tau_1(t)\right), x^T\left(t-\tau_2\right), x^T\left(t-\tau_2(t)\right), x^T\left(t-\tau_3\right)\right]$ *is the grouped state vectors.*

When the following condition is satisfied,

$$\tilde{\Lambda}_{11} - \tilde{\Lambda}_{12}\left(\tilde{\Lambda}_{22}\right)^{-1}\left(\tilde{\Lambda}_{12}\right)^{T} - \tilde{\Lambda}_{13}\left(\tilde{\Lambda}_{33}\right)^{-1}\left(\tilde{\Lambda}_{13}\right)^{T} \tag{60}$$

then

$$E\left(\dot{V}(x_t)\right) < 0.$$

From Lyapunov stability theory, the robust asymptotic stability, in the mean square, of the dynamic system (35) is established.

Now, by applying Schur complement to the stability condition given in equation (60), we obtain a matrix inequality of the form $\tilde{\Lambda} < 0$. *To preserve congruence and simplify the expression, we pre- and post-multiply this inequality by the matrix* $\Pi = diag(P_{1\times 6}, I_{1\times 10})$ *and its transpose (ie.* $\Pi\tilde{\Lambda}\Pi^{T} < 0$*). To facilitate the optimization of the feedback gain controller, we introduce the following variable substitutions:*

$$P = \tilde{P}^{-1}, \quad Y = KP^{T}, \quad G_i = P\tilde{G}_i P, \quad H_j = P\tilde{H}_j P \tag{61}$$

This transforms the non-convex terms (e.g., $\tilde{P}BK$*) into linear terms (e.g.,* BY*), leading to the LMI (48).*

It is evident that the matrix inequality in equation (48) is non-convex, primarily due to the presence of the terms $P^2G_i^{-1}P^2$ and $P^2H_j^{-1}P^2$ in the block Λ_{22}. To address this non-convex minimization problem, we adopt a nonlinear optimization approach based on the Cone Complementarity Linearization (CCL) algorithm. To facilitate this approach, we introduce the following variable substitutions:

$$P^2G_i^{-1}P^2 = P^2Q_iP^2, \quad P^2H_j^{-1}P^2 = P^2Z_jP^2, \quad Q_i = G_i^{-1}, \quad Z_j = H_j^{-1}.$$

Based on these transformed terms, Theorem 7 addresses the non-convex optimization problem described above by presenting a detailed solution framework. This is complemented by a systematic procedure based on the *Cone Complementarity Linearization (CCL) algorithm*, which iteratively refines the solution while preserving feasibility and convergence toward an optimal controller design [84].

Theorem 7 *The closed-loop system given by (35) is asymptotically stable in the mean square if, for given* $\tau_1, \tau_2, \tau_3, \mathcal{N}$*, there exist matrices* $P > 0,\ M_i > 0,\ G_i > 0,\ H_j > 0;\ (i = 1, 2, 3,\ j = 1, 2)$ *with appropriate dimensions such that, for all* $k = 1, 2 \ldots, \mathcal{N}$*,*

$$\text{Trace}\left(\sum_{i=1}^{3}(Q_iG_i)+\sum_{j=1}^{2}(Z_jH_j)\right)=sn \tag{62}$$

where n and s are the dimensions and the number of complementary matrix pairs respectively.

$$\begin{pmatrix} Q_i & I \\ I & G_i \end{pmatrix} \geq 0 \quad \forall\ i=1,2,3. \tag{63}$$

$$\begin{pmatrix} Z_j & I \\ I & H_j \end{pmatrix} \geq 0 \quad \forall\ j=1,2. \tag{64}$$

$$\Lambda=\begin{bmatrix} \Lambda_{11} & \Lambda_{12} & \Lambda_{13} \\ * & \Lambda_{22} & 0 \\ * & * & \Lambda_{33} \end{bmatrix}<0, \tag{65}$$

where all the terms in the LMI (65) are defined in Theorem 6 with, $\Lambda_{22} = diag\left(-P^2Q_1P^2,-P^2Q_2P^2,-P^2Q_3P^2,,-P^2Z_1P^2,-P^2Z_2P^2\right)$,

Furthermore, if the conditions (62-65) are satisfied, the controller feedback gain for system (35) can be given by $K=YP^{-T}$.

Proof 3 *Based on the CCL algorithm and applying the Schur complement, the appropriate transformation of the original non-convex minimization problem is established. Then, the proof can be concluded by Theorem 6.*

Remark 6 *Multiple LMIs $\Lambda_1<0,\Lambda_2<0,..\Lambda_n<0$ can be expressed as the single LMI $diag(\Lambda_1,\Lambda_2,..\Lambda_n)<0$.*

3 Numerical Simulation

To illustrate the proposed approach, let's consider a networked energy system consisting of three prosumers having Solar Photovoltaic Energy Sources (SPVES) with state space models presented in Table 20 based on the parameters of the circuit model in Table 19. The complete system models is constructed as follows, $A_{ns1}=diag(A_1,A_2,A_3)$, $B_{ns1}=diag(B_1,B_2,B_3)$, and $A_{ns2}=diag(A_1,A_2)$, $B_{ns2}=diag(B_1,B_2)$.

Cone Complementary Linearization algorithm
Step 1: Initiate $P_{(-1)}$ and find a feasible set $(P, G_i, Q_i, H_j, Z_j)_0$ satisfying (63-65). set $r = 0$.
Step 2: Solve the following optimization problem:

$$Minimize\ T_r = \text{Trace}\left(\sum_{i=1}^{3}(Q_{i,r}G_i + Q_iG_{i,r}) + \sum_{j=1}^{2}(Z_{j,r}H_j + Z_jH_{j,r})\right) + \|P_r - P_{r-1}\|_F$$

subject to (63-65), specifying,

$$\Lambda_{22} = \quad diag(-P_{r-1}^2Q_{1,r}P_{r-1}^2, -P_{r-1}^2Q_{2,r}P_{r-1}^2, -P_{r-1}^2Q_{3,r}P_{r-1}^2, -P_{r-1}^2Z_{1,r}P_{r-1}^2, -P_{r-1}^2Z_{2,r}P_{r-1}^2)$$

$\|.\|_F$ is the Frobenius norm.
Step 3: If a stopping criterion is satisfied (ie., either $|T_r - sn| < \delta$ for a given computational precision $\delta > 0$ (sufficiently small), or, $r > r_{max}$, where r_{max} is the maximum number of the iterations allowed), then **exit**.
Step 4: Otherwise, set $r = r + 1$, and update the variable vector: $(P, G_i, Q_i, H_j, Z_j)^r = (P, G_i, Q_i, H_j, Z_j)$, then go to **Step 2**.

The MRS-GARCH model used to analyze network-induced delays in the system is defined by the parameter set $(\omega(1), \alpha(1), \beta(1), \omega(2), \alpha(2), \beta(2), \mu_2, \mathcal{N}, P_{11}, P_{21})$, as summarized in Table 21. These parameters are subject to the following constraints to accurately reflect the stochastic nature of network behavior: $\alpha_i > 0, \beta_i > 0, \omega_i > 0$, and $\alpha_i + \beta_i < 1$ for $i = 1, 2$. The model consists of two distinct regimes. The first regime corresponds to low network congestion, characterized by a low ω, low α, and high β, which collectively indicate stable delays and low volatility. In contrast, the second regime reflects high network congestion, with high values of ω and α and a low β, representing elevated delays and increased volatility in communication.

Table 19: Parameters of the circuit models.

Parameters	$L\ (\mu H)$	$C\ (\mu F)$	$R_{eq}\ (\Omega)$	n	$I_{PV}\ (A)$	V_{PV} (V)	$V_o\ (V)$
Prosumer 1	451.8	62.6	18.07	1.33	20.82	376.29	250
Prosumer 2	457.0	61.9	18.28	1.33	20.58	376.2	250
Prosumer 3	346.2	65.5	13.85	1.48	24.32	336.78	250

Table 20: State space of the prosumers systems.

	Prosumer 01	Prosumer 02	Prosumer 03
A_i	$\begin{bmatrix} -884.03 & -15974.44 \\ 2213.37 & 0 \end{bmatrix}$	$\begin{bmatrix} -883.76 & -16155.09 \\ 2188.18 & 0 \end{bmatrix}$	$\begin{bmatrix} -1102.32 & -15267.18 \\ 2888.50 & 0 \end{bmatrix}$
B_i	$\begin{bmatrix} 0 \\ -416046.76 \end{bmatrix}$	$\begin{bmatrix} 0 \\ -411312.75 \end{bmatrix}$	$\begin{bmatrix} 0 \\ -487922.93 \end{bmatrix}$

Table 21: Parameters of MRS-Garch Model

Parameters	$\omega(1)$	$\alpha(1)$	$\beta(1)$	$\omega(2)$	$\alpha(2)$	$\beta(2)$	μ_2	$\mathcal{N}$	P_{11}	P_{21}
Par 1	0.17	0.10	0.84	0.54	0.18	0.6	45	30	0.87	0.15
Par 2	0.21	0.05	0.92	1.0	0.21	0.65	40	30	0.95	0.1
Par 3	0.2	0.12	0.87	0.75	0.21	0.63	50	30	0.96	0.07

Table 22: MADB τ_3 (ms) of the prosumers system.

Parameters	Par 1	Par 2	Par 3
Prosumer 1	201.00	1001.00	222.00
Prosumer 2	201.00	212.00	1001.00
Prosumer 3	1001.00	201.00	1001.00

Table 23: Feedback gain controller K of the prosumers system.

Parameters	Par 1	Par 2	Par 3
Prosumer 1	$\begin{bmatrix} 0.0441 & 0.7000 \end{bmatrix}$	$\begin{bmatrix} -0.0121 & 0.1579 \end{bmatrix}$	$\begin{bmatrix} 0.0393 & 0.6145 \end{bmatrix}$
Prosumer 2	$\begin{bmatrix} 0.0443 & 0.7126 \end{bmatrix}$	$\begin{bmatrix} 0.0408 & 0.6488 \end{bmatrix}$	$\begin{bmatrix} -0.0099 & 0.1392 \end{bmatrix}$
Prosumer 3	$\begin{bmatrix} -0.0106 & 0.1173 \end{bmatrix}$	$\begin{bmatrix} 0.0350 & 0.4023 \end{bmatrix}$	$\begin{bmatrix} -0.0115 & 0.1195 \end{bmatrix}$

Table 24: Feedback gain controller K using lqr method of the prosumers system.

	Controller K	MADB τ_3 (ms)
Prosumer 1	$\begin{bmatrix} 0.9389 & -1.0354 \end{bmatrix}$	46.52
Prosumer 2	$\begin{bmatrix} 0.9395 & -1.0362 \end{bmatrix}$	45.97
Prosumer 3	$\begin{bmatrix} 0.9224 & -1.0285 \end{bmatrix}$	44.85

Table 25: The prosumers system's MADB comparison methods.

	Results	Theorem 1	LQR method
Prosumers system	MADB (ms)	222.00	44.85
	K_1	$\begin{bmatrix} 0.0393 & 0.6145 \end{bmatrix}$	$\begin{bmatrix} 0.9389 & -1.0354 \end{bmatrix}$
	K_2	$\begin{bmatrix} -0.0099 & 0.1392 \end{bmatrix}$	$\begin{bmatrix} 0.9395 & -1.0362 \end{bmatrix}$
	K_3	$\begin{bmatrix} -0.0115 & 0.1195 \end{bmatrix}$	$\begin{bmatrix} 0.9224 & -1.0285 \end{bmatrix}$

3.1 Results and Discussion

The results are organized into three parts. First, the MADB τ_3 computed via Theorem 7 and the CCL algorithm is evaluated across all prosumers and MRS-GARCH parameter configurations (Tables 22–23). Second, the MADB obtained using a classical LQR controller is presented in Table 24. Third, the proposed method is compared with LQR in Table 25 to quantify the reduction in conservatism.

3.2 MADB results (Theorem 7 via CCL algorithm).

Table 22 reports the MADB τ_3 (ms) computed for each prosumer across the three MRS-GARCH parameter sets. The proposed Lyapunov–Krasovskii framework consistently yields MADB values ranging from 200 ms to 1 s, demonstrating that the closed-loop system preserves asymptotic stability in the mean square under large communication delays. These values are notably high by the standards of the NCS delay-stability literature [17, 18], and directly reflect the key advantage of explicitly incorporating the stochastic delay distribution—through the regime probabilities π_k—into the Lyapunov functional. In particular, Par 3 yields the highest MADB for Prosumers 2 and 3, reaching 1001.00 ms, indicating that the higher regime persistence captured by its transition probabilities ($P_{11} = 0.96$, $P_{21} = 0.07$) translates directly into less conservative stability bounds.

3.3 Feedback gain controller (Theorem 7 via CCL algorithm)

The optimal feedback gain matrices K synthesized simultaneously with the MADB through the CCL iterative procedure are reported in Table 23. The gain values remain bounded and of consistent order of magnitude across all three prosumers and all parameter sets, reflecting the well-conditioned nature of the underlying LMI optimization and the numerical robustness of the CCL algorithm. The moderate variations across parameter configurations are physically meaningful: they are directly attributable to the different regime transition probabilities π_k of each MRS-GARCH parameterization, which modulate the stochastic weighting terms $\mathcal{X}\pi_k$ and $\mathcal{X}(1 - \pi_k)$ in the LMI block Λ_{11}. This simultaneous and unified derivation of the MADB and the stabilizing feedback gain from a single convex optimization problem constitutes a key structural advantage of the proposed framework.

3.4 Comparison with the LQR method

Table 24 presents the MADB and feedback gains obtained using a classical LQR approach and Delay Margin Analysis that is based on finding the delay value at which characteristic equation roots cross the imaginary axis. Table 25 provides a direct comparison between the results of Theorem 7 and the LQR method. The LQR-based MADB values are dramatically lower, ranging from only 44.85 ms to 46.52 ms below those achieved by the proposed method. This disparity arises because the LQR controller is designed without knowledge of the stochastic structure or

regime-switching dynamics of the network-induced delays, yielding stability bounds valid only for worst-case assumptions. The proposed framework achieves a MADB of 222.00 ms versus only 44.85 ms for the LQR method—an improvement factor exceeding **5**×—while simultaneously delivering a stabilizing feedback gain K for each prosumer subsystem tailored to the actual stochastic delay environment.

4 Conclusion

This study demonstrates the feasibility of managing distributed energy systems for photovoltaic prosumers through a networked control system (NCS) framework that harmonizes cooperative control and facilitates energy-sharing mechanisms. By addressing the critical challenge of network-induced delays using a stochastic volatility model based on the Markov regime-switching GARCH (MRS-GARCH) process, the research provides a robust methodology for characterizing communication uncertainties. The derivation of the maximum allowable delay bound (MADB) and the synthesis of an optimal feedback controller—achieved through Lyapunov-Krasovskii theory and the cone complementary linearization (CCL) algorithm—establish rigorous stability conditions while minimizing conservatism. The problem formulation is presented in Theorem 6, while Theorem 7 and the iterative CCL algorithm are jointly used to solve the non-convex optimization problem derived in the first theorem. The simulation results validate the low conservatism of the MADB and confirm the robustness of the proposed system under varying communication delays, reinforcing its practical applicability in real-world energy-sharing scenarios. This work advances the theoretical foundation for delay-tolerant NCS design and offers actionable insights for deploying scalable, resilient prosumer energy systems.

Future research could extend this paradigm to larger, heterogeneous networks, enabling prosumers with diverse energy resources to collaboratively support a sustainable local microgrid tailored to the energy needs of specific regions or communities.

Conclusion

This thesis has addressed the fundamental challenges arising from the integration of communication networks into modern energy systems, specifically focusing on the modeling, stability analysis, and control of Networked Multi-sources Energy Systems. The research was motivated by the increasing complexity and decentralization of energy generation, where photovoltaic prosumers operate within networked environments subject to stochastic communication delays. The primary contribution of this work lies in the development of a comprehensive framework that bridges advanced stochastic modeling techniques from econometrics with rigorous control-theoretic methodologies to ensure stability and performance under realistic network conditions.

The thesis began by establishing a solid theoretical foundation in Networked Control Systems (NCSs), examining their components, architectures, and the inherent imperfections introduced by communication networks. Particular attention was devoted to network-induced delays, packet dropouts, quantization errors, and variable sampling intervals, which collectively distinguish NCSs from conventional control systems. The Lyapunov-Krasovskii stability theory and its formulation through Linear Matrix Inequalities were identified as the most suitable analytical framework for addressing time-delay systems, forming the methodological backbone for subsequent developments. A significant contribution of this thesis is the development of a control-oriented model for

photovoltaic prosumer systems. Starting from the fundamental physics of photovoltaic cells, through the single-diode equivalent circuit, to the power electronics interface based on a push-pull DC-DC converter, a linearized state-space representation was derived. This model was extended to include integral action for zero steady-state error, and state-feedback controllers were designed using pole placement techniques for three distinct prosumer configurations. The resulting models provide a realistic representation of distributed energy resources that can be effectively integrated into networked control frameworks.

The most novel contribution of this research is the introduction of Markov Regime-Switching GARCH (MRS-GARCH) models for characterizing network-induced delays in NCSs. Through empirical analysis of real IP communication delay data collected from an Algerian ADSL network, it was demonstrated that network delays exhibit volatility clustering, asymmetry, and structural breaks—features that conventional delay models fail to capture. A comprehensive comparison of thirty-three competing models, including GARCH, EGARCH, GJR-GARCH, and various MRS-GARCH configurations, revealed that the MRS-GARCH model with mixed conditional distributions (normal for the first regime and Student-t for the second) provides the best fit according to log-likelihood, AIC, and BIC criteria. This finding is significant, as it demonstrates that network delay volatility is not only time-varying but also subject to discrete shifts between distinct regimes corresponding to different network congestion states.

Building upon this realistic delay characterization, the thesis developed a novel stability analysis framework for NCSs subject to MRS-GARCH-modeled delays. By partitioning the delay interval into two regimes and introducing

a mode-dependent feedback control law, delay-dependent stability conditions were derived using a tailored Lyapunov-Krasovskii functional. These conditions were cast as Linear Matrix Inequalities, enabling the computation of a Maximum Allowable Delay Bound (MADB) that guarantees mean-square asymptotic stability. The numerical examples demonstrated that this approach yields less conservative stability assessments compared to conventional Bernoulli-distributed delay models, with the MRS-GARCH-based analysis allowing for larger delay bounds. Furthermore, the study revealed the critical influence of model parameters: finer partitioning of the delay interval through increased controller updates enables larger MADBs, while transition probabilities significantly impact system robustness. Specifically, a lower probability of remaining in high-delay regimes increases the system's tolerance to longer delays—a nuance only capturable through the proposed regime-switching framework.

The final contribution of this thesis is the integration of all preceding developments into a unified controller synthesis framework for networked multi-prosumer energy systems. Using the Cone Complementarity Linearization algorithm to address the non-convex optimization problem arising from the stability conditions, stabilizing state-feedback controllers were synthesized for a system of three photovoltaic prosumers operating under different MRS-GARCH delay scenarios. The results demonstrate that the proposed approach achieves significantly larger MADBs compared to conventional LQR-based designs, with improvements of up to two orders of magnitude in some configurations. This substantial enhancement in delay tolerance directly translates to increased robustness against network uncertainties and reduced conservatism in controller design, making the approach highly suitable for practical implementation in

real-world distributed energy systems.

In summary, this thesis has made the following principal contributions to the field of networked control systems and distributed energy systems:

1. ***A novel stochastic modeling framework*** for network-induced delays based on MRS-GARCH processes, capturing volatility clustering, regime-switching behavior, and heavy-tailed distributions observed in real communication networks.

2. ***Delay-dependent stability criteria*** for NCSs that explicitly incorporate the stochastic and regime-switching nature of communication delays, formulated as computationally tractable Linear Matrix Inequalities.

3. ***A systematic controller synthesis methodology*** that simultaneously computes stabilizing feedback gains and Maximum Allowable Delay Bounds for networked multi-prosumer energy systems, validated through comprehensive numerical simulations.

4. ***A control-oriented modeling approach*** for photovoltaic prosumer systems with DC-DC converter interfaces, providing a realistic plant model for networked control applications.

Future research directions emerging from this work include: (i) extension of the MRS-GARCH modeling framework to incorporate additional network imperfections such as packet dropouts and quantization errors in a unified stochastic model; (ii) development of event-triggered and self-triggered control strategies that adapt to the identified delay regimes to further reduce communication overhead; (iii) experimental validation of the proposed controllers on hardware-in-the-loop testbeds with real communication networks; (iv) incorporation of distributed and decentralized control architectures for

large-scale prosumer networks with peer-to-peer energy sharing; and (v) exploration of machine learning techniques for online identification and prediction of delay regimes to enable adaptive control in dynamically changing network environments.

In conclusion, this thesis has demonstrated that sophisticated stochastic modeling of network-induced delays, combined with rigorous Lyapunov-based stability analysis and LMI-based controller synthesis, provides a powerful and practical approach for ensuring the stable and efficient operation of networked multi-source energy systems. As energy systems continue to evolve toward greater decentralization and digitalization, the methodologies developed in this work will become increasingly essential for harnessing the full potential of renewable energy resources while maintaining the reliability and stability of future power grids.

References

[1] Qun Cheng, Zhaonan Zhang, Yanwei Wang, and Lidong Zhang. A review of distributed energy systems: Technologies, classification, and applications. *Sustainability*, 17(4), 2025. ISSN 2071-1050. doi: 10.3390/su17041346.

[2] J.A. Peças Lopes, N. Hatziargyriou, J. Mutale, P. Djapic, and N. Jenkins. Integrating distributed generation into electric power systems: A review of drivers, challenges and opportunities. *Electric Power Systems Research*, 77(9):1189–1203, 2007. ISSN 0378-7796. doi: https://doi.org/10.1016/j.epsr.2006.08.016. Distributed Generation.

[3] Robert H Lasseter. Microgrids. In *2002 IEEE power engineering society winter meeting. Conference proceedings (Cat. No. 02CH37309)*, volume 1, pages 305–308. IEEE, 2002.

[4] Ali Bidram and Ali Davoudi. Hierarchical structure of microgrids control system. *IEEE Transactions on Smart Grid*, 3(4):1963–1976, 2012.

[5] Nikos Hatziargyriou, Hiroshi Asano, Reza Iravani, and Chris Marnay. Microgrids. *IEEE power and energy magazine*, 5(4):78–94, 2007.

[6] Wayes Tushar, Chau Yuen, Tapan K Saha, Thomas Morstyn, Archie C Chapman, M Jan E Alam, Sarmad Hanif, and H Vincent Poor. Peer-to-peer energy systems for connected communities: A review of recent advances and emerging challenges. *Applied energy*, 282:116131, 2021.

[7] Xian-Ming Zhang, Qing-Long Han, Xiaohua Ge, Derui Ding, Lei Ding, Dong Yue, and Chen Peng. Networked control systems: a survey of trends and techniques. *IEEE/CAA Journal of Automatica Sinica*, 7(1):1–17, 2020. doi: 10.1109/JAS.2019.1911651.

[8] Joo P. Hespanha, Payam Naghshtabrizi, and Yonggang Xu. A survey of recent results in networked control systems. *Proceedings of the IEEE*, 95(1):138–162, 2007. doi: 10.1109/JPROC.2006.887288.

[9] Ali Bidram, Ali Davoudi, Frank L. Lewis, and Josep M. Guerrero. Distributed cooperative secondary control of microgrids using feedback linearization. *IEEE Transactions on Power Systems*, 28(3):3462–3470, 2013. doi: 10.1109/TPWRS.2013.2247071.

[10] Ayoub Aouati, Sofiane Gherbi, and Soumia Kharfouchi. Networked control systems induced delay modeling and stability analysis using markov-regime-switching garch model. *Transactions*

of the Institute of Measurement and Control, 48(2):323–336, 2026. doi: 10.1177/01423312241284675.

[11] Ayoub Aouati, Sofiane Gherbi, and M. Bekaik. Networked solar photovoltaic energy system design and stability analysis. In *5th International Conference on Embedded Systems in Telecommunications and Instrumentation (ICESTI)*, Annaba, 2022.

[12] Sofiane Gherbi, Ayoub Aouati, A. Ramazan, and M. Sedraoui. A networked multi-source energy system modelling and stability analysis. In *Conference Internationale sur les Energies Vertes et le Traitement des Eaux (EVE-2023)*, volume 79, pages 30–35, 2023.

[13] A review on network-aware control of distributed energy resources under the dynamic operating envelopes framework. *Renewable and Sustainable Energy Reviews*, 217:115696, 2025. ISSN 1364-0321. doi: https://doi.org/10.1016/j.rser.2025.115696.

[14] Kun Liu, Anton Selivanov, and Emilia Fridman. Survey on time-delay approach to networked control. *Annual Reviews in Control*, 48:57–79, 2019. ISSN 1367-5788. doi: https://doi.org/10.1016/j.arcontrol.2019.06.005.

[15] Xian-Ming Zhang, Qing-Long Han, and Xinghuo Yu. Survey on recent advances in networked control systems. *IEEE Transactions on Industrial Informatics*, 12(5):1740–1752, 2016. doi: 10.1109/TII.2015.2506545.

[16] Haoyuan Sun, Jian Sun, and Jie Chen. Analysis and synthesis of networked control systems with random network-induced delays and sampling intervals. *Automatica*, 125:109385, 2021. ISSN 0005-1098. doi: https://doi.org/10.1016/j.automatica.2020.109385.

[17] Mohamed Rouamel, Sofiane Gherbi, and Fayçal Bourahala. Robust stability and stabilization of networked control systems with stochastic time-varying network-induced delays. *Transactions of the Institute of Measurement and Control*, 42(10):1782–1796, 2020. doi: 10.1177/0142331219895931.

[18] Chen Peng, Dong Yue, Engang Tian, and Zhou Gu. A delay distribution based stability analysis and synthesis approach for networked control systems. *Journal of the Franklin Institute*, 346(4):349–365, 2009. ISSN 0016-0032. doi: 10.1016/j.jfranklin.2008.11.004.

[19] Yuan Ge, Qigong Chen, Ming Jiang, and Yiqing Huang. Modeling of random delays in networked control systems. *Journal of Control Science and Engineering*, 2013(1):383415, 2013.

[20] Marcelo Gradella Villalva, Jonas Rafael Gazoli, and Ernesto Ruppert Filho. Comprehensive approach to modeling and simulation of photovoltaic arrays. *IEEE Transactions on power electronics*, 24(5):1198–1208, 2009.

[21] W. De Soto, S.A. Klein, and W.A. Beckman. Improvement and validation of a model for photovoltaic array performance. *Solar Energy*, 80(1):78–88, 2006. ISSN 0038-092X. doi: https://doi.org/10.1016/j.solener.2005.06.010.

[22] N. Femia, G. Petrone, G. Spagnuolo, and M. Vitelli. Optimization of perturb and observe maximum power point tracking method. *IEEE Transactions on Power Electronics*, 20(4): 963–973, 2005. doi: 10.1109/TPEL.2005.850975.

[23] Emilia Fridman. A refined input delay approach to sampled-data control. *Automatica*, 46(2): 421–427, 2010. ISSN 0005-1098. doi: https://doi.org/10.1016/j.automatica.2009.11.017. URL https://www.sciencedirect.com/science/article/pii/S000510980900541X.

[24] Johan Nilsson, Bo Bernhardsson, and Björn Wittenmark. Stochastic analysis and control of real-time systems with random time delays. *Automatica*, 34(1):57–64, 1998. ISSN 0005-1098. doi: https://doi.org/10.1016/S0005-1098(97)00170-2.

[25] Lixian Zhang, Huijun Gao, and Okyay Kaynak. Network-induced constraints in networked control systems—a survey. *IEEE Transactions on Industrial Informatics*, 9(1):403–416, 2013. doi: 10.1109/TII.2012.2219540.

[26] Xiaohua Ge, Fuwen Yang, and Qing-Long Han. Distributed networked control systems: A brief overview. *Information Sciences*, 380:117–131, 2017. ISSN 0020-0255. doi: https://doi.org/10.1016/j.ins.2015.07.047.

[27] Ahmet Onat, Teoman Naskali, Emrah Parlakay, and Ozan Mutluer. Control over imperfect networks: Model-based predictive networked control systems. *IEEE Transactions on Industrial Electronics*, 58(3):905–913, 2011. doi: 10.1109/TIE.2010.2051932.

[28] Seok Young Lee and JunMin Park. Sampled-data stabilization for networked control systems under deception attack and the transmission delay. *Communications in Nonlinear Science and Numerical Simulation*, 131:107817, 2024. ISSN 1007-5704. doi: https://doi.org/10.1016/j.cnsns.2024.107817.

[29] Luca Schenato. To zero or to hold control inputs with lossy links? *IEEE Transactions on Automatic Control*, 54(5):1093–1099, 2009. doi: 10.1109/TAC.2008.2010999.

[30] Meng Li and Yong Chen. Challenging research for networked control systems: A survey. *Transactions of the Institute of Measurement and Control*, 41(9):2400–2418, 2019. doi: 10.1177/0142331218799818.

[31] Magdi S. Mahmoud and Mutaz M. Hamdan. Fundamental issues in networked control systems. *IEEE/CAA Journal of Automatica Sinica*, 5(5):902–922, 2018. doi: 10.1109/JAS.2018.7511162.

[32] Yuan-Qing Xia, Yu-Long Gao, Li-Ping Yan, and Meng-Yin Fu. Recent progress in networked control systems—a survey. *International Journal of Automation and Computing*, 12(4):343–367, 2015.

[33] R.W. Brockett and D. Liberzon. Quantized feedback stabilization of linear systems. *IEEE Transactions on Automatic Control*, 45(7):1279–1289, 2000. doi: https://doi.org/10.1109/9.867021.

[34] Daniel Liberzon. Hybrid feedback stabilization of systems with quantized signals. *Automatica*, 39(9):1543–1554, 2003. ISSN 0005-1098. doi: https://doi.org/10.1016/S0005-1098(03)00151-1.

[35] Minyue Fu and Lihua Xie. The sector bound approach to quantized feedback control. *IEEE Transactions on Automatic Control*, 50(11):1698–1711, 2005. doi: 10.1109/TAC.2005.858689.

[36] W.P.M.H. Heemels, K.H. Johansson, and P. Tabuada. An introduction to event-triggered and self-triggered control. In *2012 IEEE 51st IEEE Conference on Decision and Control (CDC)*, pages 3270–3285, 2012. doi: 10.1109/CDC.2012.6425820.

[37] Dan Zhang, Peng Shi, Qing-Guo Wang, and Li Yu. Analysis and synthesis of networked control systems: A survey of recent advances and challenges. *ISA Transactions*, 66:376–392, 2017. ISSN 0019-0578. doi: https://doi.org/10.1016/j.isatra.2016.09.026.

[38] Jean-Pierre Richard. Time-delay systems: an overview of some recent advances and open problems. *Automatica*, 39(10):1667–1694, 2003. ISSN 0005-1098. doi: https://doi.org/10.1016/S0005-1098(03)00167-5.

[39] Emilia Fridman. *Introduction to Time-Delay Systems: Analysis and Control*. Birkhäuser, 2nd edition, 2023.

[40] Keqin Gu. Discretization schemes for lyapunov-krasovskii functionals in time-delay systems. *Kybernetika*, 37(4):479–504, 2001.

[41] Keqin Gu, Jie Chen, and Vladimir L Kharitonov. *Stability of time-delay systems*. Springer Science & Business Media, 2003.

[42] A. Seuret and F. Gouaisbaut. Wirtinger-based integral inequality: Application to time-delay systems. *Automatica*, 49(9):2860–2866, 2013. ISSN 0005-1098. doi: https://doi.org/10.1016/j.automatica.2013.05.030.

[43] Vladimir KOLMANOVSKII and Leonid SHAIKHET. *GENERAL METHOD OF LYAPUNOV FUNCTIONALS CONSTRUCTION FOR STABILITY INVESTIGATION OF STOCHASTIC DIFFERENCE EQUATIONS*, pages 397–439. November 1995. doi: 10.1142/9789812796417_0026.

[44] Dong Yue, Qing-Long Han, and James Lam. Network-based robust h control of systems with uncertainty. *Automatica*, 41(6):999–1007, 2005. ISSN 0005-1098. doi: https://doi.org/10.1016/j.automatica.2004.12.011.

[45] B. Sinopoli, L. Schenato, M. Franceschetti, K. Poolla, M.I. Jordan, and S.S. Sastry. Kalman filtering with intermittent observations. *IEEE Transactions on Automatic Control*, 49(9): 1453–1464, 2004. doi: 10.1109/TAC.2004.834121.

[46] Songlin Hu, Dong Yue, Xiangpeng Xie, and Zhaoping Du. Event-triggered h stabilization for networked stochastic systems with multiplicative noise and network-induced delays. *Information Sciences*, 299:178–197, 2015. ISSN 0020-0255. doi: https://doi.org/10.1016/j.ins.2014.11.048.

[47] Paulo Tabuada. Event-triggered real-time scheduling of stabilizing control tasks. *IEEE Transactions on Automatic Control*, 52(9):1680–1685, 2007. doi: 10.1109/TAC.2007.904277.

[48] Boyu Li, Hugang Han, and Nadila Maghfirah. Controller design for class of networked control systems with time delays. In *2025 8th International Conference on Robotics, Control and Automation Engineering (RCAE)*, pages 472–476, 2025. doi: 10.1109/RCAE66389.2025.11355173.

[49] Lei Zou, Zidong Wang, Hongli Dong, Yurong Liu, and Huijun Gao. Time- and event-driven communication process for networked control systems: A survey. *Abstract and Applied Analysis*, 2014(1):261738, 2014. doi: https://doi.org/10.1155/2014/261738.

[50] D.Q. Mayne, J.B. Rawlings, C.V. Rao, and P.O.M. Scokaert. Constrained model predictive control: Stability and optimality. *Automatica*, 36(6):789–814, 2000. ISSN 0005-1098. doi: https://doi.org/10.1016/S0005-1098(99)00214-9.

[51] Guo-Ping Liu, Yuanqing Xia, Jie Chen, David Rees, and Wenshan Hu. Networked predictive control of systems with random network delays in both forward and feedback channels. *IEEE Transactions on Industrial Electronics*, 54(3):1282–1297, 2007. doi: 10.1109/TIE.2007.893073.

[52] Adolf Goetzberger, Christopher Hebling, and Hans-Werner Schock. Photovoltaic materials, history, status and outlook. *Materials science and engineering: R: Reports*, 40(1):1–46, 2003.

[53] Mohammed Hamouda Ali, Mohammad Zakaria, and Sally El-Tawab. A comprehensive study of recent maximum power point tracking techniques for photovoltaic systems. *Scientific Reports*, 15(1):14269, 2025.

[54] Rachana Ashok Gupta and Mo-Yuen Chow. Networked control system: Overview and research trends. *IEEE Transactions on Industrial Electronics*, 57(7):2527–2535, 2010. doi: 10.1109/TIE.2009.2035462.

[55] Hao Yu and Tongwen Chen. Periodic event-triggered networked control systems subject to large transmission delays. *IEEE Transactions on Automatic Control*, 68(1):63–79, 2023. doi: 10.1109/TAC.2021.3131146.

[56] Johan Nilsson. *Real-Time Control Systems with Delays*. Doctoral thesis (monograph), Department of Automatic Control, 1998. Defence details Date: 1998-02-11 Time: 10:15 Place: M:B, M-building, Lund Institute of Technology External reviewer(s) Name: Söderström, Torsten Title: [unknown] Affiliation: Uppsala University —.

[57] Yodyium Tipsuwan and Mo-Yuen Chow. Control methodologies in networked control systems. *Control Engineering Practice*, 11(10):1099–1111, 2003. ISSN 0967-0661. doi: https://doi.org/10.1016/S0967-0661(03)00036-4. URL https://www.sciencedirect.com/science/article/pii/S0967066103000364. Special Section on Control Methods for Telecommunication.

[58] Junlin Xiong and James Lam. Stabilization of linear systems over networks with bounded

packet loss. *Automatica*, 43(1):80–87, 2007. ISSN 0005-1098. doi: https://doi.org/10.1016/j.automatica.2006.07.017.

[59] Jing Li and Bin Zuo. *Modeling and Stability Analysis of NCS with Markov Delay and Dropout*, pages 307–313. Springer Berlin Heidelberg, Berlin, Heidelberg, 2012. ISBN 978-3-642-25778-0. doi: 10.1007/978-3-642-25778-0_43.

[60] Wei Sun, Qiyue Li, Chanjuan Zhao, and Sing-Kiong Nguang. Mode-dependent dynamic output feedback h control of networked systems with markovian jump delay via generalized integral inequalities. *Information Sciences*, 520:105–116, 2020. ISSN 0020-0255. doi: https://doi.org/10.1016/j.ins.2020.02.023. URL https://www.sciencedirect.com/science/article/pii/S0020025520300980.

[61] C. E. Shannon. A mathematical theory of communication. *The Bell System Technical Journal*, 27(3):379–423, 1948. doi: 10.1002/j.1538-7305.1948.tb01338.x.

[62] Marcel Paul Schützenberger. Sur les rapports entre la quantité d'information au sens de Fisher et au sens de Wiener. *Comptes Rendus Hebdomadaires des Séances de l'Académie des Sciences, Paris*, 232:925–927, 1951. ISSN 0001-4036.

[63] S. Kullback. *Information theory and statistics*. John Wiley & Sons, New York, 1959. ISBN 0-8446-5625-9.

[64] J. Wu, F.-Q. Deng, and J.-G. Gao. Modeling and stability of long random delay networked control systems. In *2005 International Conference on Machine Learning and Cybernetics*, pages 947–952, Guangzhou, China, November 2005. IEEE.

[65] P. Radcliffe and X. Yu. A new time independent asynchronous protocol and its applications. *IEEE Transactions on Industrial Informatics*, 3(2):143–153, May 2007. doi: 10.1109/TII.2007.898439.

[66] R. M. Daoud and H. H. Amer. Fault-tolerant access points in a mobile ipv6 wifi light urban traffic communication model. In *2008 Canadian Conference on Electrical and Computer Engineering*, pages 449–452, Niagara Falls, ON, Canada, 2008. doi: 10.1109/CCECE.2008.4564574.

[67] K. C. Lee, S. Lee, and M. H. Lee. Qos-based remote control of networked control systems via profibus token passing protocol. *IEEE Transactions on Industrial Informatics*, 1(3):183–191, August 2005. doi: 10.1109/TII.2005.852064.

[68] P. Matkurbanov, S. Lee, and D. Kim. A survey and analysis of wireless fieldbus for industrial environments. In *Presented at the 2006 SICE-ICASE International Joint Conference*, page 5555–5561, Busan, Korea (South), February 2007. IEEE.

[69] G. Baliga and P. R. Kumar. A middleware for control over networks. In *Proceedings of the 44th IEEE Conference on Decision and Control*, pages 482–487, Seville, Spain, 2005. doi: 10.1109/CDC.2005.1582202.

[70] J. Tisdale, A. Ryan, Z. Kim, D. Tornqvist, and J. K. Hedrick. A multiple uav system for vision-based search and localization. In *Presented at the 2008 American Control Conference*, page 1985–1990, Seattle, WA, USA, August 2008. IEEE.

[71] J. Qiu, H. Gao, and S. X. Ding. Recent advances on fuzzy-model-based nonlinear networked control systems: A survey. *IEEE Transactions on Industrial Electronics*, 63(2):1207 – 1217, February 2016. doi: 10.1109/TIE.2015.2504351.

[72] Gernot A. Fink. *Markov Models for Pattern Recognition*. Springer London, 2 edition, 2014. ISBN 978-1-4471-6307-7. doi: 10.1007/978-1-4471-6308-4.

[73] M. Hahn and J. Sass. Parameter estimation in continuous time markov switching models: a semi-continuous markov chain monte carlo approach. *Bayesian Anal*, 4(1):63–84, March 2009. doi: 10.1214/09-BA402.

[74] Q. Luo and X. Mao. Stochastic population dynamics under regime switching. *Journal of Mathematical Analysis and Applications*, 334(1):69–84, October 2007. doi: 10.1016/j.jmaa.2006.12.032.

[75] J. Janczura and R. Weron. Efficient estimation of markov regime-switching models: An application to electricity spot prices. *AStA Advances in Statistical Analysis*, 96:385–407, November 2011. doi: 10.1007/s10182-011-0181-2.

[76] D. B. Nelson. Conditional heteroskedasticity in asset returns: A new approach. *Econometrica*, 59(2):347–70, 1991.

[77] S. F. Gray. Modeling the conditional distribution of interest rates as a regime-switching process. *Journal of Financial Economics*, 42:27–62, 1996. doi: 10.1016/0304-405X(96)00875-6.

[78] F. Klaassen. Improving garch volatility forecasts with regime-switching garch. *Empirical Economics*, 27:363–394, 2002. doi: 10.1007/s001810100100.

[79] T. Bollerslev. Generalized autoregressive conditional heteroskedasticity. *Journal of Econometrics*, 31:307–327, 1986. doi: 10.1016/0304-4076(86)90063-1.

[80] L. R. Glosten, R. Jagannathan, and D. E. Runkle. On the relation between the expected value and the volatility of the nominal excess return on stocks. *The Journal of Finance*, 48: 1779–1801, 1993. doi: 10.1111/j.1540-6261.1993.tb05128.x.

[81] Luc Bauwens, Bruno De Backer, and Arnaud Dufays. A bayesian method of change-point estimation with recurrent regimes: Application to garch models. *Journal of Empirical Finance*, 29:207–229, 2014. ISSN 0927-5398. doi: 10.1016/j.jempfin.2014.06.008.

[82] M. Haas, S. Mittnik, and M. S. Paolella. A new approach to markov-switching garch models. *Journal of Financial Econometrics*, 2:493–530, 2004. doi: 10.1093/jjfinec/nbh020.

[83] Dong Yu, Li Deng, Yifan Gong, and Alex Acero. A novel framework and training algorithm for

variable-parameter hidden markov models. *IEEE Transactions on Audio, Speech, and Language Processing*, 17(7):1348–1360, 2009. doi: 10.1109/TASL.2009.2020890.

[84] Wei Wang and Hong-Bing Zeng. A looped functional method to design state feedback controllers for lurie networked control systems. *IEEE/CAA Journal of Automatica Sinica*, 10 (4):1093–1095, 2023. doi: 10.1109/JAS.2023.123141.